UNIVERSITÄTSKLINIKUM HAMBURG-EPPENDORF

Institut für Immunologie

Prof. Dr. Marcus Altfeld

Targeting Clostridioides difficile CDTb and TcdB toxins with Nanobodies developed from *Camelus dromedarius*

Dissertation

zur Erlangung des Doktorgrades Dr. rer. biol. hum. / PhD
an der Medizinischen Fakultät der Universität Hamburg.

vorgelegt von:

Intissar Chahbani
aus Djerba, Tunisia

Hamburg 2021

Angenommen von der
Medizinischen Fakultät der Universität Hamburg am: 26.10.2021

Veröffentlicht mit Genehmigung der
Medizinischen Fakultät der Universität Hamburg.

Prüfungsausschuss, der/die Vorsitzende: Prof. Dr. Friedrich Koch-Nolte

Prüfungsausschuss, zweite/r Gutachter/in: PD Dr. Andrea Kristina Horst

Table of Content

1. Introduction

1.1 Clostridioides difficile infection

Clostridium difficile (*C. difficile*) is a gram-positive, anaerobic, spore-forming, toxin-producing bacillus, which was officially renamed in 2016 to *Clostridioides difficile*. The new name reflects the taxonomic differences between this species and other members of the Clostridium genus (Czepiel et al., 2019). The abbreviations *'C. diff*,' 'CDAD,' and others remain applicable (Ghizzone, 2019). The transmission of *C. difficile* spores occurs by the fecal-oral route. The potential reservoirs for *C. difficile* include asymptomatic carriers, infected patients, the contaminated environment and animal intestinal tract (canine, feline, porcine, avian) (Czepiel et al., 2019). *Clostridium difficile* is the leading cause of antibiotic-associated diarrhea. The most important risk factor for CDI is broad-spectrum antibiotic treatment that causes an imbalance of the intestinal microflora allowing the germination of *C. difficile* spores with subsequent colonization and proliferation of the bacteria (Banawas, 2018). *Clostridium difficile* infection (CDI) is considered nowadays a significant healthcare-associated infection with a considerable economic impact in Europe, the United States, and worldwide. The incidence of CDI in Germany is estimated to be 83 cases per 100 000 persons according to the German Federal Office of Statistics, with more than 30,000 primary inpatient cases and more than 74,000 secondary inpatient cases in the years 2013 and 2014 (Lubbert et al., 2016). In the United States, CDI is thought to cause approximately 453,000 infections and 29,000 deaths every year, with an annual economic burden ranging from $436 million to $3 billion dollars (Peng et al., 2018).

The clinical symptoms of CDI range from mild to severe diarrhea, which can lead to fulminant colitis, toxic megacolon, bowel perforation, sepsis, and ultimately death (Mastrantonio, 2018). CDI has been more frequent, virulent, and refractory due to the emergence of a hypervirulent strain (NAP1/BI/027), (Song and Kim, 2019). About 15-35% of CDI patients suffer from recurrent infections. Recurrent CDI (rCDI) occurs usually within 8 weeks after the first CDI episode. The relapse could arise from the same strain or reinfection by a different strain. The second recurrence rate of patients with resolved first recurrence is approximately 40%. The recurrence rate of patients who have already recurred more than twice is approximately 45% to 65% (Song and Kim, 2019).This high rate of CDI recurrence contributes to increased health care costs. The main virulence factors of *C. difficile* are high-molecular-weight clostridial toxins: toxin A (TcdA) and toxin B (TcdB). TcdA and TcdB enter the colonic epithelium, causing proinflammatory chemokine and cytokine production, influx of neutrophils, disruption of tight junctions, fluid secretion and epithelial cell death (Ooijevaar et al., 2018). In recent years, newly recognized hypervirulent strains such as the *C. difficile* BI/ NAP1/027 are responsible for severe infections and increasing mortality worldwide (Banawas, 2018). These

strains express *C. difficile* transferase (CDT), a binary toxin in addition to TcdA and TcdB. This binary toxin can induce microtubule-based protrusions on epithelial cells (Blanke et al., 2009).

1.2 *C. difficile* glucosylating cytotoxins TcdA and TcdB

Toxins A and B share similar structural and functional characteristics (**Fig. 1.1**). TcdA 308 kDa, and TcdB 270 kDa have 2,710 and 2,366 amino acids, respectively (Gupta et al., 2017). TcdA and TcdB share a common domain structure with 44% sequence identity and approximately 66% sequence similarity, the greatest diversity in sequence is confined to their C-terminal binding domains (Di Bella et al., 2016). These toxins share a multi-modular domain structure described as the ACDB model (A: biological activity; C: cutting; D: delivery; B: binding) (Di Bella et al., 2016). Region A is a 63 kDa glucosyltransferase domain (GTD) located at the N-terminus, which is a biologically active enzyme acting on the small GTPases involved in regulation of the cytoskeleton, region B, located at the C-terminus, is involved in receptor binding and consists of combined repeated oligopeptides (CROPs) that form the receptor binding domain (RBD); region C is the cysteine protease domain (CPD) that promotes the auto-catalytic cleavage of the toxins; Finally region D called also the delivery domain (DD) is important for toxin´s translocation into the cytosol, as well as their binding to target cells (**Fig. 1.1A**) (Di Bella et al., 2016).

To initiate the cellular uptake, *C.difficile* toxins bind to specific receptors on the host cell surface. The receptor binding domain of TcdA and TcdB covers amino acid residues, 1,833–2,710 and 1,834–2,366, respectively, and is characterized by repetitive sequences called combined repetitive peptides (CROPs) (Aktories et al., 2017). Toxin A interacts with different cell surface carbohydrate structures, mainly with two proteins, the sucrase-isomaltase and the glycoprotein gp96 (Gerhard, 2017), while host receptors of toxin B were identified as CSPG4 (chondroitinsulphate proteoglycan-4), PVRL3 (poliovirusreceptor-like 3) and members of the Wnt receptor frizzled family, such as FZD2 (Mastrantonio, 2018). After binding to their specific receptors on the surface of gut epithelial cells, the intoxication process of TcdA and TcdB begins with their endocytic uptake through a clathrin and dynamin-dependent mechanism (Aktories et al., 2017). In response to the low pH of endosomes, TcdA and TcdB delivery domain structure changes that leads to the exposure of hydrophobic segments. These segments insert into the host membrane forming a pore through which the glucosyltransferase domain translocate into the cytosol (Orrell et al., 2017).

Once in the cytosol, the toxins undergo an autocatalytic cleavage dependent on the presence of Insp6 leading to the release of the GTD domain which glucosylates several members of the Rho subfamily of GTPases by transferring a glucose moiety from the UDP-glucose to the Thr35/37 residue of Rho proteins (Di Bella et al., 2016). Glucosylation of Rho proteins causes their inactivation, resulting in the loss of the cytoskeletal structure, disassembly of focal adhesions and disruption of tight junctions. These effects result in the characteristic cell rounding phenotype (also termed the cytopathic effect).

The glucosylation-dependent cytopathic effect is thought to play an important role in the context of disease by increasing intestinal permeability and inflammation. In addition to the cytopathic effect, inactivation of Rho GTPases by TcdA and TcdB can promote epithelial cell death (referred to as a cytotoxic effect) (**Fig. 1.1B**) (Chandrasekaran and Lacy, 2017).

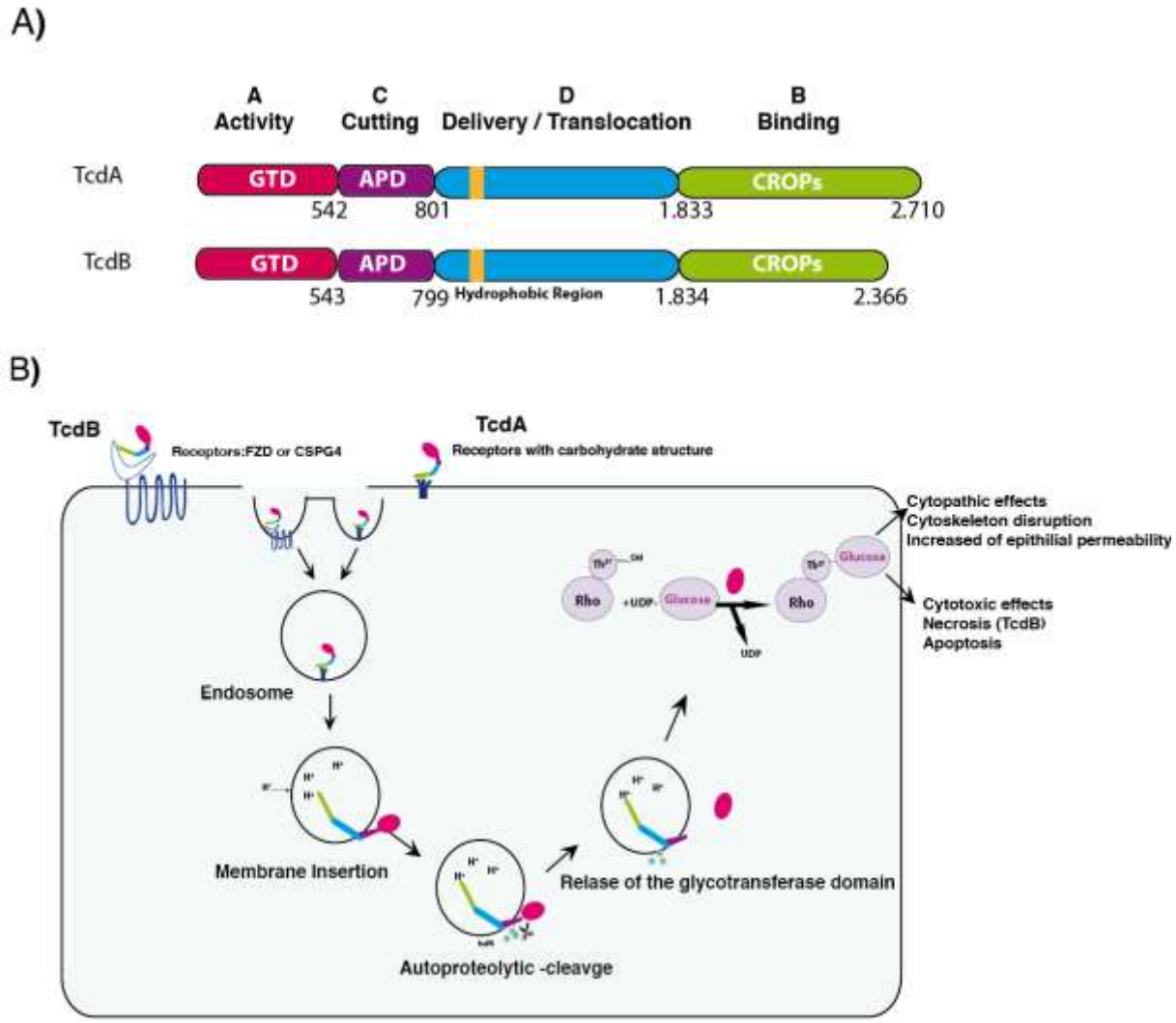

Figure 1.1. **Schematic diagrams of TcdA and TcdB and their mode of action**. A) TcdA and TcdB are organized in four functional domains, with the glucosyltransferase domain (GTD) in red, the autoprotease domain (APD) in purple, the delivery or translocation domain in blue, the hydrophobic region in orange, and the C-terminal binding repetitive region (CROP) in green. B) Mode of action of TcdA and TcdB. TcdA and TcdB bind to cell surface receptors. Certain carbohydrate structures (and gp96) have been identified to be host cell receptors for TcdA. Endocytosis of TcdA involves PACSIN2 (also called syndapin-II) and dynamin pathway but not clathrin. For TcdB, three proteins have been identified to be the host cell receptors (CSPG4, FZD, PVRL3). After binding to the receptor, TcdB is endocytosed in a clathrin-and dynamin-dependent manner. Both toxins reach an acidic endosomal compartment, where the hydrophobic region of the translocation domain inserts into the endosomal membrane, forming a double helical hairpin pore. The GTD and APD domains translocate through the pore into the cytosol, where the inositol hexakisphosphate (InsP6) activates the protease, thereby cleaving the toxin and releasing GTD into the cytosol. The free GTD glucosylates Rho family GTPases (RhoA at Thr37; Cdc42 and Rac at Thr35), leading first to cytopathic effects, and later to cytotoxic effects. At high doses of TcdB, a necrotic pathway is stimulated that is independent of the GTD domain.

TcdB is 100-10,000 times more potent than TcdA in several cells type (Di Bella et al., 2016). At low concentrations, TcdB induces apoptosis in a glucosylation-dependent manner, while at high concentrations (100 pM or above); TcdB causes a necrotic form of cell death without either the

autoprocessing or glucosyltransferase activities of the toxin (Chandrasekaran and Lacy, 2017). The necrotic death can be observed in both cell culture and colon explant models after 2-4 hours of intoxication and is marked by rapid ATP depletion, breakdown of the plasma membrane and cellular leakage, and chromatin condensation. TcdB induced-necrosis causes an aberrant production of reactive oxygen species (ROS) through the assembly of the NADPH oxidase (NOX) complex on endosomes. High levels of ROS promote cellular necrosis likely through DNA damage, lipid peroxidation, protein oxidation and/or mitochondrial dysfunction (Chandrasekaran and Lacy, 2017).

1.3 The binary ADP-ribosylating *C. difficile* toxin (CDT)

Strains producing the binary toxin or *C. difficile* transferase (CDT) in addition to TcdA and TcdB, have been associated with an increased CDI severity (e.g., ribotype BI/NAP1/027) (Aktories et al., 2017). CDT consists of two components; CDTa, an ADP-ribosyltransferase, targeting the actin, and CDTb, a binding component, which binds to the cell receptors and translocate CDTa into the cytosol (**Fig. 1.2**). The enzyme component CDTa (53 kD) consists of 463 amino acids, with an N-terminal signal peptide sequence of 43 amino acids, which is cleaved by proteolysis. The mature CDTa has a size of 48 kD (420 amino acids) consists of two domains with similar folding. Amino acids 1-215 interact with CDTb, whereas amino acids 224–420 harbor the catalytic ADP-ribosyltransferase domain (**Fig. 1.2A**) (Mastrantonio, 2018). The binding component CDTb (98.8 kDa, 876 amino acids) is divided into four domains. The N-terminal 257 residues form the activation domain I. Domain II (residues 258-480) is involved in membrane insertion and pore formation. Domain III (amino acids 481-591) participates in oligomerization, and the C-terminal domain IV (amino acids 592–876) is involved in receptor binding (Gerding et al., 2014). CDTb is activated by proteolytic cleavage by serine-type proteases which leads to the removal of a 20 kD peptide from the N-terminus domain I (Mastrantonio, 2018). This cleavage allows oligomerization and formation of heptamers. This process might occur in solution or on the surface of target cells after receptor binding (**Fig. 1.2A**).

Activated CDT binds to the lipolysis-stimulated lipoprotein receptor (LSR), followed by accumulation in lipid rafts, oligomerization, and binding of the enzyme component. The toxin receptor complex is endocytosed to reach a low pH compartment. CDTb then forms pores in endosomal membranes that serve as translocation channels for CDTa (Mastrantonio, 2018). Translocation of CDTa and refolding in the cytosol depend on helper proteins including Hsp90, peptidyl-prolyl cis-/trans-isomerase cyclophilin A, and FK506-binding protein 51 (Aktories et al., 2017). In the cytosol, CDTa transfers ADP-ribose from nicotinamide adenine dinucleotide (NAD^+) to Arg-177 of monomeric G-actin, thereby inhibiting actin polymerization by trapping it in its monomeric form (Chandrasekaran and Lacy, 2017). ADP ribosylated actin acts also as a capping protein that binds at the barbed ends of F-actin blocking its polymerization. This induces microtubule-based protrusions on epithelial cells that increase adherence of bacteria (**Fig. 1.2B**) (Aktories et al., 2017).

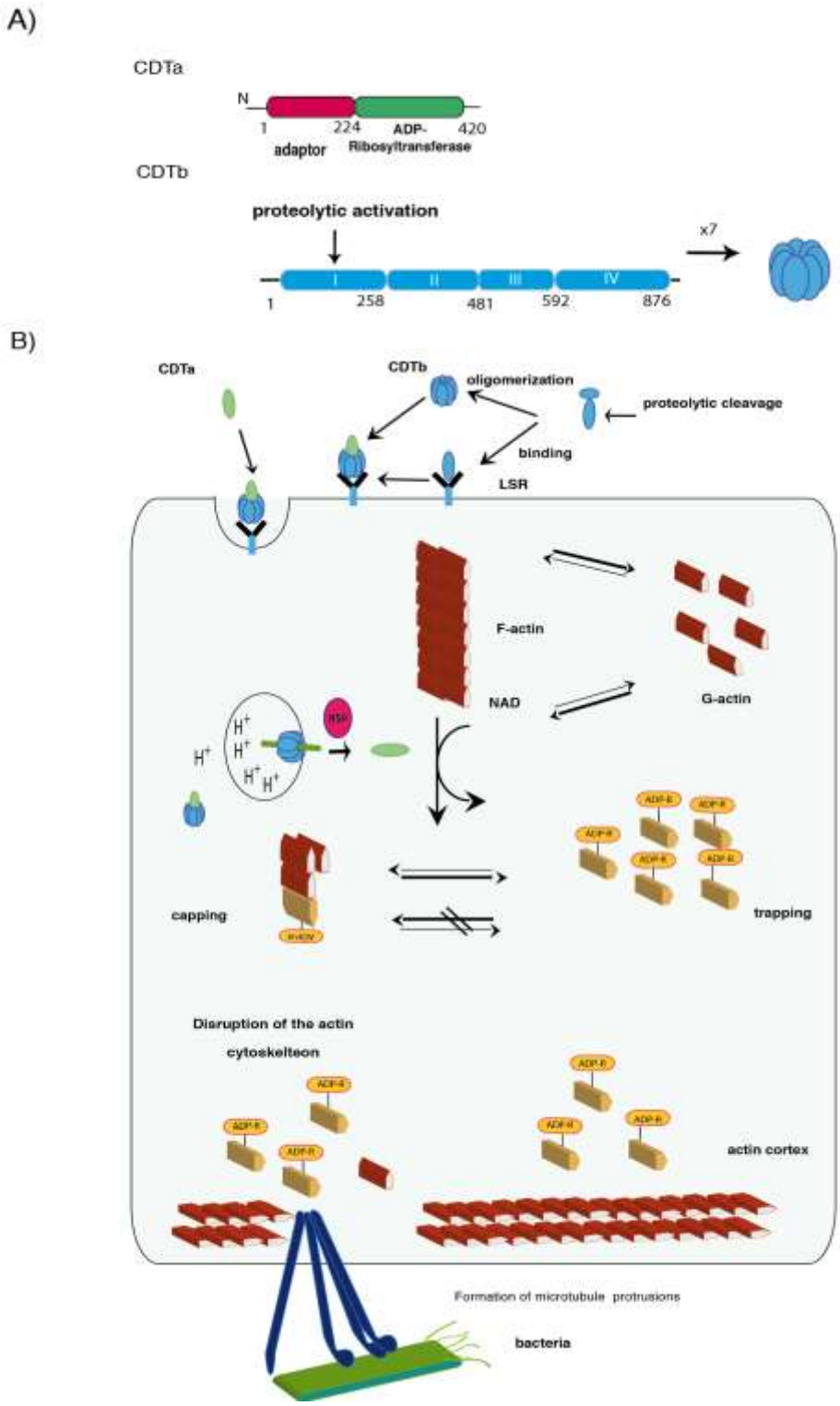

Figure 1.2. **Schematic diagram of the CDT binary toxin and its mode of action**. A) CDT consists of an enzymatic component CDTa and a binding component CDTb. The N-terminal domain of mature CDTa (red) is responsible for CDTb binding, while the C-terminal domain (green) carries the ADP-ribosyltransferase activity. CDTb consists of four domains. Activation of domain I by proteolytic cleavage triggers formation of heptamers. B) CDTb binds to the lipolysis-stimulated lipoprotein receptor (LSR) and undergoes proteolytic activation and oligomerization on the cell surface. CDTa binds to CDTb and the toxin-receptor complex is internalized. At low-pH of endosomes, CDTb undergoes conformational changes, inserts into the endosomal membrane and forms a pore through which CDTa is translocated into the cytosol. Translocation and refolding of CDTa is facilitated by chaperones, heat shock protein 70 (Hsp70), Hsp90, and cyclophilin A (CypA). In the cytosol, CDTa ADP-ribosylates actin at arginine-177. ADP-ribosylation of actin results in the disruption of the actin cytoskeleton, cytopathic cell rounding, and the formation of microtubule-based protrusions that enhance bacterial adherence.

1.4 Advances and limitations of *C. difficile* diagnosis

An effective diagnosis of CDI requires both clinical symptoms and a positive laboratory test (Peng et al., 2018). Currently, there is n o single test that can be considered as a reference standard or stand-alone test for the diagnosis of CDI. Early toxin detection is critical for CDI treatment as this allows earlier diagnosis that can significantly reduce the morbidity, mortality and the medical cost of CDI (Peng et al., 2018). Several assays are available for CDI detection such as the toxinogenic culture (TC) (in which *C. difficile* is cultured from stool and isolates are tested for cytotoxin production by cytotoxicity assay). This test has limited utility for clinical diagnosis; it is slow (requiring 72 to 96 hours), non-standardized, and unsuitable for routine clinical testing. An additional disadvantage of this technique is its ability to examine only the in vitro toxin production, which may not reflect the strain's production of toxins in the in vivo environment (Pollock, 2016). A second assay known for CDI diagnosis is cytotoxicity neutralization assay (CCNA), in which stool sample filtrate is inoculated onto an in vitro cell monolayer (Vero cells, HeLa cells, human fibroblast cells) and at 24- and 48-hours intervals, the obtained cell cultures are evaluated for the characteristic rounding effect (Mastrantonio, 2018). The TC or CCNA methods were the most frequently used standard for CDI diagnosis for many years (Peng et al., 2018), but since they are labor intensive and have a slow turnaround time, they are less used in clinical diagnosis routine (Mastrantonio, 2018).

Alternative easy-to perform rapid assays have been developed. These include enzyme immunoassays (EIA) for GDH and for TcdA/TcdB, and nucleic acid amplification tests (NAATs) for toxin genes. These assays are suited for clinical use, but each of them suffers from shortcomings (Mastrantonio, 2018). The glutamate dehydrogenase test (GDH) is easy to perform and cheap. This assay detects glutamate dehydrogenase, an enzyme that is produced by both toxigenic and non-toxigenic strains. GDH-EIA test methods are sensitive for screening *C. difficile* but are unable to differentiate toxigenic and non-toxigenic strains as both strains produce GDH (Peng et al., 2018). Other enzyme immunoassay (EIA) detects *C. difficile* toxins directly in a stool sample at low cost and rapid turnaround time (about 1–2 hours). A drawbacks is the variable specificity (Pollock, 2016). NAATs are regarded as the most effective method for CDI diagnosis and detect the genes of TcdB, TcdA, and/or the binary toxins (Peng et al., 2018). However, in addition to the high cost, NAAT are unable to differentiate between active toxin production in vivo and only *C. difficile* colonization (Peng et al., 2018).

In light of the these assay limitations, multi-step algorithmic testing for CDI diagnosis was recommended by the European Society of Clinical Microbiology and Infectious Diseases (ESCMID), the Society for Healthcare Epidemiology of America and the Infectious Diseases Society of America (SHEA/IDSA) (Cohen et al., 2010, Crobach et al., 2016). Algorithmic testing starts with either NAATs or GDH-EIA that have high negative predictive value. The second test should be a test with

high positive predictive value, i.e. toxin A/B EIAs. If the first test is negative, it excludes CDI. If the first test is positive, the second test (toxin A/B EIAs) should be performed. If the second test is positive, it confirms CDI. If the second test is negative, the case needs to be clinically evaluated, and such result can be seen in three situations: CDI with toxin levels below the threshold of detection, false-negative toxin A/B EIA result, or *C. difficile* carriage. Samples with a negative GDH result but are positive for toxins need to be retested, as this is an invalid result (Czepiel et al., 2019).

Other tests are used for diagnosing CDI in clinical routine. If the first diagnosis of CDI results are suspected or no response to standard course of antibiotics is observed, direct endoscopy and visualization /or biopsy of the bowel mucosa is needed (Bartlett, 2002, Bartlett and Gerding, 2008). Endoscopy is an invasive procedure with perforation risks and is often expensive. Moreover, abdominal imaging (X-ray, ultrasound) is a good method to detect CDI. Patients with CDI reveals distended bowel loops, often with wall thickening (Czepiel et al., 2019). Computer tomography of the abdomen and pelvis with oral and intravenous contrast could be also useful in diagnosing fulminant CDI and pseudomembranous colitis (PMC) helping to detect toxic megacolon, bowel perforation, or other findings warranting surgical intervention (Czepiel et al., 2019). Imaging is less sensitive when compared with NAAT or stool toxin tests but can be useful when there is a need for quick results (Bartlett and Gerding, 2008). Other markers such as immune modulating interleukins and cytokines that may play a role in CDI and may correlate to disease severity are under investigation (Mastrantonio, 2018). An optimized and accurate diagnostic modality that can accurately differentiate CDI versus colonization is urgently needed.

1.5 Current and emerging treatment strategies of *C. difficile* infection (CDI)

Antimicrobial therapy still is the first choice for CDI, The three antimicrobial agents approved for CDI treatment are metronidazole, vancomycin and fidaxomicin. Metronidazole has historically been the most commonly used option for treating CDI (Mastrantonio, 2018). However, new guidelines no longer recommend it as first-line therapy. For both mild and severe CDI, either vancomycin or fidaxomicin are selected, metronidazole is used if neither is available or tolerated. The antimicrobial therapeutic approach is based on the severity of CDI infection (Rao and Malani, 2020). Unfortunately, antibiotic therapy is less effective for recurrent CDI (rCDI). In cases of multiple recurrences or refractoriness through standard antibiotics, fecal microbiota transplant (FMT) is considered. Studies have shown that FMT produced a primary cure rate of approximately 90% in patients with rCDI (Song and Kim, 2019).

However, FMT remains experimental and the US Food and Drug Administration (FDA) only permits its clinical and non-investigational use for rCDI (Rao and Malani, 2020). The European Society of Clinical Microbiology and Infectious diseases guidelines recommend the use of FMT as non-antibiotic therapy of choice for the management of recurrent CDI. However, several aspects of FMT

remain to be optimized, such as the timing, preparation, and route of delivery. Despite strict screening protocols for donors' fecal matter, FMT still has the potential of transmitting infectious diseases. Also changes in gut microbiota upon FMT can affect various extra-intestinal disorders, such as metabolic, neuropsychiatric, and autoimmune diseases and tumors (Song and Kim, 2019).

In 2016, the FDA approved Merck' s ZINPLAVA™ (bezlotoxumab) to reduce recurrency of CDI in patients with high risk of CDI recurrence. Bezlotoxumab is a human monoclonal antibody that blocks the binding of *C. difficile* TcdB to host cells and thereby limits epithelial damage and facilitates microbiome recovery (Bartlett, 2017). The registration trial, which included over 2500 patients, showed that bezlotoxumab together with standard oral antibiotic therapy was associated with a significantly lower rate of recurrent infection than oral antibiotic therapy alone (17 versus 28%) (Czepiel et al., 2019). Fidaxomicin and bezlotoxumab have been shown to reduce the risk of recurrent CDI by 40–50% in comparison with vancomycin alone (Mastrantonio, 2018).

An emerging preventative strategy to reduce the incidence of CDI, is the use of β-lactamases to reduce the initial microbial disruption caused by β-lactam antibiotics while preserving systemic drug activity (Dieterle et al., 2019). Oral probiotics such as BioK and VSL#3 are also considered as preventative measures, as an adjunct to antibiotic prescriptions, to restore the balance of gut microbiota (Kalakuntla et al., 2019). However, evidences for their efficient use are still limited (Mastrantonio, 2018). Vaccines (VLA84, ACAM-CDIFF, PF-06425090, CDVAX) are evaluated as a preventive strategy to boost host antibody-mediated immunity and decrease the ability of *C. difficile* to proliferate. Lactoferrin therapy, which is a growth modulator, has been shown to delay *C. difficile* growth and reduce toxin production (Dieterle et al., 2019). Toxin binders (calcium alumino silicate), and immune modulators (alanyl-glutamine) can be used to reduce the mucosal damage caused by CDI toxins, helping in reducing the severity of CDI. Bowel prep solutions such as Nu-Lytely, which is a formulation of an osmotic laxative PEG 3350 and electrolytes, are also used to flush out the luminal toxin content of the intestines to prevent severe CDI (Dieterle et al., 2019).

New antibiotics for CDI treatment (cadazolid, CRS3123, LFF571, ridinilazole, surotomycin,) are designed to reach high luminal concentrations with high activity against *C. difficile* without broad activity against other native bacteria (Dieterle et al., 2019). Microbiome based therapeutics aim to restore colonization and promote resistance by supplementing the microbiota with bacterial replacement therapies (SER-109, RBX2660,) (Dieterle et al., 2019, Mastrantonio, 2018). Administration of non-toxigenic *C. difficile* (VP20261) could be useful to compete with toxigenic *C. difficile* cells and reduce the risk of CDI. These approaches are in advanced clinical trials (Dieterle et al., 2019).

1.6 Nanobodies: the soluble variable domain of heavy chain antibodies (VHH)

In 1993, functional heavy chain antibodies (hcAbs) lacking light chains and the CH1 domain were discovered in the serum of Camelidae (Camelus dromedarius, Camelus bactrianus, Lama glama, Lama guanicoe, Lama pacos, and Lama vicugna), in addition to conventional IgG. HcAbs constitute approximately 50% of the IgG in llama serum and as much as 75% of the IgG in dromedary serum (Daley et al., 2005). They have a molecular mass of 95 kDa, while their variable antigen-binding domains (VHH) are usually 12-14 kDa. The small size in the low nanometer size range inspired Ablynx to register the name Nanobody® as a trademark; nanobody is also commonly used as a generic name for recombinant VHH (Jovcevska and Muyldermans, 2020).

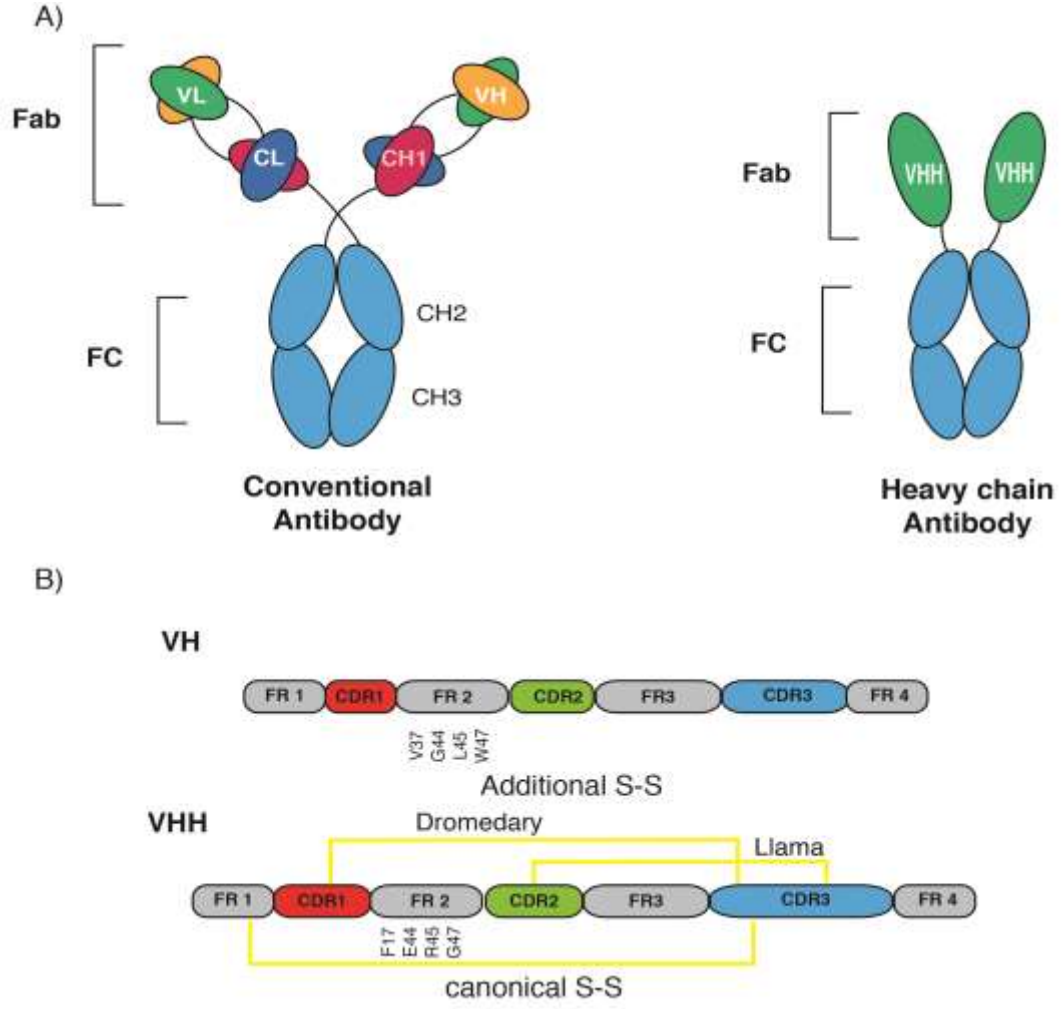

Figure 1.3. Schematics of a conventional antibody and a heavy-chain antibody hcAb. A) The conventional IgG consist of two light (L) chains, comprising the VL and CL domains, and two heavy (H) chains composed of the VH, CH1, hinge, and CH2 and CH3 domains; the hcAb consists only of heavy chains; each of which contains a VHH, hinge, CH2, and CH3 domains. The antigen-binding fragment (Fab) of IgG consists of VH-CH1 and VL_CL, while the antigen-binding fragment of hcAbs consists of a single variable domain (VHH or nanobody). B) The complementarity determining regions (CDRs) that determine the specificity of an antibody are color coded: CDR1 is indicated in red; CDR2 in green, CDR3 in blue, The CDR3 of VHHs is often larger than that of VHs, a hallmark difference between VH and VHH are amino acids substitutions in framework 2 that confer a hydophobic interface of VH with a VL, but a hydophylic surface to the VHH and high solubility as a recombinant protein. VHHs often carry an extra disulfide bond (S–S) connecting the CDR3 with the end of the CDR1 (dromedaries) or the beginning of the CDR2 (llamas). The extra disulfide bond is indicated in yellow.

Similarly to the VH domains of human immunoglobulin, VHHs contain four conserved framework regions (FR) surrounding three hypervariable antigen-binding loops (complementarity-determining regions (CDR). A hallmark difference between a human VH and a camelid VHH is observed within the framework 2 region where four highly conserved and hydrophobic amino acids (V42, G49, L50 and W52 in VH) are substituted in nanobodies by hydrophilic amino acids (F42 or Y42, E49, R50 and G52) (amino acid numbering is according to the international ImMunoGeneTics (IMGT) information system), which makes the VHH domain more soluble than a VH domain (**Fig. 1.3B**) (de Marco, 2020).

HcAbs bind to their target with only the three antigen-binding loops of the VHH, whereas conventional antibodies bind their target antigen with paired VH-VL domains containing six CDRs (**Fig. 1.3A**). The extended CDR3 loop of nanobodies has the capacity to form a finger-like structure or a convex paratope able to penetrate into cavities on the surface of an antigen such as the concave surface in the catalytic site of an enzyme. However, the paratope of VH-VL pairs from human or mouse antibodies often forms a flat surface to interact with larger epitopes on proteins, or might form a groove or cleft to recognize linear peptides or haptens (Jovcevska and Muyldermans, 2020, Muyldermans and Smider, 2016). Nanobodies show many other advantageous proprieties such us strong antigen-binding affinity, low immunogenicity, efficient tissue penetration, thermal stability, and ease of production in prokaryotic and eukaryotic expression systems (Kunz et al., 2018). VHHs are used in protein structural characterization as crystallization chaperones. They are also suitable for noninvasive in vivo PET/ SPECT imaging as convenient carriers for radioisotopes with a short half-life. Furthermore, they are excellent capturing agents to purify targets from complex mixtures or for chromatin immunoprecipitation (de Marco, 2020).

1.7 IgA immunoglobulin; a first line defense at mucosal surfaces

IgA is the second most abundant antibody class in human serum at 2–3 mg/mL (after IgG at 10 mg/ml). IgA is localized mainly at mucosal surfaces such as gastrointestinal, genitourinary, and respiratory tracts. It has been calculated that around 60 mg of IgA is produced per kilogram of body weight per day (de Sousa-Pereira and Woof, 2019). In humans, there are two subclasses of IgA, named IgA1 and IgA2, which can exist as monomer in serum or as dimers in mucosal secretions. IgA1 comprises 80–85% of total human serum IgA (1–3 mg/ml) and is prevalent on many mucosal surfaces including the nasal, bronchial, gastric, and small intestinal mucosa. IgA2 is predominantly present in the colon (Breedveld and van Egmond, 2019). The two IgA subtypes differ at various sites in the heavy chain, IgA1 contains two N-linked glycosylation sites per heavy chain whereas IgA2 has four N-glycans per heavy chain (Breedveld and van Egmond, 2019). A notable difference is found in the hinge region where IgA2 lacks 13 amino acids and multiple O-linked glycans compared to IgA1 (**Figs. 1.4A and 1.4B**). The shorter hinge region of IgA2 leads to a reduced susceptibility to bacterial

proteases, which possibly explains the higher prevalence of IgA2 in mucosal secretions (Hansen et al., 2019). At the C-terminus of both subclasses lies an 18 amino acid extension known as the tailpiece, which contains an N-linked sugar at residue Asn459. It has been reported recently that the latter can interact directly with certain viruses and thereby neutralize them (de Sousa-Pereira and Woof, 2019).

Serum IgA is produced by plasma cells in the bone marrow, spleen, and lymph nodes. IgA at mucosal surfaces is produced by local plasma cells as dimeric molecules. In dimeric IgA (dIgA), the Fc regions of the two monomers are covalently linked by disulfide bridges to the J chain (**Fig. 1.4C)**. In particular, the penultimate residue of the tailpiece, Cys471, of one of the heavy chains of each monomer forms a disulfide bridge to the J chain (Woof and Russell, 2011). J chain is a 15kDa polypeptide, expressed by antibody-producing cells, and is also present in larger IgA polymers and pentameric IgM. It is incorporated into polymeric IgA or IgM prior to secretion (de Sousa-Pereira and Woof, 2019). Dimeric IgA secreted by plasma cells in the lamina propria of the intestine is transported across the epithelium via the poly-immunoglobulin receptor (pIgR) and is released into the gut lumen upon proteolytic cleavage of the pIgR together with a fragment of pIgR referred to as the secretory component (Hansen et al., 2019). These secretory IgA antibodies (sIgA) bind and regulate the intestinal microbiota and protect the epithelial barrier from pathogens (**Fig. 1.4D)**. Secretory component is a hydrophilic and highly (N and O linked) glycosylated negatively charged molecule, which protects sIgA from degradation in luminal secretions (Breedveld and van Egmond, 2019).

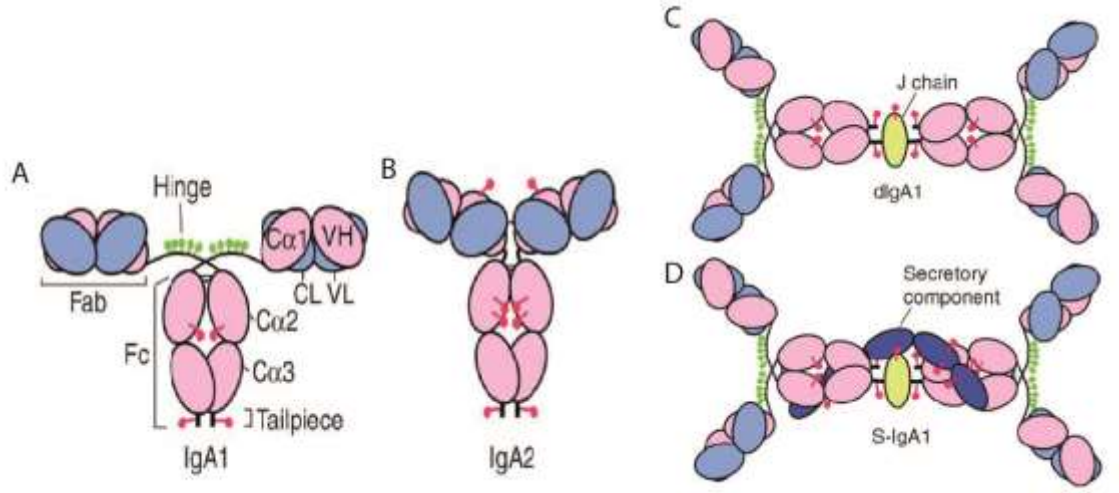

Figure1.4. Schematics of human IgA subclasses and formats. A, IgA1 subclass; B, IgA2 subclass; C, dimeric IgA1; D secretory IgA1. IgA heavy-chain domains are colored in pink, light-chain domains in blue, J chain in yellow, and pIgR domains (secretory component) in dark blue. N-and O-linked oligosaccharides are shown in red and green, respectively (Woof and Russell, 2011).

sIgA is a major immune effector at mucosal surfaces that acts via three mechanisms: immune exclusion, antigen excretion and intracellular antigen neutralization (de Sousa-Pereira and Woof,

2019) (**Fig. 1.5**). Immune exclusion refers to the ability of sIgA to prevent microbial pathogens (and antigens) from gaining access to the intestinal epithelium through a stepwise series of events involving agglutination, entrapment in mucus, and/or clearance via peristalsis (Mantis et al., 2011). Antigen excretion takes place in the lamina propria, where antigens are bound to dimeric IgA and are subsequently transported to the luminal surface of the epithelial cells following endocytosis of the antigen–dimeric IgA–pIgR complex and its release into the mucosal lumen (Strugnell and Wijburg, 2010). Intracellular neutralization occurs where endosomes carrying sIgA from the basolateral surface intersect and fuse with endosomes from the apical surface containing endocytosed virus or toxins. The interaction between the specific sIgA and viral proteins, or bacterial toxins, present in endosomes can lead to inhibition of viral replication steps, such as removal of the capsid, and the trafficking of toxins to their intracellular receptors (**Fig. 1.5)** (Strugnell and Wijburg, 2010).

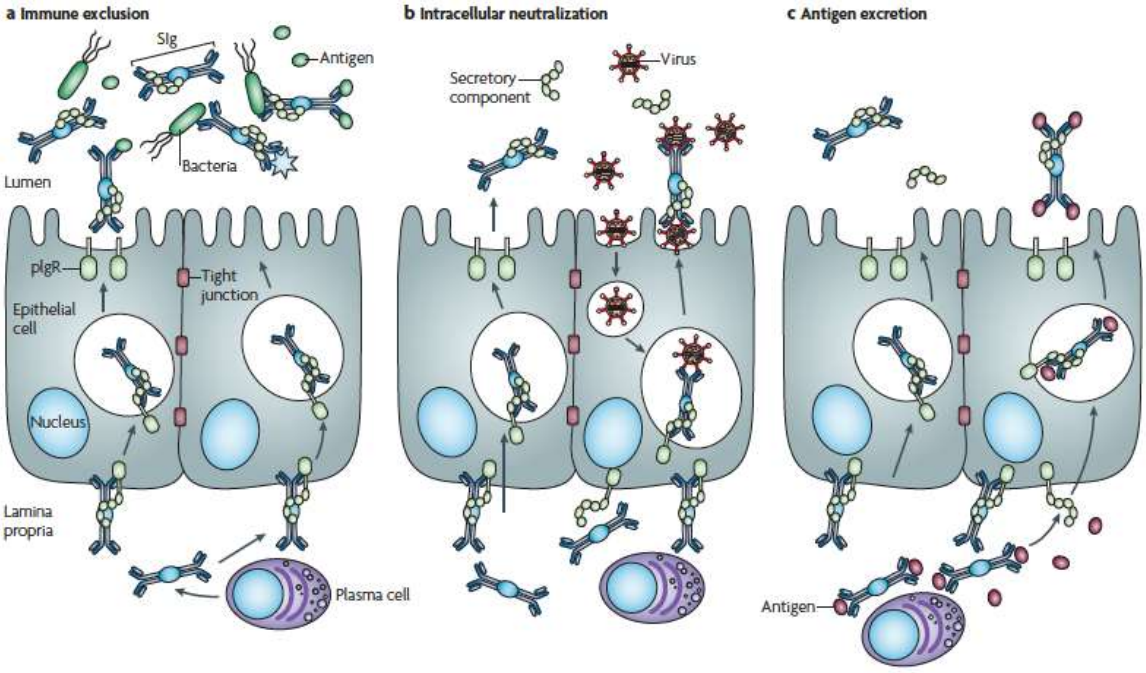

Figure.1.5. Protective functions of secretory IgA in the mucosal compartment. Secreted antibodies can protect mucosal surfaces by immune exclusion, antigen excretion, and intracellular neutralization (Strugnell and Wijburg, 2010)

Thus, together with the mucus layer, sIgA forms a barrier against pathogens, and commensals by preventing colonization and penetration of the mucosal epithelium, thereby avoiding infection and antigen leakage into the systemic circulation (Breedveld and van Egmond, 2019). Furthermore, IgA can modulate inflammation, both at mucosal and non-mucosal sites by binding to specific IgA Fc receptors (FcαRI; also known as CD89) on myeloid cells (Hansen et al., 2019). The co-stimulation of FcαRI affects pro-inflammatory cytokine production by dendritic cell subsets, macrophages, monocytes, and Kupffer cells. FcαRI-induced inflammation plays a crucial role in orchestrating human host defense against pathogens, as well as in the generation of tissue-specific immunity (Hansen et al., 2019).

1.8 Goals of the study

The goal of this study was to generate and to evaluate novel nanobody-based heavy chain antibodies as a basis for new diagnostics and therapeutics of *C. difficile* associated disease.

Specific aims were:

- To select high affinity nanobodies from dromedaries that had been immunized with the enyzmatic domains of TcdB (CPD-GTD) and the receptor-binding subunit of CDT (CDTb) using phage display technology.
- To assess the affinity, epitope specificity and neutralization potential of the selected nanobodies in vitro.
- To reformat the selected nanobodies into rabbit IgG and mouse IgA heavy chain antibodies.
- To develop high sensitivity sandwich ELISAs for detecting TcdB and CDTb in stool samples.

2. Materials and Methods

2.1 Materials

2.1.1 Laboratory equipment

Equipment	Model/Type	Company
Analytical scale	Analytical Plus	Ohaus
Autoclave	2540 EK Varioklav	Tuttnauer H&P Labortechnik
Bacteria incubator	Multitron Pro	Infors HT
Centrifuge	Rotanta 460 R 5417R 5430 Biofuge pico	Hettich Eppendorf Eppendorf Heraeus
CO_2 incubator	MCO-20AIC	Sanyo Electric Co.
Electrophoresis Equipment	MicroPulser	Bio-Rad Laboratories, Inc.
ELISA plate reader	Victor3 1420	Perkin-Elmer
Freezer	HFC 586 Basic	Heraeus
Heat block	Thermomixer Compact	Eppendorf
Micropipettes	Modell Research	Eppendorf
Microwave	M 637 EC	Miele
Neubauer cell chamber		LaborOptik
pH meter	Toledo MP220	Mettler
Photometer	Nanodrop 2000c	PEQLAB Biotechnologie GmbH
Photometer	Ultraspec 2000	Pharmacia Biotech
Power supply for Agarose gel electrophoresis	Standard power pack P25 BIO1015 LVD	Biometra, Göttingen
Power supply for SDS PAGE and electroblot	Power Pac 200	BioRAD, Munich
Roller	Mixer SRT6	Stuart
Scanner	CanonScan 9800F	Canon
Sterile work bench	BSB4, HeraSafe, Type TI 1	GELAIR Heraeus Biometra
Table scale	Scout Pro	Ohaus
Thermocycler	T3/T Gradient	Biometra
UV transilluminator	Type TI 1	Biometra Vertical electrophoresis system for SDS-PAGE Xcell SureLock MiniCell Thermo Fisher
Vortex		Neolab
Water bath	Type 1007	Labortechnik

2.1.2 Consumables

Consumable	Type/Size	Manufacturer
Cell culture flask	T-25, T-75, T-225	Greiner bio one/NuncTM
Disposable pipette tips	Different sizes	Sarstedt
Erlenmeyer flask		PP Corning Inc
Electroporation cuvette	Gene pulser 0,1 cm	Bio-Rad Laboratories
Falcon tubes	Volume 15 ml, 50 ml	Greiner
Gloves	Perform	Aurelia
Nunc 96 well-plate	NuncTM MaxiSorp	Thermo Fisher Scientific
Petri dishes	various sizes c	Thermo Fischer Scientific
SDS-PAGE gels	10% and 12% NuPAGE	Invitrogen

2.1.3 Chemicals

Chemicals	Manufacturer
2xYT	BD/Difco
AEBSF	Merck
Agar	BD/Difco
Agarose	Invitrogen
Aqua ad iniectabilia	Braun
Bacto-Agar	Braun
Bacto-Trypton	Gibco-BRL
BSA	Sigma-Aldrich/Merck
Carbenicillin	Sigma-Aldrich/Merck
DMEM medium	GibcoTM /Thermo Fisher Scientific
DMEM medium	GibcoTM/Thermo Fisher Scientific
DNA Gel Loading Dye (6x)	New England Biolabs
dNTPs	Invitrogen
DTT	Invitrogen
Fetal calf serum (FCS)	GibcoTM /Thermo Fisher Scientific
GeneRuler 1 kb-DNA-Ladder	Fermentas
Glycerol	Sigma-Aldrich/Merck
HEPES	GibcoTM /Thermo Fisher Scientific
IgG Elution buffer pH 2,8	Thermo Fisher Scientific
Imidazole	Sigma-Aldrich/Merck
IPTG (Isopropyl-1-thio-"-D galactopyranoside)	Fermentas (St. Leon-Rot)
jetPEI	Polyplus
Kanamycin	Sigma-Aldrich/Merck
L-Glutamine, 200 mM	GibcoTM /Thermo Fisher Scientific
LB Agar	BD/Difco
LB Broth	BD/Difco
NuPAGE LDS Sample Buffer (4x)	Invitrogen/Thermo Fisher Scientific
NuPAGE Sample Reducing Agent (10x)	Invitrogen/Thermo Fisher Scientific
Paraformaldehyde (PFA)	Sigma-Aldrich/Merck
Phosphate buffered saline (PBS)	GibcoTM/Thermo Fisher Scientific
Polyethylenglycol (PEG) MW 8000	Carl Roth GmbH + Co.

Roti Gel-Stain	Carl Roth
Sodium Chloride	Baker
Sodium hydroxide	Merck
Sodium pyruvate	GibcoTM /Thermo Fisher Scientific
TAE-Puffer (50x) UltraPure DNA Typing Grade	Thermo Fisher Scientific
TMB substrate	Pierce
Tris-Base	Sigma Aldrich
Tris-Cl	Sigma Aldrich
Triton X-100	Sigma-Aldrich/Merck
Trypsin, 10x	Invitrogen
Tween-20	Sigma-Aldrich/Merck
β-mercaptoethanol	GibcoTM

2.1.4 Culture media

Bacterial culture Media	
Medium	**Composition**
2xYT	31 g/l in de-ionized water
LB LB-Agar	25 g/l in de-ionized water 30.5 g/l in de-ionized water
SOC-Medium	2 % Trypton, 0,5 % yeast extract, 8,6 mM NaCl, 2,5 mM KCl, 20 mM MgSO4, 20 mM Glucose
Eukaryotic cell culture media	
Medium	**Composition**
Complete DMEM	DMEM medium 2 mM L-Glutamine 1 mM Sodium pyruvate 10 mM HEPES 1x NEM (non-essential amino acids) 5 % FCS

2.1.5 Buffers

Buffer	Composition
Buffers for ELISA:	
Coating buffer (ELISA)	0,1 M NaHCO3, pH 8,8
Blocking solution	5% BSA in PBS
Dilution Buffer	1 % BSA in PBS
Washing Buffer	0,05 % Tween-20 in PBS
Stop Solution	1 M H2SO4
Bacterial cell lysis buffer	
TS lysis buffer	30 mM Tris-HCl, pH 8, 20% Saccharose, 500 mM AEBSF, 1% Lysozym in de-ionized water
Buffers for SDS-PAGE	
NuPAGE Sample Reducing Agent (10x)	500 mM Dithiothreitol (DTT)
NuPAGE LDS Sample Buffer (4x)	Lithiumdodecylsulfat (pH 8,4)

MES Running Buffer	50 mM MES, 50 mM TrisBase, 1 % SDS, 1 mM EDTA (pH 7,3)
Buffers for affinity chromatography for protein purification	
IgG Elution Buffer (Protein A/G)	Thermo Fisher Scientific (pH 2,8)
Neutralisationspuffer (Protein A/G)	1 M Tris-Hcl (pH 9)
Washing buffer	PBS (1X)
Buffer for Agarose gel electrophoresis	
TAE gel running buffer	1x TAE buffer (thermofischer) in de-ionized buffer
Sample preparation buffer	1x DNA loading dye (Fermentes)

2.1.6 Antibiotics

Antibiotic	Concentration
Carbenicilin (stock solution)	100 mg/ml
Kanamycin (stock solution)	100 mg/ml

2.1.7 Antibodies

Specificity	Host	Clone	Manufacturer
Anti-c-myc tag	mouse	9E10	Nolte Group
anti-c-Myc-HRP	rabbit	polyclonal	Sigma-Aldrich/Merck
Anti-rabbit IgG-HRP	Donkey	polyclonal	GE Healthcare

2.1.8 Kits

Kit	Manufacturer
BCA Protein Assay Reagent	Pierce
EZ-Link Sulfo-NHS-Biotin	Thermo Scientific™
Plasmid preparation QIAprep Spin Miniprep Kit	QIAGEN, Hilden
Plasmid preparation QIAprep Spin Maxiprep Kit	QIAGEN, Hilden

2.1.9 DNA and protein standards

Type of standard	Manufacturer
DNA	
GeneRuler 1 Kb DNA ladder	Thermo Fisher Scientific
Protein	
Supermark	75 µg/ml IgG, 100 µg/ml BSA, 10 µg/ml Lysozym
Precision Plus Protein	Bio-Rad

2.1.10 Restriction Enzymes

Polymerases	**Manufacturer**
KOD Hot Start Polymerase	Novagen
Enzymes	**Manufacturer**
T4 DNA Ligase	NEB
NotI-HF	NEB
NcoI	NEB
SfiI	NEB
XbaI	NEB

2.1.11 Plasmid

Vector name	**Manufacturer**
pHEN2 (see appendix 6.1)	Institut Leloir, Buenos Aires (Argentinien)
pCSE2.5_rb-Fc IgG (see appendix 6.1)	Provided by Prof. Thomas Schirrmann, Braunschweig
pCSE2.5_HISmyc (see appendix 6.1)	Nolte Group

2.1.12 Proteins

Recombinant toxins from *C. difficile*

Bacterial toxins of *C. difficile* used during this study; **TcdB full length** 1–2366 (GTD, CPD, DD, RBD), **TcdB 1–807 (**GTD, CPD), **CDTa full length, CDTb full length,** were provided by the group of Prof. Dr Klaus Aktories from the University Hospital Freiburg.

2.1.13 E. coli strains

Strain	**Genotype**	**Manufacturer**
TG1	[F´ traD36 proAB lacIq Z ΔM15] supE thi-1 Δ(lac-proAB) Δ(mcrB-hsdSM)5(rK– mK–)	Lucigen
HB2151	K12 D(lac-pro), ara, nalr, thi/F'[proAB, lacIq, lacZDM15	Amersham
XL10-Gold	endA1 glnV44 recA1 thi-1 gyrA96 relA1 lac Hte Δ (mcrA)183 Δ (mcrCB-hsdSMR-mrr)173 tetR F'[proAB lacIqZΔ M15 Tn10(TetR Amy CmR)]	Stratagene,
XL-1 Blue	recA1 endA1 gyrA96 thi-1 hsdR17 supE44 relA1 lac [F´ proAB lacIq ZΔM15 Tn10 (Tetr)]	Stratagene

2.1.14 Eucaryotic cell lines

Cell line	**Provider**
HEK293-6E	Provided by Dr. Yves Durocher, NRC Canada
HT-29: Human Colorectal Adenocarcinoma Cell Line (ATCC HTB-38)	Provided by Prof. Dr. Holger Kalthoff, Universität Kiel

2.2 Methods in molecular biology

2.2.1 Reverse transcription of RNA to cDNA

Total RNA was isolated from peripheral blood lymphocytes using the *innuPREP RNA Mini Kit* from *Analytik Jena* according to the manufacturer's instructions.

The isolated RNA was used to generate complementary DNA (cDNA) per reverse transcription. In a first step, isolated RNA was incubated with random hexamers and dNTPs as follows:

X µl RNA	1,5 µg Total RNA
3 µl	Random Hexamers (200 ng/µl)
1 µl	dNTPs (10mM)
to 15 µl	ddH_2O

Then, the reaction was incubated for 5 min at 65°C.

To check the quality of the RNA, 5 µl of the reaction was loaded on agarose gel. The rest of the reaction was used for cDNA synthesis using the M-MLV RT Reverse Transcriptase (Moloney Murine Leukemia Virus Reverse Transcriptase), which is an RNA-dependent DNA polymerase that can be used in cDNA synthesis with long messenger RNA templates (>5kb).

10µl	RNA/from previous reaction
4 µl	5x 1^{st} Strand Buffer
2 µl	DTT (0,1 M)
1 µl	M-MLV Reverse Transcriptase (200 U/µl)
to 20 µl	ddH_2O

Table. 2.2.1: Program for cDNA synthesis

Step	**Temperature**	**Duration**
Annealing	25 °C	10 min
cDNA-Synthesis	37 °C	50 min
Termination	70 °C	15 min

2.2.2 Polymerase chain reaction (PCR)

The polymerase chain reaction (PCR) is an in vitro DNA amplification technique. The amplification reaction includes target DNA, a DNA polymerase, two oligonucleotide primers, deoxynucleotide triphosphates (dNTPs), reaction buffer and magnesium. A PCR consists mainly of three steps. The first step is **Denaturation:** The reaction temperature is increased to 95 °C, permitting the disruption of the hydrogen bonds between complementary bases which transform all double stranded DNA into

single-stranded DNA (ssDNA). Second step is **Annealing:** The temperature is decreased to approximately 5°C below the melting temperature (T_m) of the primers (often 45–60°C) to promote primer binding to the template and the last step is **Elongation** where temperature is increased to (69-72°C) which is the optimum for DNA polymerase activity to allow the hybridized primers to synthetize the complementary strands. The aforementioned steps are performed in a cyclical manner, resulting in exponential amplification of the amplicon.

PCR reactions are used for amplification of DNA fragment, incorporation of restriction sites, DNA sequencing and genotyping. In this project, the following PCR reactions were performed.

- **First PCR Amplification of VHH and VH fragments from cDNA.**

2 µl	of cDNA
5 µl	dNTPs (2 mM)
5 µl	reaction buffer (10x)
1 µl	cVHH lead seq forward (see appendix 6.2).
1µl	cVHH CH2 rev (see appendix 6.2).
3 µl	$MgSO_4$ (25 mM)
1 µl	KOD-DNA-Polymerase
33 µl	H_2O
	Σ 50 µl

- **Nested PCR for the amplification of VHH fragments**

2 µl	Template
2 µl	dNTPs (2 mM)
2 µl	reaction buffer (10x)
1 µl	cVHH FR1 for (see appendix 6.2).
1 µl	cVHH FR4 rev (see appendix 6.2).
0.8 µl	$MgSO_4$ (25 mM)
0.5 µl	KOD-DNA-Polymerase
10,7 µl	H_2O
	Σ 20 µl

Table. 2.2.2: Program for the two PCR

Step	Temperature	Duration	Cycle
Intial denaturation	95°C	2min	1
Denaturation	95°C	30s	
Annealing	52°C	30s	30
Elongation	70°C	60s	
Final Elongation	70°C	7min	1

2.2.3 DNA sequencing

DNA sequencing was carried out by eurofins Genomics services. 15 µl of 50-100 ng/µl of plasmid DNA were mixed with 2 µl of 10 µM of respective primer in a total volume of 17 µl. The volume was adjusted with de-ionized water when required.

2.2.4 Agarose gel electrophoresis of DNA and RNA fragments

Using agarose gel electrophoresis, DNA/RNA fragments are separated according to their size, charge or conformation. Gels with 0.8% or 1% agarose were prepared using TAE buffer with 5 µl of Roti®-Gel stain. Samples were mixed with DNA loading buffer and loaded in the correspondent well. The electrophoresis was run at a voltage of 90-120 V for 40-60 minutes. DNA bands were visualized afterwards by UV-illuminator and photographed for documentation.

2.2.5 Extraction of DNA fragments from agarose gel

The extraction of DNA fragments from agarose gels was carried out with the QIAquick gel extraction kit (QIAGEN) following the manufacturer's protocol. DNA fragments were eluted with 15-50 µl of de-ionized water.

2.2.6 Restriction digestion of DNA

In a first step of DNA cloning, doubled-stranded DNA fragments were digested with respective restriction enzymes provided from New England Biolabs (NEB) in recommended temperature and buffers. Digestion was carried out in PCR cycler in 20 µl-50 µl reaction volumes and incubated from 3 to 16 hours. At the end, the enzymes were heat inactivated at 65°C for 10min.

2.2.7 Dephosphorylation of DNA fragments

In order to minimize the self-ligation of the vector backbone, plasmid vectors were dephosphorylated using the Antarctic Phosphatase from New England Biolabs. 1 µl of the enzyme and 3 µl of the 10x buffer were added directly to the digested plasmid reaction. The final volume was adjusted with de-ionized water to 30 µl. The reaction was incubated for 60 min at 37°C, followed by inactivation of the Antarctic Phosphatase at 65 °C for 20 minutes.

2.2.8 Ligation of DNA fragments

Ligation reactions were performed using the T4 ligase, which catalyzes the joining of two strands of DNA between the 5´-phosphate and the 3´-hydroxyl groups of adjacent nucleotides in a reaction volume of 20 µl. A molar ratio of 1:3 vector: insert was used for ligation. The reactions were incubated at 16°C during 16 hours followed by heat inactivation of the ligase for 10 min at 65°C.

2.2.9 Transformation of chemically competent bacteria

50 µl-100 µl of chemically competent bacteria strains (XL-1 Blue, XL10-Gold) were thawed and incubated with 5 µl of DNA-plasmid vector on ice for 30 min, then heat shocked in a water bath at 42°C for 30 seconds and put on ice for further 2 min. Pre-warmed SOC medium were added to the cell suspension and incubated for 1 hour at 37°C, 300 rpm in a heat block. Defined amount of the transformed bacteria was plated on LB agar plates containing respective antibiotics and incubated overnight at 37 °C.

2.2.10 Transformation of electro-competent bacteria

50 µl of electrocompetent TG1 bacteria cells (Lucigen) were thawed on ice for 30 min and incubated with 3 µl of desalted ligation reaction on ice for 30 min. The mixture was pipetted in a pre-cooled electroporation cuvette then pulsed with 1800 V for 4-5 ms (program EC1, MicroPulser, Biorad). 900 µl of SOC medium were added to the electoporated cells and incubated for 90 min at 37°C, 250 rpm. Defined amount of the electroporated bacteria was plated on LB agar plates containing antibiotics and incubated overnight at 37°C.

2.2.11 Preparation of plasmid DNA

Isolation of plasmid-DNA was performed using Qiaprep® Spin Miniprep for small scale or Maxiprep kits for large-scale production following the manufacturer's protocol. Generally, a single bacterial colony is inoculated in 5 ml or 100 ml of LB medium containing antibiotics and cultivated overnight at 37°C, 230 rpm.

2.2.12 Phage display technology

Phage display is a selection technique in which a peptide or protein is fused with a bacteriophage coat protein and displayed on the surface of a viron (Wu et al., 2016).

Screening of phage-displayed peptide libraries is an effective means of identifying peptides that can bind with high affinity to target molecules (**Fig. 2.2.1**).

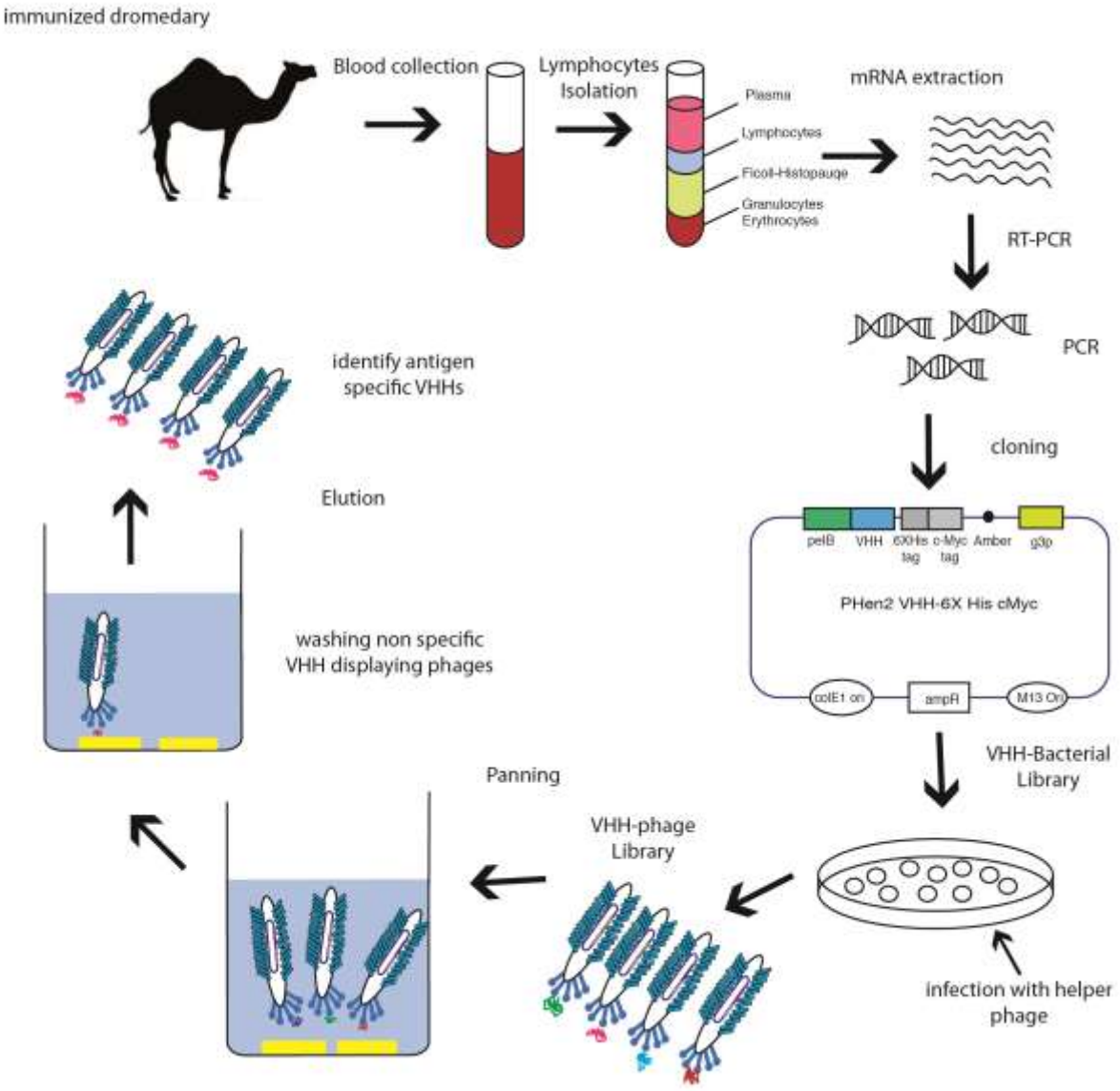

Figure 2.2.1 Schematic overview of phage display technology

The first step of a VHH phage library generation consists in isolating peripheral blood mononuclear cells (**PBMC)** by density centrifugation over Histopaque from blood samples collected from immunized dromedaries with TcdB (CPD-GTD) and CDTb. Second, total RNA was prepared from the PBMC and used as template for first strand cDNA synthesis by reverse transcriptase RT-PCR. VHH coding regions were amplified by PCR from cDNA using two-step PCR amplification strategy. The obtained PCR products corresponding to VHH fragments and the pHEN2 vector used for cloning were subjected to digestion with restriction endonucleases; SfiI for 16 hours and subsequently with NotI-HF for 3 hours. The purified digested vector and VHH inserts were ligated at 16°C overnight, and used for TG1 electroporation. The VHHs were cloned upstream of the phage coat protein M13 gIII gene. The phagemid vector pHEN2 contains a bacterial origin of replication as well as a wildtype M13 origin of replication (**Fig. 2.2.2**). Electroporated cells were plated on LB agar plates with

carbenicilin and glucose and incubated overnight at 37°C. To check the integrity of the generated bacterial libraries, plasmid-DNA obtained from 24 single colonies of each library were subjected to DNA sequence analyses using primers flanking the VHH insert. The remaining colonies were harvested and stored in 20% glycerol stocks at -80°C.

Figure 2.2.2 Schematic diagram of the M13 phage display phagemid vector pHEN2 used for VHH libraries cloning. The VHH coding regions are cloned downstream of an inducible bacterial promoter (Lac promoter) which induces protein expression in the presence of IPTG, (a non-metabolizable lactose analog), and in-frame behind a periplasm signal sequence (PelB). Downstream the VHH come the 6XHis and Myc Tags, which are used for affinity purification and for ELISAs and Western Blots. The tags coding regions are followed by amber stop codon, which is recognized as a translation termination site in some bacterial strains (e.g. HB2151) for the expression of VHH fragments and translated as pyrrolysine in other strains (TG1) for the display of VHH fragments as fusion proteins with phage. The amber stop codon is followed by the coding sequence of the M13 phage head capsid protein gIIIp.

2.2.13 Generation of VHH phage Library

To obtain the phage libraries, an aliquot of each glycerol stock of transformed bacteria was scooped (30 µl in total) in 10 ml 2xYT medium Carb-100 Glu-2% and cultured to exponential growth ($O.D._{600}$ 0.5-0.7), then super-infected with M13KO7 (10^{11} pfu/ml) helper phage from NEB at a multiplicity of infection index (MOI) of 10. The super infected culture was incubated at 37°C 150 rpm for 30 min, then centrifuged at 4000 rpm for 10 min, the pellet was resuspended in 50 ml 2xYT Carb-100 Kana-50 and cultivated for phage production for a maximum of 6 hours at 28°C, 250 rpm. Phages were subsequently precipitated from supernatants.

2.2.14 Phage precipitation

Helper-phage infected TG1 cells cultures were centrifuged at 4600 rpm for 10 min at 4°C. 40 ml of recuperated phage containing supernatants were transferred into 50 ml Falcon tubes containing 8 ml of PEG/NaCl (20% PEG 8000 in 2.5 M NaCl), mixed thoroughly and incubated for 60 min at 4°C. Phages were pelleted by centrifugation at 4600 rpm for 10 min at 4°C. The pellet was resuspended in 1 ml PBS and transferred to a 1.5 ml Eppendorf tube and centrifuged at 14000 rpm for 1 min to remove residual components.

Supernatant was transferred to a chilled 1.5 ml Eppendorf tube containing 250 µl PEG/NaCl for a second phage precipitation step. After incubating on ice for 60 min, precipitated phages were pelleted by centrifugation at 14000 rpm for 10 min at 4°C and resuspended in 1 ml PBS. To remove non-soluble debris, phages in PBS were centrifuged at 14000 rpm for 4 min. Phage-containing supernatant

was transferred to a fresh 1.5 ml Eppendorf tube. The centrifugation and transfer step (14000 rpm, 4 min) were repeated until no further debris pellet was observed. Soluble phages in PBS were stored at 4°C.

2.2.15 Biopannig of phage libraries

Biopanning is an affinity selection-based strategy where phage libraries are screened for the enrichment of peptides that specifically bind to the target of interest (Aghebati-Maleki et al., 2016). In our study, the biopanning process was performed using polystyrene ELISA well surface. 100 ng of the antigen TcdB (GTD-CPD) or CDTb diluted in 100 µl volume of coating buffer (0.1M $NaHCO_3$ pH 8.8) were coated at 4°C overnight. Free binding sites were blocked with 5% milk-PBS solution, and then wells were washed with PBS. Phages which were pre incubated with blocking buffer (5%milk-PBS) for two hours at 4°C were added to the correspondent well and incubated further for two hours at 4°C. After incubation, the supernatant was discarded and the wells undergo washing step; 50 times with 0.05% Tween20-PBS and 50 times with PBS only. Bound phages were eluted by incubation with 120 µl trypsin for 15 min. Supernatant containing eluted phages were transferred to a fresh tube where 12 µl of AEBSF was added to inactivate the trypsin.

To amplify eluted phages, 120 µl of eluted phages were added to 2.5 ml of a logarithmically growing culture of TG1 culture at OD600 ≈ 0.5 and incubated for 30 min at 37°C 150 rpm. Infected TG1 culture was centrifuged at 4000 rpm for 10 min at 4°C and the pellet was resuspended in 500 µl 2xYT medium carb 100 and plated directly on large LB Agar Carb-100 plates and diluted 1:100 in small plates to be able to pick single colonies for sequencing. The plates were incubated at 30°C overnight. The following day, bacterial colonies were scrapped off from the large culture plates with 10 ml of 2xYT Carb-100 and incubated at room temperature for 10 min with rolling. Suspension were centrifuged at 4600 rpm for 10 min and stored in 1 ml 20% glycerol stock. Single colonies from dilution plates were picked and undergo plasmid extraction using mini prep preparation kit to check the sequence of the VHH isolated after one round of panning.

2.3 Methods in protein biochemistry

2.3.1 Periplasmic expression of the VHHs in E. coli HB2151

To express VHHs as secretory proteins with a C-terminal c-myc-His6x in E.coli HB2151 periplasm, single colonies of pHEN2 transformed bacteria were cultivated in 5ml 2xYT Carb medium overnight at 37°C and 240 rpm. 50 µl of the primary culture were inoculated in 20ml of 2xYT at 37°C and 240 rpm and cultivated until an OD between 0.3 to 0.5, then lactose analogue, Isopropyl-β-D-thiogalactopyranoside (IPTG, 1mM), was added and incubated for 4 hours at 37°C and 240 rpm. The presence of the pelB leader sequence in the pHEN2 vector allows the release of the recombinant VHHs into the periplasmic compartment of the bacteria. The culture was centrifuged for 10 min at 4000 rpm, the pellet was briefly dried and resusupended in 500 µl Lysis buffer and incubated for 1

hour on ice. After incubation, the lysates were centrifuged at 2000 rpm for 5 min. The pellet was then resuspended in 500 µl of MgCl (5mM) and incubated on ice for further 30 min to initiate the osmotic shock and facilitate the release of the expressed VHHs from the periplsamic compartment. The suspension was centrifuged and the harvested periplasmic lysate was checked for the expression of VHH by SDS-PAGE.

2.3.2 Reformatting of nanobodies into bivalent format

2.3.2.1 Expression of rabbit-Fc VHH constructs

The rabbit-Fc fused VHHs were obtained by using the eucaryotic expression vector (pCSE2.5) that already contained the coding region for the 'hinge-CH2-CH3' region of rabbit IgG. The VHH inserts were subcloned into pCSE2.5 using NcoI and NotI restriction endonucleases.

2.3.2.2 Expression of monomeric and dimeric mouse IgA VHHs

Mouse IgA and J chain sequences were ordered as gene blocks (Integrated DNA Technologies,IDT), codon optimized for expression in human eukaryotic cells and flanked by appropriate restriction sites for sub-cloning into expression vector pCSE2.5. First, the rabbit Hinge-CH2 and CH3 domains were removed from pCSE2.5 vector and replaced by mouse Hinge-CH2-CH3 domains of IgA using NotI and XbaI restriction endonucleases. Then VHHs were subcloned into the new generated pCSE 2.5 _mIgA backbone vectors using NcoI and NotI restriction endonucleases. The J chain was cloned into another eukaryotic vector upstream c-myc-His6x in a pCSE2.5 c-myc-His6x. The dimeric format of IgA nanobodies was obtained after co-transfection of HEK293 6E with both VHH mIgA and J chain constructs (see Result 3.1.4).

2.3.3 Immobilized affinity chromatography using protein G and A

Reformatted VHHs into rabbit-Fc antibodies were purified from transfected HEK293 culture supernatants using affinity chromatography via the affinity of the Fc domain of heavy chain antibodies toward protein G. Supernatants of transfected HEK cell cultures were harvested and centrifuged at 4600 rpm for 10 min, then loaded on a column with 2 ml of protein G Sepharose 4 Load Fast Flow (GE Healthcare). Columns were washed with 20 ml of PBS and eluted with elution buffer in three fractions (eluate 1: 1.2 ml, eluate 2 and 3: 2.5 ml). Each fraction was collected and neutralized in neutralization buffer. The second and the third fraction of eluted proteins were loaded in PD-10 desalting columns (GE Healthcare) to desalt and change storage buffer to PBS, then protein fractions were concentrated using Amicon Ultra Centrifugal filter columns (Millipore) with suitable molecular weight cut-off. Purified heavy chain antibodies were stored at 4°C. Reformatted VHHs into monomeric and dimeric mouse IgA-Fc were purified using the affinity of certain amino acids present in the sequences of VHHs toward protein A. The purification procedure of IgA VHHs from HEK cell supernatants was similar to the above method but using protein A 4 Fast Flow (GE Healthcare).

2.3.4 Sodium dodecyl sulfate polyacrylamide gel electrophoresis (SDS-PAGE)

SDS-PAGE (sodium dodecyl sulphate-polyacrylamide gel electrophoresis) is an electrophoresis method by which proteins are separated based on their molecular weight.

Protein analysis by SDS-PAGE was carried out with SDS-PAGE NuPAGE® Bis-Tris precast Gels (Invitrogen). For the reducing SDS-PAGE, the proteins were mixed with the LDS sample buffer (4x) and the reducing agent (10x) (Invitrogen) and incubated at 70°C for 10 minutes. The gel electrophoresis was performed with MES buffer at a voltage of 200 V for 40-45 minutes.

The visualization of proteins in SDS-PAGE gels was performed by coomassie blue staining. The gel was stained for at least 3 hours at room temperature with the Coomassie blue staining solution from the Colloidal Blue Staining Kit (Invitrogen).

Non-specific staining of the gel was removed by washing the gel in de-ionized water. Distained gels were soaked in Novex® Gel-Dry drying solution for 5 minutes and mounted in a frame, between two transparent cellophane films to dry.

2.3.5 Quantification of proteins

Protein quantification was carried out using the BCA protein assay kit from Pierce; the unknown protein concentrations were determined through a BSA standard titration curve. Absorbance was measured at a wavelength of 562 nm with a photometer.

2.3.6 Biotinylation of the antibodies

Biotin labeling of the heavy chain antibodies was carried out using the Thermo Scientific EZ-Link Sulfo-NHS-LC-Biotin kit according to the manufacturer's instructions.

NHS-activated biotins react efficiently with primary amino groups (-NH2) of antibodies to form stable amide bond.

2.4 Methods in cell biology

2.4.1 Cell culture of human embryonic kidney cells (HEK293-6E cells)

HEK293-6E cells cultures were cultivated in complete DMEM medium with 10% FCS in cell culture flasks in a steam-saturated incubator maintained at 37°C and 5% CO2. Adherent HEK-293 cells were splitted, sub-cultured (1:5 – 1:10) every 2–3 days and transferred into new flasks after been washed with PBS and detached with Trypsin.

2.4.2 Cell count using a Neubauer chamber

Cell counting was performed using the Neubauer counting chamber (Laboroptik). First, cells were diluted in trypan blue solution to distinguish dead cells from live cells, then live cells were counted in the major quadrants under microscope. The cell number per ml is calculated according to the following equation: mean of the cell number in major quadrants x10000 x dilution factor.

2.4.3 Transfection of eukaryotic cells

HEK293-6E cells were transfected with pCSE2.5 vector containing VHHs using transfection reagent jetPEI (Polyplus, Illkirch, France) following the manufacturer's protocol. The cells were cultivated at cell incubator at 37°C for 5 days. Then, the supernatants were harvested and centrifuged at 4000 rpm for 10 min. VHHs fused to rabbit-Fc or to mouse IgA-Fc in monomeric and dimeric formats were purified by affinity chromatography using protein G and A.

2.4.4 Cytotoxicity assay

HT29 human colon carcinoma cells (25.000 cells/well) were seeded and cultured on glass-bottom 96 well microtiter plates to subconfluency. Constant amount of CDTa and CDTb for CDT cytotoxicity assay experiment and TcdB (full length toxin) for TcdB cytotoxicity assay were preincubated for 60 min at 37°C with or without nanobodies before addition to HT29 cells. Cells were subsequently incubated for 4 h to 22 hours at cell incubator at 37°C.

After incubation, in TcdB cytotoxicity assay, cell morphology was observed and documented by differential interference contrast microscopy using a Zeiss Axiovert 200M, whereas, in CDT cytotoxicity assay, cells were gently washed with PBS, and fixed in 4% paraformaldehyde. Fixed cells were counterstained with rhodamine-phalloidin (1:3500) (Abcam), which binds with high affinity to F-actin, and Hoechst 33342 (1:3000) (Molecular Probes, Life Technologies, Carlsbad, CA), and analyzed by Zeiss Axiovert 200M microscope equipped with an Apotome (Zeiss, Oberkochen, Germany).

2.5 Immunological Methods

2.5.1 Enzyme linked immunosorbent assay (ELISA)

CDTb and TcdB (CPD-GTD) antigens (100ng /well) were coated in a 96-well Nunc Maxisorp plates in $NaHCO_3$, pH 8.8 overnight at 4°C. Wells were blocked with 5% BSA-PBS at room temperature for 2 hours. Subsequently, wells were washed with 0.05% Tween-20-PBS. VHHs from the periplasmic lysates (10 µl) or HEK cells supernatants (10 µl) diluted in 90 µl of 1% BSA-PBS were added to the correspondent well and incubated for 1 hour at room temperature. After incubation, the wells were washed four times with 0.05% Tween-20-PBS.

VHHs with c-Myc-tag were detected by incubation for 60 minutes at room temperature with a peroxidase-conjugated anti-c-myc secondary antibody developed in rabbit diluted 1:5000 in 1% BSA-PBS. Whereas, VHH-rabbit Fc fusion proteins were detected with anti-rabbit IgG HRP-linked diluted 1:5000 in 1% BSA-PBS. After six cycles of washing with 0.05% Tween-20-PBS and PBS, 100 µl of TMB substrate were added to the well and incubated until signal development. The reaction was stopped with 100 µl of 1 M sulfuric acid. The optical density at 450 nm was measured on an ELISA reader (Victor, Perkin-Elmer Waltham, USA).

In sandwich ELISA experiment, capture antibody (100ng /well) were coated in a 96-well Nunc Maxisorp plates using NaHCO3, pH 8.8 as a coating buffer overnight at 4 °C. Wells were blocked by adding 5% BSA-PBS and incubating for 2 hours at room temperature. Depending on the type of the experiment; toxin standards, spiked samples or infected mice stools, diluted in 1% BSA-PBS, were added to the wells and incubated at room temperature for 2 hours. After incubation, several washing cycles were performed with 0.05% Tween20-PBS and PBS. Next, biotinylated antibodies (100ng /well), used as a detector, were added and incubated for 1 hour at room temperature. Washing steps were repeated as previously mentioned and 100 µL of a 1/10,000 dilution of streptavidin-poly HRP (Pierce) were added and incubated 1 h at room temperature. At the end, 100 µl of TMB substrate were added and incubated in the wells until signal development. The reaction was stopped with 100 µl of 0.5 M sulfuric acid. The optical density at 450 nm was measured on an ELISA reader (Victor, Perkin-Elmer Waltham, USA).

2.5.2 Cross-blockade analyses

Recombinant CDTb or TcdB_GTD-CPD were coated in 96 well plates and wells were blocked with BSA as described above in 2.5.1. Wells were preincubated with excess nanobody rabbit-IgG hcAbs (10 µl of HEK-6E cell supernatants containing 0.2-2 µg hcAb) for 60 min at RT. Without washing, a second c-myc-tagged Nb precomplexed with peroxidase-conjugated anti-c-myc mAb 9E10 (45ng/well) in CDTb Cross-blockade ELISA and a biotinylated rabbit-IgG hcAb (50ng/well) in TcdB Cross-blockade ELISA was added and incubation was continued for 30 min at RT. Wells were washed and bound antibody was detected with TMB in CDTb Elisa and with HRP-conjugated streptavidin (1:1000 in 1%BSA-PBS) and TMB in TcdB ELISA as described above in 2.5.1

2.5.3 Detection of toxins in stool samples

Fecal extracts were prepared by resuspending feces in 4 volumes (weight/volume) in PBS containing 5% BSA and 1x protease inhibitor cocktail, EDTA-free (Halt, Thermofisher) for 2 h on ice with vortexing every 15 min (corresponding to ≈250 mg feces/ml PBS). Insoluble material was pelleted by centrifugation (20 min at 8000rpm). Supernatants were filtered by centrifugation through 0.2 µm filters. Cleared supernatants were diluted in PBS/BSA in a $\sqrt{10}$ dilution series. CDTb and TcdB were detected by sandwich ELISA as described above in 2.5.1.

2.6 *C.difficile* mouse model

C57BL/6J mice were pretreated with an antibiotic cocktail in the drinking water on day -6 to -3 prior to infection (kanamycin 0.4 mg/ml, gentamicin 0.035 mg/ml, colistin 850 U/ml, metronidazole 0.215 mg/ml and vancomycin 0.045 mg/ml). On day -1, 200 µg of clindamycin was injected intraperitoneally. On day 0, mice were infected, by gavage, with 10^6 CFU of *C. difficile* strain (ribotype 027). Mice were monitored every day for weight loss and signs of infection.

3. Results

The first section presents the selection production and reformatting of nanobodies directed against CDTb and TcdB, followed by two sections on their characterization and functionality-assessment, and a final section describing the establishment of a sandwich ELISA immunoassay using as capture and detector nanobody-based heavy chain antibodies.

3.1 Selection, production and reformatting of anti-CDTb and anti-TcdB nanobodies

3.1.1 Immunization strategy and cloning of anti-CDTb and anti-TcdB VHH repertoire

To isolate specific binders, immune dromedary libraries were constructed. Two dromedaries (*Camelus dromedarius*) Dr.1406 and Dr.1409 were immunized with recombinant TcdB (GTD-CPD) and CDTb (**Fig. 3.1**). Four and ten days after the last boost, 200 ml of peripheral blood were collected.

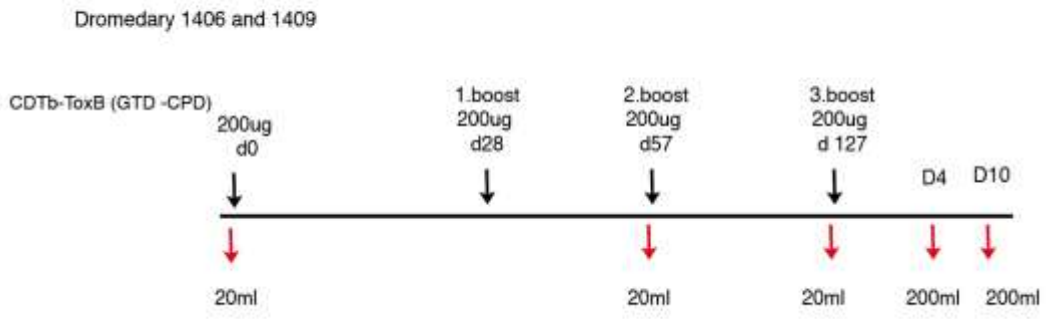

Figure 3.1. Immunization scheme of dromedaries (1406 and 1409) with recombinant TcdB (GTD-CPD) and CDTb. Two dromedaries were injected subcutaneously with a mixture of each TcdB (GTD-CPD) and CDTb in PBS mixed with Freund‘s adjuvant. The dromedaries received three more boost and were bled as indicated on the scheme by red arrows. Phage libraries were generated from lymphocytes purified on the fourth and tenth day (D4, D10) after the 3rd boost.

To generate VHH libraries, total RNA was prepared from peripheral blood mononuclear cells (PBMCs) of the immunized dromedaries and used as template for first strand cDNA synthesis by reverse transcription. The VHH coding region was amplified by PCR from cDNA using two amplification steps. In the first step a primer combination corresponding to the leader sequence (cVHH lead for) as a forward primer and the CH2 exon (cVHH CH2 rev) as a reverse primer. Two bands were obtained, corresponding to fragments derived from conventional IgG (1000 bp) and heavy chain antibodies (hcAbs) (700 bp)**.** The 700 bp fragments were purified and used as template for the second, nested PCR using primers corresponding to framework 1 (cVHH FR1 for) and framework 4 (cVHH Fr4 rev).

To generate VHH phage libraries, the PCR products were cloned into the pHEN2 vector. The purified PCR products and the pHEN2 vector were digested with SfiI for 16 hours and subsequently with NotI

for 3 hours. The digested vector and VHH inserts were gel purified and ligated at 16°C overnight. The ligation product was desalted and used for electroporation of TG1 electrocompetent cells. Plasmid DNA obtained from 12 colonies of each library was subjected to DNA sequence analyses using primers flanking the VHH insert. The results showed that 80-90 % of clones derived from dromedaries 1406 and 1409 contained coding sequences for intact VHHs (see **appendix 6.3**).

3.1.2 Generation of VHH-displaying phage libraries and selection of toxin-specific nanobodies

To obtain phage libraries, an aliquot of transformed bacteria was super-infected with M13KO7 helper phage. Libraries with phage titers of $9x10^{15}$ /ml were obtained. VHHs were selected by panning of the phage libraries on immobilized recombinant TcdB (GTD-CPD) and CDTb. Sequencing of selected clones revealed clones derived from several distinct VHH families (**Table 3.1**), with CDR3 lengths ranging from 8 to 22 amino acid residues. Most of the selected clones have a pair of cysteine residues in addition to those of the canonical disulfide bond between FR1 and FR3, consistent with an extra disulfide bond between CDR1 or FR2 and CDR3, a characteristic feature of many dromedary VHH domains.

Specificity	Dromedary	Family	Isolate	CDR3
CDTb	1409	+10	1	PNWRLESPCY
	1406	+18a	5	VPGSFASGGACYPDGHSY
	1409	+18b	1	VPGDFASGGACYPTGHTY
	1409/1406	+19.2	31	RNPRDLQNYGGACQGPFGY
	1406	-20	1	NSRQWVPAASRFLYETSYNN
	1406	+20.1a	4	GEYGGVCRDWMRGPPEDYTD
	1406	+20.1b	1	GQYGGVCRDWMRGPPEGYTD
	1406	+20.2	1	TLAGSGGACYSPLDQYGQSY
TcdB	1406	-8	3	GSVWALGT
	1406	+11	2	GDGRFCRGDCY
	1409	+15	1	SEGVFCYLRTNAYNY
	1406	-16	5	RALGDIRRLQPVDWSL
	1406	+22	9	DRYDYCSDSWSDADLVEYGYNY

Table 3.1. **Characteristics of nanobodies selected on immobilized recombinant CDTb and TcdB (GTD-CPD).** Family names indicate the absence (-) or presence (+) of an extra disulfide bond connecting CDR1 or FR2 and CDR3, and the length of the CDR3 in numbers of amino acid residues. Isolates indicates the number of clones selected per family.

3.1.3 Production of recombinant nanobodies as epitope-tagged monomers and as bivalent rabbit-IgG1 heavy chain antibodies

To determine the binding specificity of the obtained nanobodies against CDTb and TcdB, I produced them as soluble proteins with a C-terminal chimeric His6x c-myc tag in *E. coli* HB2151 cells. Periplasma lysates were prepared 4 hours after induction of transcription with IPTG. Proteins in the lysates were size fractionated by SDS-PAGE and visualized by Coomassie staining. The results show prominent bands at 14–20 kDa corresponding to the predicted size of recombinant nanobodies (**Fig. 3.2**). However, levels of nanobodies in the *E. coli* periplasm varied considerably.

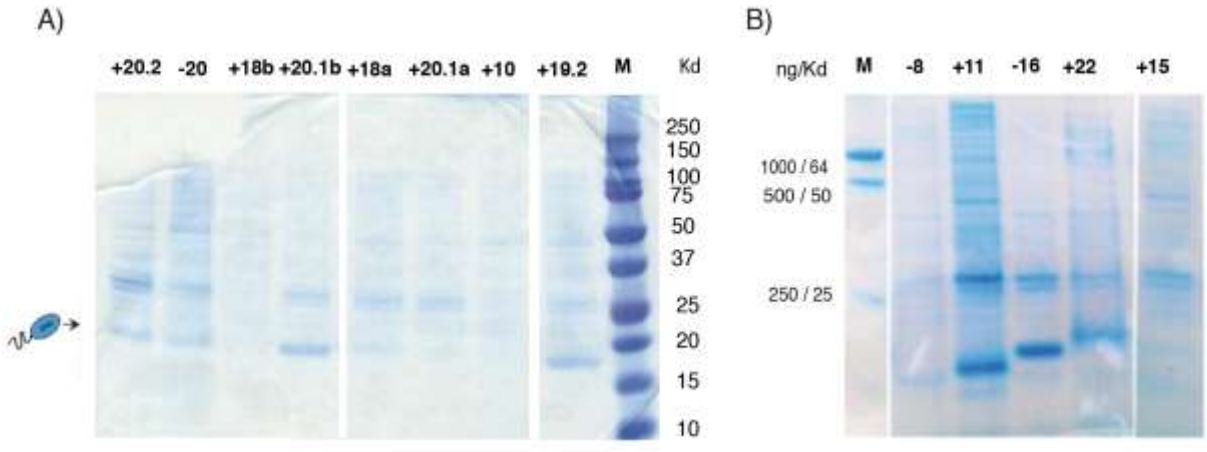

Figure 3.2. Production of monovalent VHHs in the periplasm of *E. coli* HB2151. Nanobodies selected by panning on CDTb **(A)** or TcdB (GTD-CPD) **(B)** were produced as monovalent secretory proteins in *E. coli* HB2151 periplasm. After transformation with VHH-encoding pHEN2 vectors, *E. coli* were cultured to an OD of 0.5 and expression of VHHs was induced by IPTG for 4 h at 37°C. Bacteria were harvested by centrifugation, resuspended in periplasma lysis buffer, incubated for 30 min on ice. Spheroblast were pelleted by centrifugation and supernatants (periplamsa lysates) were collected. A 10 µl aliquot of each lysate was analyzed by SDS-PAGE. Proteins were visualized by staining with Coomassie brilliant blue. M = marker proteins.

ELISA analyses were performed with crude periplasma lysates on immobilized CDTb or TcdB (GTD-CPD) using peroxidase-conjugated anti-c myc antibodies (**Fig. 3.3**). The results indicate that most of the selected VHHs bind specifically to their target toxin but not the control (BSA). The CDTb-specific VHHs +10, +20.1a, +18a showed a clear signal in the ELISA (**Fig. 3.3A)**, although no clear band was detectable by SDS-PAGE (**Fig. 3.2A)**, indicating the specificity of these selected VHHs. Similarly, TcdB-specific VHHs -8 and +15 were not strongly produced in the bacteria lysates (**Fig. 3.2B)**, but showed a clear signal by ELISA (**Fig. 3.3B)**.

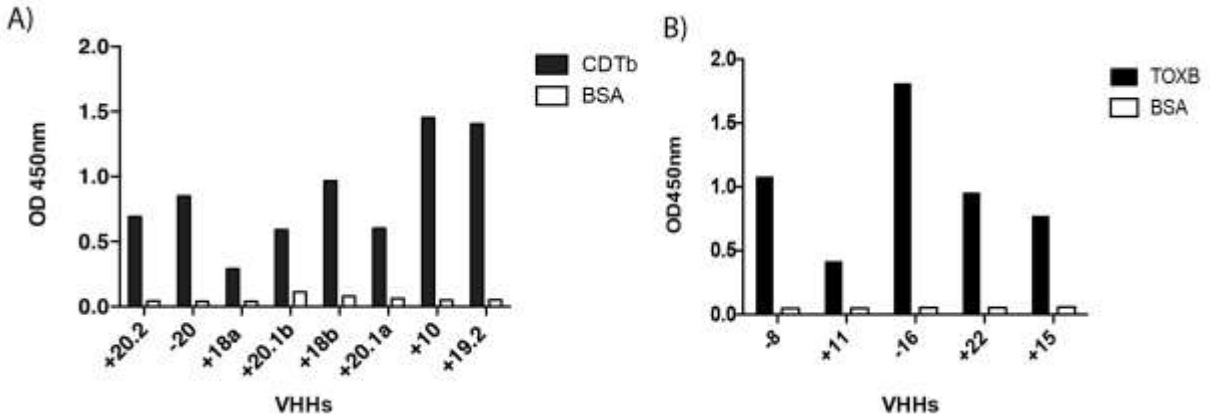

Figure 3.3. Analysis of binding specificity of the epitope-tagged nanobodies by ELISA. Wells of a 96-microtiter plate were coated overnight at 4˚C with recombinant CDTb **(A)** or TcdB (GTD-CPD) **(B)** or BSA as a control (100ng /well). Free binding sites were blocked for 2 h with 5% BSA in PBS. VHH-containing periplasma lysates were diluted 1:10 in 1% BSA-PBS, and added to the wells for 1 h at RT. Wells were washed four times with PBS-Tween 20 (0.005%), bound VHHs were detected with peroxidase conjugated rabbit anti-c-myc antibody (1:5000) and TMB substrate. Measurement was performed at 450 nM using an ELISA reader. The data points are from single measurements. The experiment was performed only once.

In order to improve their use for diagnostic and therapeutic applications, selected nanobodies were reformatted into bivalent rabbit IgG heavy chain antibodies (hcAbs). To this end, the VHH coding region was subcloned into a eukaryotic expression vector (pCSE2.5_rbFc) that already contained the coding region for the 'hinge-CH2-CH3' region of rabbit IgG. These constructs were used to transfect HEK293-6E cells. Supernatants containing the secreted nanobody-based hcAbs were harvested six days after transfection. SDS-PAGE analyses revealed distinct bands at the expected size of 50 Kd. By comparison to marker proteins, yields were estimated at 1-2 µg per 10 µl of cell supernatant (**Fig. 3.4)**. Heavy chain antibodies were purified by affinity chromatography using protein A or G.

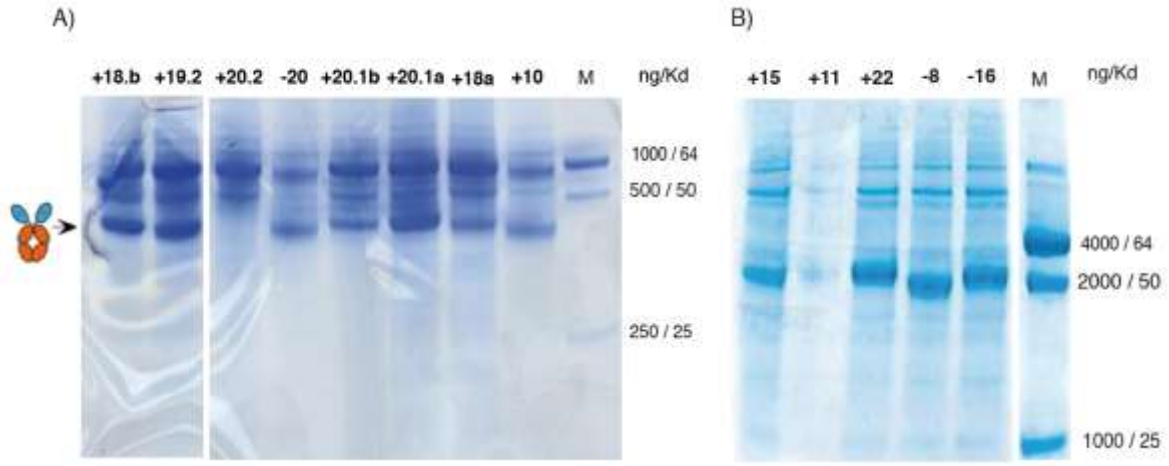

Figure 3.4. Production of CDTb and TcdB specific nanobody based heavy chain antibodies in HEK 6E cells. HEK-6E cells were transfected with cDNA-expression vectors encoding CDTb-specific **(A)** or TcdB-specific **(B)** VHHs fused to the hinge, CH2-CH3 domains of rabbit IgG. Transfected cells were cultured in serum free medium for 6 days. Proteins in cell supernatants (10 µl/well) were analyzed by SDS-PAGE and Coomassie staining.

The heavy chain antibodies in HEK cell supernatants were analyzed for specific binding to CDTb and TcdB by ELISA (**Fig. 3.5**). The results show high specific signals for all hcAbs. CDTb-specific hcAb +20.2, which was not well produced in HEK cells (**Fig. 3.4A)**, showed the weakest signal by ELISA (**Fig. 3.5A)**. This hcAb was reproduced later and then showed a strong specific signal (see **appendix 6.4**).

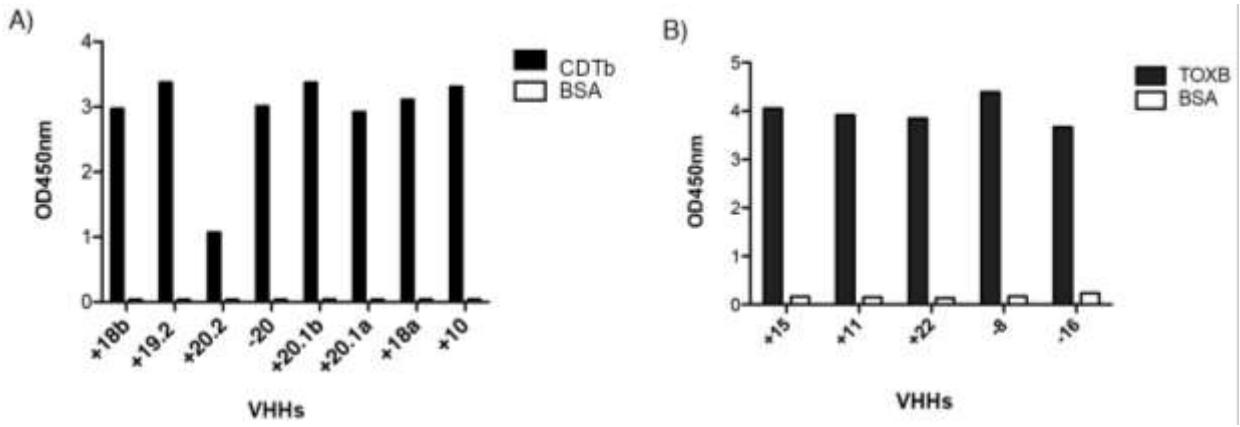

Figure 3.5. ELISA analysis of the binding specificities of CDTb- and TcdB-specific rabbit IgG heavy chain antibodies. CDTb **(A)** and TcdB (GTD-CPD) **(B)** (100ng/well) were immobilized on a 96-well microtiter plate at 4˚C overnight. Wells were blocked for 2 h with 5% BSA at RT, incubated for 60 min with HEK cell supernatants (diluted 1:10 in PBS/BSA) containing nanobody-based hcAbs. Bound antibodies were detected using peroxidase-conjugated rabbit IgG. The data points are from single measurements. The experiment was performed only once.

3.1.4 Reformatting VHHs into monomeric and dimeric IgA heavy chain antibodies

Since the *C.difficile* toxins target mainly the mucosal surface of the gastro-intestinal tract and the most abundant antibody class on mucosal surfaces is IgA, we decided to reformat CDTb-specific hcAbs +20.1a, +10, +18.a and -20 to monomeric/bivalent and dimeric/tetravalent IgA hcAbs. The sequences for the hinge, CH2 and CH3 domains of mouse IgA and for the J chain were codon optimized for expression in HEK cells (see **appendix 6.5**) and cloned into the pCSE2.5 vector. The VHH coding region was cloned upstream of the hinge. HEK293-6E cells were co-transfected with expression constructs for the mouse J chain and the nanobody-based IgA hcAbs in a 1:1 molar ratio. Transfected cells were cultured in serum free medium for 6 days. Proteins in supernatants were analyzed by SDS-PAGE under non-reducing conditions. The results reveal prominent bands at the expected size of ~100 and 200 kD for monomeric and dimeric IgA hcAbs, respectively (**Fig. 3.6A**). The reformatted hcAbs were purified by affinity chromatography using protein A and analyzed by SDS-PAGE and Coomassie staining. The results confirm high purity and yields (2-3 mg/ml) for both, monomeric and dimeric IgA hcAb formats (**Fig. 3.6B**).

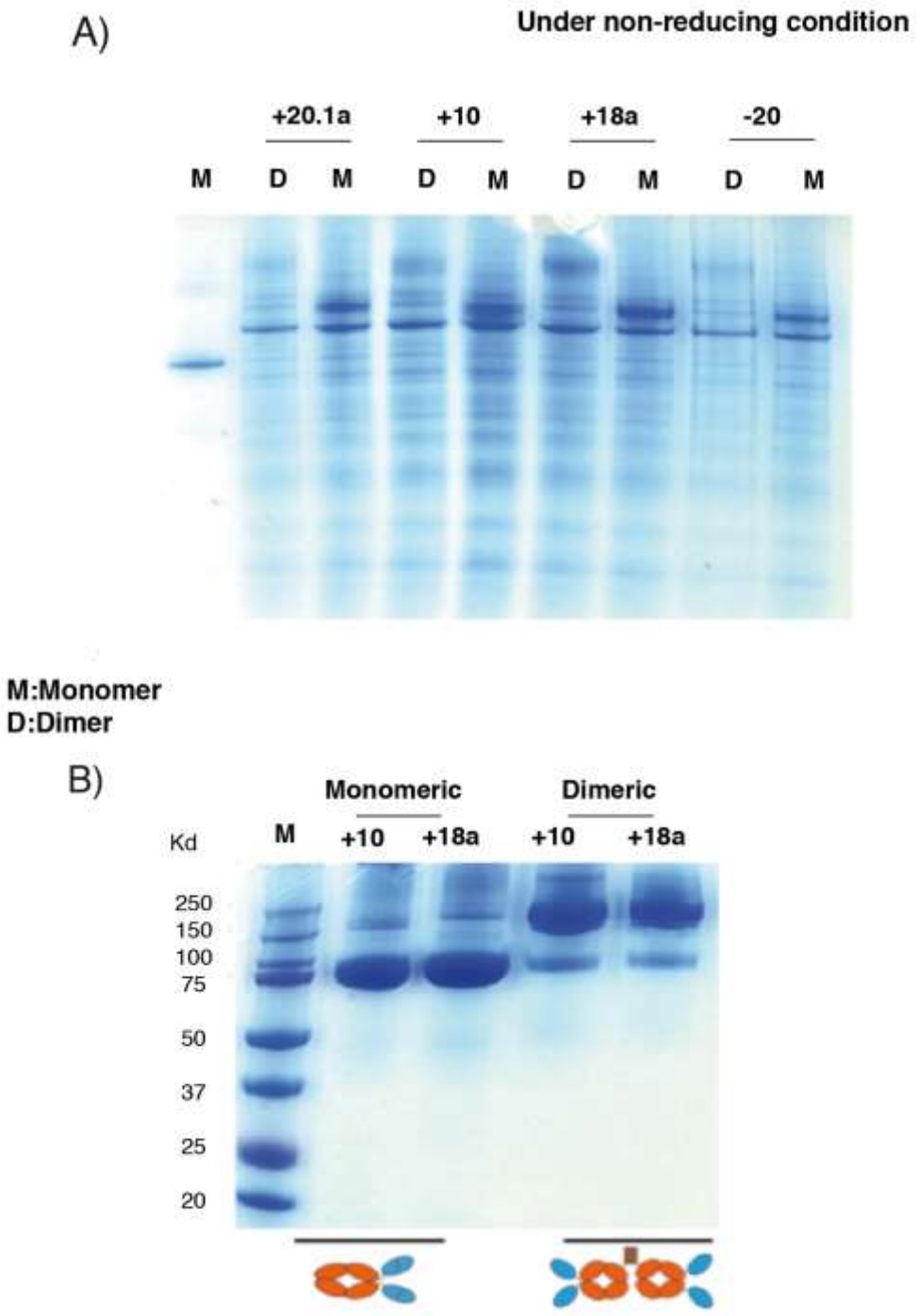

Figure 3.6. Production and purification of reformatted CDTb-sepcific nanobody-based IgA heavy chain antibodies. **A)** HEK293-6E cells were transfected with a cDNA-expression construct encoding nanobodies fused to the hinge, CH2 and CH3 domains of mouse IgA either alone (M) or in combination with an expression construct encoding the mouse J chain. Cells were cultured in serum free medium for 6 days and proteins in cell supernatants were analyzed by SDS-PAGE and Comassie staining. **B)** Nanobody-based hcAbs were purified from cell supernatants by affinity chromatography using protein A immobilized on sepharose beads. Purified proteins were analyzed by SDS-PAGE and Comassie staining.

3.2 Characterization of CDTb-specific nanobodies

3.2.1 Qualitative comparison of nanobody affinities

To estimate the affinities of selected nanobodies, an ELISA was performed using serial dilutions of bacterial lysates containing CDTb-specific monovalent c-myc-His 6x tagged nanobodies (**Fig. 3.7**). The detection was performed with a peroxidase-conjugated monoclonal antibody directed against the c-myc tag. The Kd of the tested nanobodies was estimated as the concentration of the half maximum of the signal. CDTb-specific VHHs +19.2, +10, -20, +20.2, +18a and +20.1b showed an estimated Kd of ~ 0.5nM. VHHs +18.b and +20.1a presented a higher dissociation constant (lower affinity) of > 10 nM (**Fig. 3.7**).

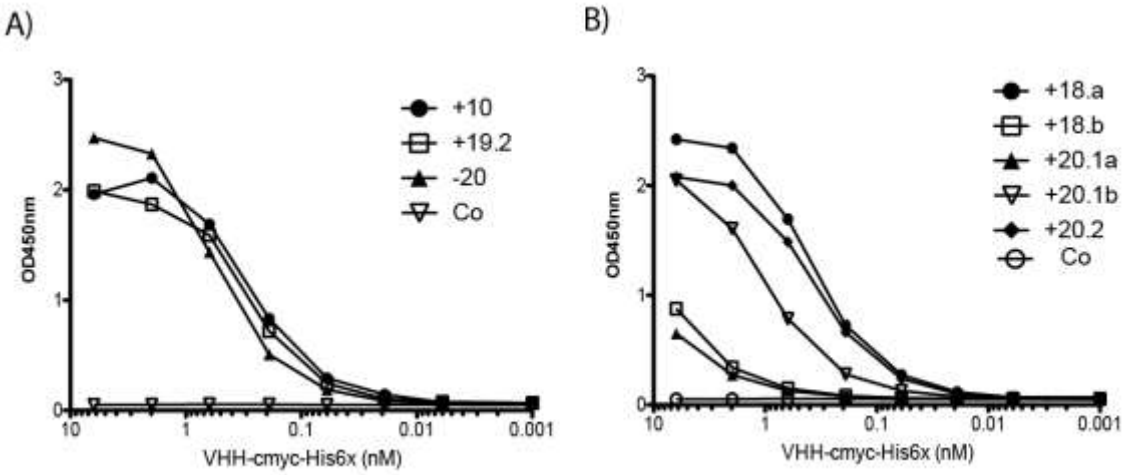

Figure 3.7. Comparative analyses of the dissociation constants of CDTb-specific nanobodies. CDTb was coated overnight at 4˚C onto a 96-microtiter plate (100ng/well). Free binding sites were blocked with 5% BSA-PBS at RT for 1 h. Wells were incubated with serial dilutions of c-myc-tagged VHHs for 1 h at RT. Bound antibodies were detected with peroxidase-conjugated monoclonal antibody 9E10 directed against the c-myc tag using TMB as substrate. The reaction was stopped by addition of the H_2SO_4 and absorbance was measured at 450 nM on an ELISA reader. A c-myc tagged nanobody directed against CD38 was used as control (Co). The data points are from single measurements. The experiment was performed only once.

3.2.2 Crossblockade analyses for epitope mapping of selected nanobodies

In order to assess whether the selected nanobodies recognize overlapping or distinct epitopes on CDTb, crossblockade analyses were performed. The experimental set up is illustrated schematically in **Figure 3.8A**. Monovalent c-myc nanobodies were converted to a bivalent format for detection by incubation for 30 min with peroxidase-conjugated anti-c-myc mAb 9E10. CDTb was immobilized on 96-well plates and pre-incubated with excess of a first nanobody-rabbit-IgG hcAb before addition of the preformed complexes of a second nanobody with PO-conjugated mAb 9E10. The results permit grouping of nanobodies according to their relative epitope specificities.

Nanobodies +10 and +19.2 block the binding of one another (**Fig 3.8 B, C**). Binding of these two

nanobodies is not blocked by any of the other six nanobodies, and they do not block binding of the other nanobodies (**Fig. 3.8 D-I**). Nb +19.2 evidently shares the same epitope with Nb +10 (epitope 1). Binding of VHH -20 was blocked only by itself (**Fig. 3.8D**) and did not block binding of any of the other nanobodies (**Fig 3.8 B-I**), suggesting that this nanobody binds a distinct epitope (epitope 2). Nanobodies of the same family, e.g. +20.1a and +20.1b, blocked binding of one other (**Fig. 3.8 E, F**) (epitope 3). Similarly, Nbs +18a and +18b blocked one another (**Fig. 3.8 G, H**) (epitope 4). Binding of Nb +20.2 was blocked by both, Nbs +18a and +18b (**Fig. 3.8I**), suggesting that this nanobody shares the same epitope with the VHH family +18 (epitope 4).

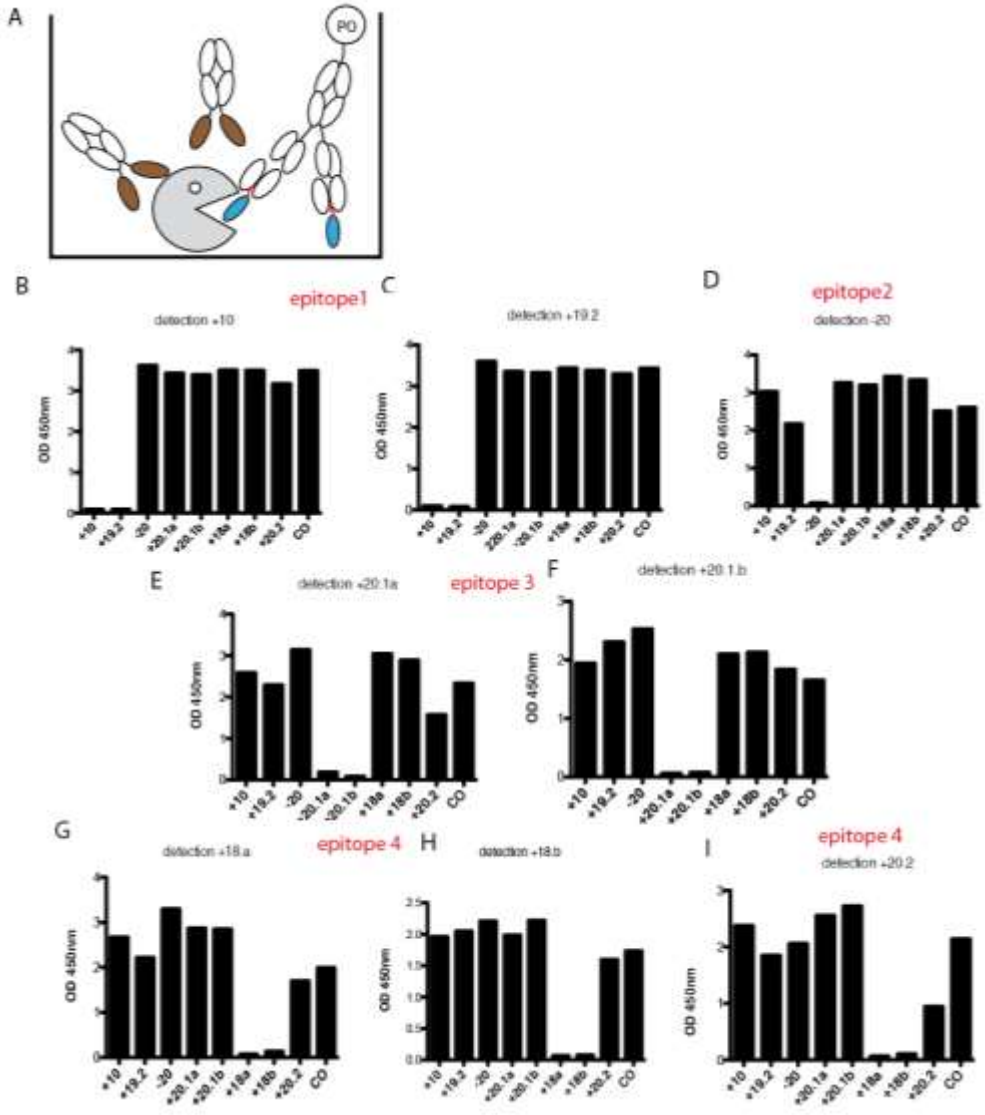

Figure 3.8. Epitope mapping of CDTb-specific nanobodies. CDTb (100ng/well) was coated on a 96 well-microtiter plate overnight at 4˚C. Free binding sites were blocked with 5% BSA-PBS for 2 h at RT. Excess of the first rabbit IgG hcAb (2 µg/well) was added to each well and incubated for 60 min before addition of the second c-myc-tagged Nb precomplexed with peroxidase-conjugated anti-c-myc mAb 9E10 (45ng/well) and further incubation for 30 min. Wells were washed and bound antibodies visualized with TMB as substrate. The data points are from single measurements. The experiment was performed only once.

3.2.3 Evaluation of the capacity of CDTb-specific VHH to neutralize CDT-mediated cytotoxicity

In order to monitor CDT-mediated disruption of the actin cytoskeleton, a phalloidin actin-staining assay was performed using human HT-29 colon carcinoma cells. Cells were cultured for two days to subconfluency. A mixture of the two subunits of the binary CDT toxin, CDTa and CDTb, were preincubated for 60 min at 37°C with a 12 molar excess of CDTb-specific rabbit IgG hcAbs before addition to cells and further incubation for 4 hours. Cells were fixed and counterstained with fluorescently labeled Rhodamin-phalloidin which binds to filamentous actin, but not to monomeric actin. While healthy cells show a bright red staining indicative of an intact cytoskeleton, cells treated with CDT toxin alone show only barely detectable fluorescence, indicating CDT-mediated disruption of filamentous actin (**Fig. 3.9).** The results of this assay indicate that CDTb-specific Nb +20.1a effectively protects HT29 cells from the cytotoxic effects of CDT; Nbs +10, -20 and +20.2 mediate partial protection and Nbs +19.2 and +18a only weak protection against CDT-mediated cytotoxicity (**Fig. 3.9**).

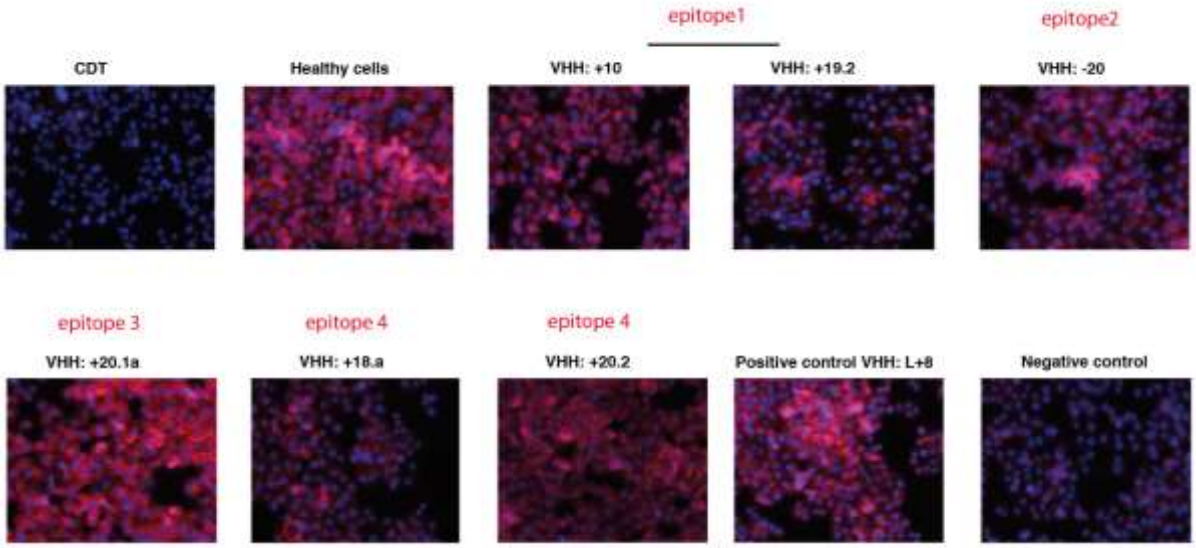

Figure 3.9. Capacity of CDTb-selected nanobodies to inhibit CDT-induced disruption of the actin cytoskeleton of HT29 cells. Adherent HT29 human colon carcinoma cells (25 000 cells/well) were cultured to subconfluency on a glass-bottom 96 well microtiter plate. CDTa (0.25nM) and CDTb (0.35nM) were pre-incubated in complete DMEM medium for 60 min at 37°C with 12 folds molar excess of CDTb-specific rabbit IgG hcAbs (4 nM) before addition to HT29 cells. After 4 h further incubation, cells were washed and fixed with 4% paraformaldehyde. The cellular cytoskeleton was stained with the F-actin-staining dye Rhodamin-Phalloidin, cell nuclei was stained with Hoechst 33342 for 15 min at RT. Cells were then analyzed by microscopy with a Zeiss Axiovert 200M microscope equipped with digital interference contrast and an apotome. A P2X7-specific rabbit IgG hcAb was used as negative control, the CDTa-sepcific VHH l+8 mouse IgG hcAb was used as positive control (Unger et al., 2015). Images shown are from single samples. The experiment was repeated twice with similar results.

3.3 Characterization of TcdB-specific nanobodies

3.3.1 Qualitative comparisons of nanobody affinities

To estimate the affinities of selected TcdB-specific nanobodies, an ELISA was performed using serial dilutions of HEK cell supernatants containing TcdB-specific rabbit-IgG hcAbs. The detection of bound antibodies was performed with a peroxidase-conjugated rabbit IgG-specific peroxidase-conjugated antibody. The Kd of the tested nanobodies was estimated as the concentration of the half maximum of the signal (**Fig. 3.10**). All VHHs showed Kds in the lower nM range, with VHHs -8 and -16 showing 2-5 fold lower Kds (higher affinities) than the three other VHHs (**Fig. 3.10**).

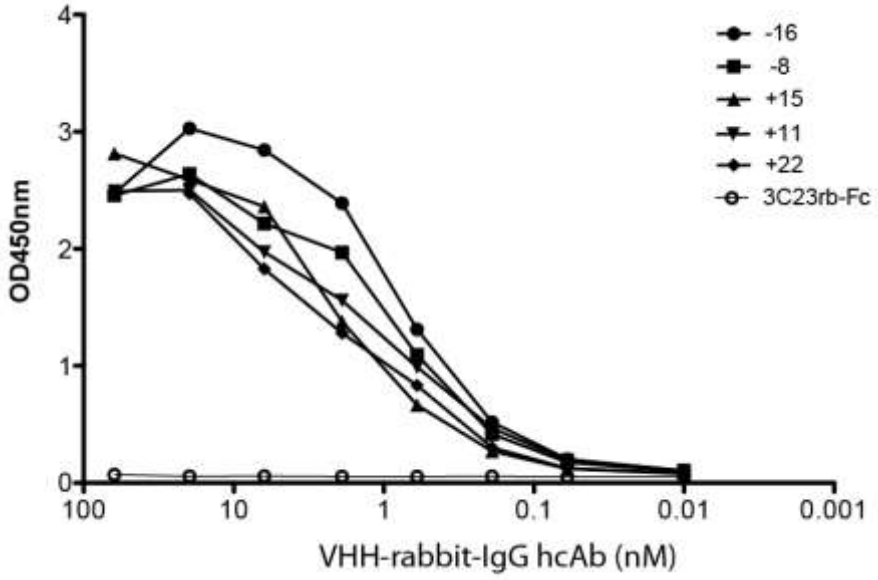

Figure 3.10. Comparative analyses of the dissociation constants of TcdB-specific heavy chain antibodies. Wells of a 96-well microtiter plate were coated overnight with TcdB_GTD-CPD (100ng/well) at 4˚C. Free binding sites were blocked with 5% of BSA-PBS at RT for 1 h. Wells were incubated with serial dilutions of VHH-rabbit-IgG hcAbs for 1 h at RT. Wells were washed four times with PBS-Tween 20 (0.05%) and PBS. Bound antibodies were detected with peroxidase-conjugated anti-rabbit IgG and with TMB as substrate. The reaction was stopped by addition of the H_2SO_4 and absorbance was measured at 450 nM on an ELISA reader. P2X7-specific VHH 3c23 rabbit-IgG hcAb was used as negative control. The data points are from single measurements. The experiment was repeated twice with similar results.

3.3.2 Crossblockade analyses for epitope mapping of selected nanobodies

In order to assess whether the selected nanobodies recognize overlapping or distinct epitopes on TcdB, crossblockade analyses were performed. The experimental set up is illustrated in **Figure 3.8A**. Recombinant TcdB (GTD-CPD) was immobilized on 96 well plates and preincubated with excess nanobody rabbit-IgG hcAbs for 30 min. Without washing, a second biotinylated rabbit-IgG hcAb was added and incubation continued for 30 min. Wells were washed and bound biotinylated hcAbs were detected with peroxidase-conjugated streptavidin (**Fig. 3.11A**). The results show that VHH +11 recognizes the same or an overlapping epitope with -8 (epitope 1) (**Fig. 3.11 B, C**). However, the binding of VHH +15 is blocked only by preincubation with VHH +15, but not with any of the other

VHHs (**Fig. 3.11D**). Moreover, VHH+15 does not inhibit binding of any of the other VHH-hcAbs (**Fig. 3.11, B-F**), indicating that VHH+15 binds to TcdB independently to the other four VHHs (epitope 2). VHH +22 recognizes the same or an overlapping epitope with VHH -16 (epitope 3) (**Fig 3.11 E, F**). Interestingly, precinbuation with VHH -8 inhibits binding of VHH +22 (**Fig. 3.11 F**) but binding of VHH +22 does not seem to impede binding of VHH -8 (**Fig. 3.11B**).

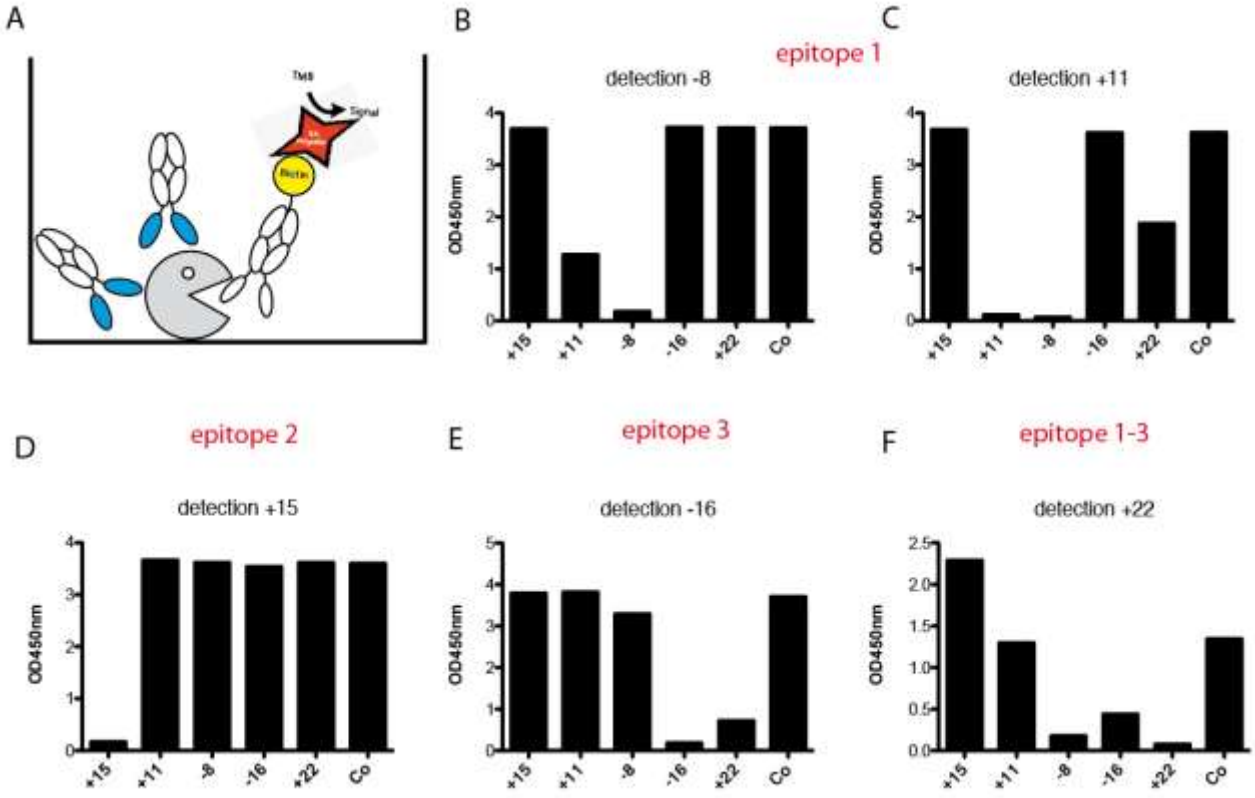

Figure 3.11. Epitope mapping of TcdB-specific nanobodies. TcdB_GTD-CPD (100ng/well) was immobilized overnight at 4˚C on 96-well microtiter plates. Free binding sites were blocked with 5% BSA and wells were pre-incubated with excess of a nanobody-rabbit-IgG hcAb (2 µg/well) for 60 min at RT (indicated on the bottom of each panel). Then a second, biotinylated nanobody-rabbit-IgG hcAb (50 ng/ well) was added (indicated on the top of each panel) and samples were further incubated for 30 min at RT. Wells were washed six times with PBS-Tween 20 (0.05%) and PBS. Bound antibodies were detected with peroxidase-conjugated Streptavidin and TMB as substrate. A P2X7-specific VHH-hcAb was used as negative control (Co). The data points are from single measurements. The experiment was performed once.

3.3.3 TcdB-specific VHHs do not neutralize ToxB, even at at very high mola ratios

In order to assess the ability of selected VHHs to neutralize ToxB, a microscopic assay of ToxB-induced rounding of HT-29 human colorectal carcinoma cells was performed. A sublethal dose of full length TcdB toxin (0.74 pM) was incubated with a 10.000 fold molar excess of TcdB-specific VHHs for 60 min at 37˚C before addition to HT-29 cells. The morphological changes of the cells were monitored by differential interference contrast microscopy after 4 hours and 22 hours (**Fig. 3.12**). The results show that incubation with ToxB alone resulted in extensive rounding of cells. Addition of TcdB-specifc VHHs did not significantly improve cell vitality compared to the control VHH (**Fig.**

3.12). This assay was repeated with titrated VHH concentrations, but none of the five TcdB-specific VHHs was able to neutralize the cytopathic effect of TcdB (not shown).

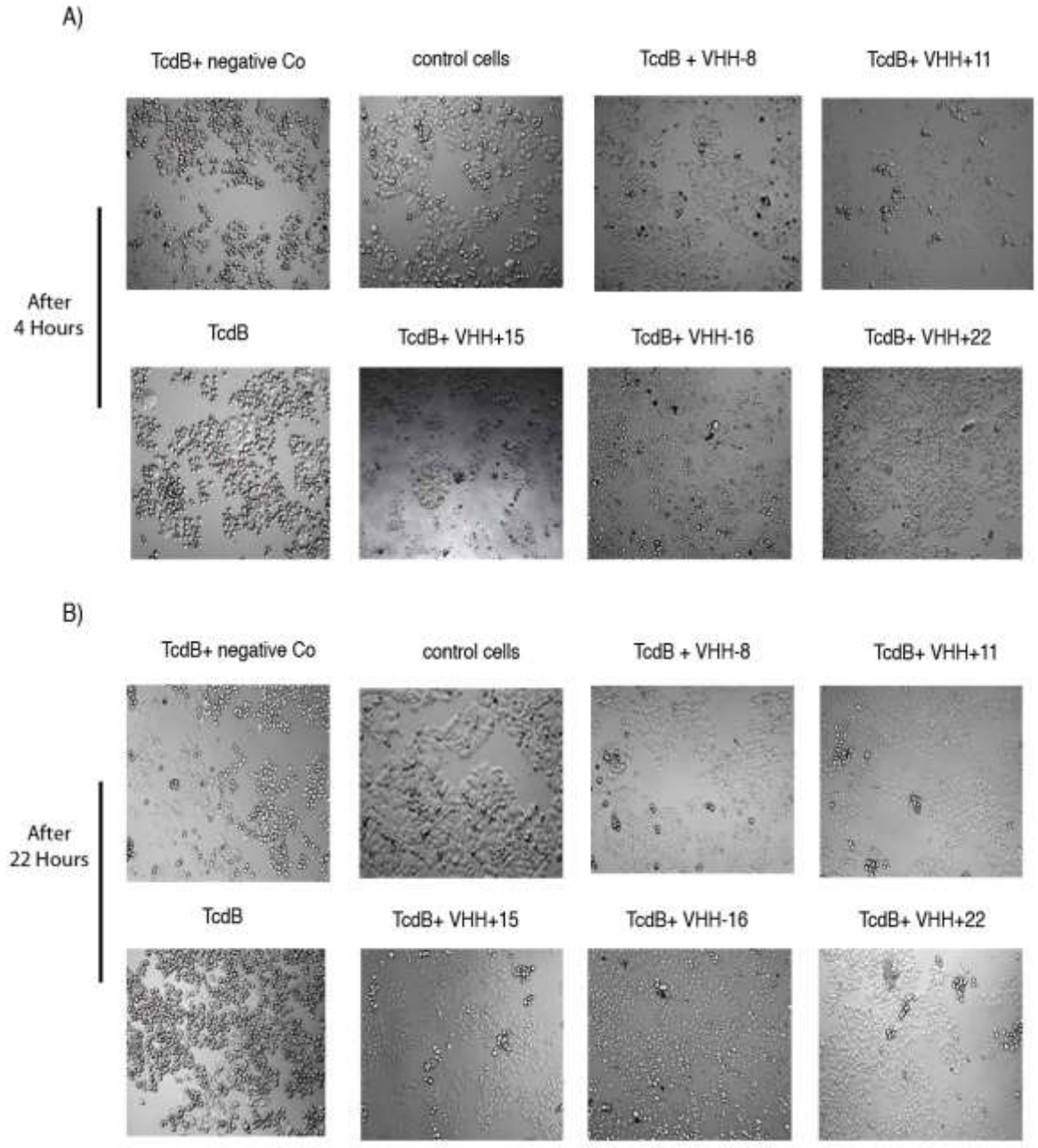

Figure 3.12. Neutralization assay of TcdB selected nanobodies. Adherent HT29 human colon carcinoma cells were cultured to subconfluency on glass-bottom 96 well microtiter plates. ToxB full length protein 40 pg/100 µl (0.74pM) was preincubated for 60 min without (-Nb) or with a 10.000 fold molar excess of the indicated TcdB-specific nanobodies (100ng/100 µl) (6 nM) before addition to adherent HT29 cells. Cells were further incubated at 37°C for 4 h (A) or 22 h (B) and then analyzed for rounding by microscopy with a Zeiss Axiovert 200M microscope. P2X7-specific nanobody was used as negative control (Co). Control cells were incubated without ToxB. Images shown are from single samples. The experiment was repeated twice with similar results.

3.4 Evaluation of the diagnostic potential of CDT-specific nanobodies

3.4.1 Selecting pairs of hcAbs for detecting CDTb and TcdB by sandwich ELISA

To establish a sensitive sandwich ELISA system, pairs of hcAbs binding to non-overlapping epitopes (as determined by cross-blockade analyses in **Fig. 3.8** and **Fig 3.11**) were screened for their capacity to detect CDTb and TcdB in a sandwich ELISA. **Figure 3.13** shows a schematic diagram of the assay in which an unconjugated hcAb was used as a capture and a second, biotinylated hcAb as a detector **(Fig. 3.13)**. A total of 17 pairwise combinations were evaluated for the detection of recombinant CDTb (**Fig. 3.14A**) and 6 pairwise combinations for the detection of TcdB (**Fig. 3.14.B**). The results show that most of the analyzed pairs of hcAbs were able to detect recombinant CDTb **(Fig. 3.14A)** and TcdB (GTD-CPD) **(Fig. 3.14B)**. Based on the strength of their signal, five pairs of CDTb-specific hcAbs (catcher/detector: +20.2 e4/+19.2 e1, +10 e1/-20 e2, -20 e2/+20.1b e3, -20 e2/+20.2 e4, +20.1b e3/+20.2 e4) and three pairs of TcdB-specific hcAbs (-8 e1/+15 e2, -8 e1/-16 e3, -16 e3/+15 e2), marked with an asterisk in **Figure. 3.14A-B,** were chosen for the next experiments.

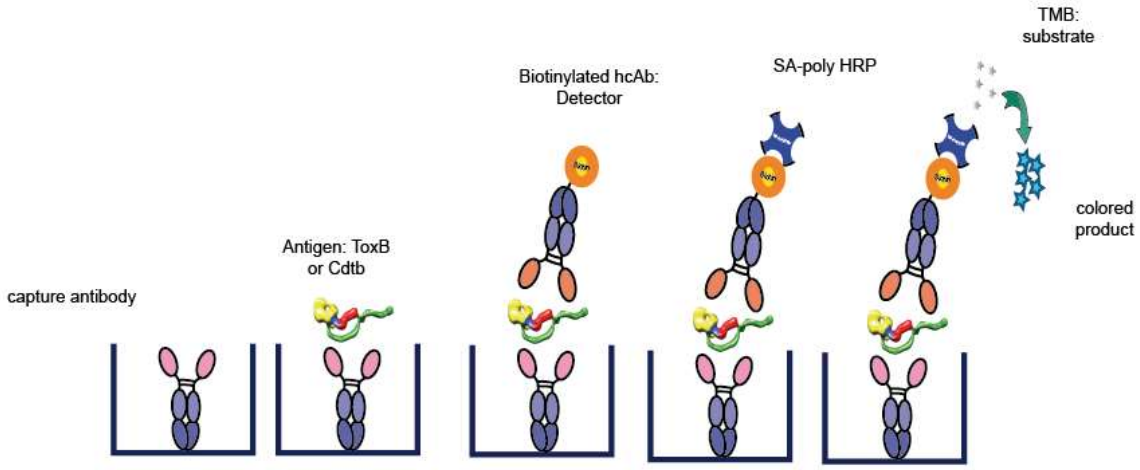

Figure 3.13. Schematic diagram of the sandwich ELISA for detecting CDT and TcdB. The assay uses a classic sandwich ELISA system with a pair of hcAbs that bind to non-overlapping epitopes on the toxin. An unconjugated hcAb is used as a capture and a second biotin labeled hcAb as a detector. The catcher antibody is coated overnight in a 96-well microtiter plate, free binding sites are blocked using BSA, and toxin-containing samples are added to the coated wells for 2 hours at room temperature. Bound toxins are detected by sequential incubation with the second biotinylated hcAb, poly-HRP-conjugated streptavidin and TMB as substrate. The reaction is stopped with H_2SO_4 and product is detected with a plate reader at 450nM.

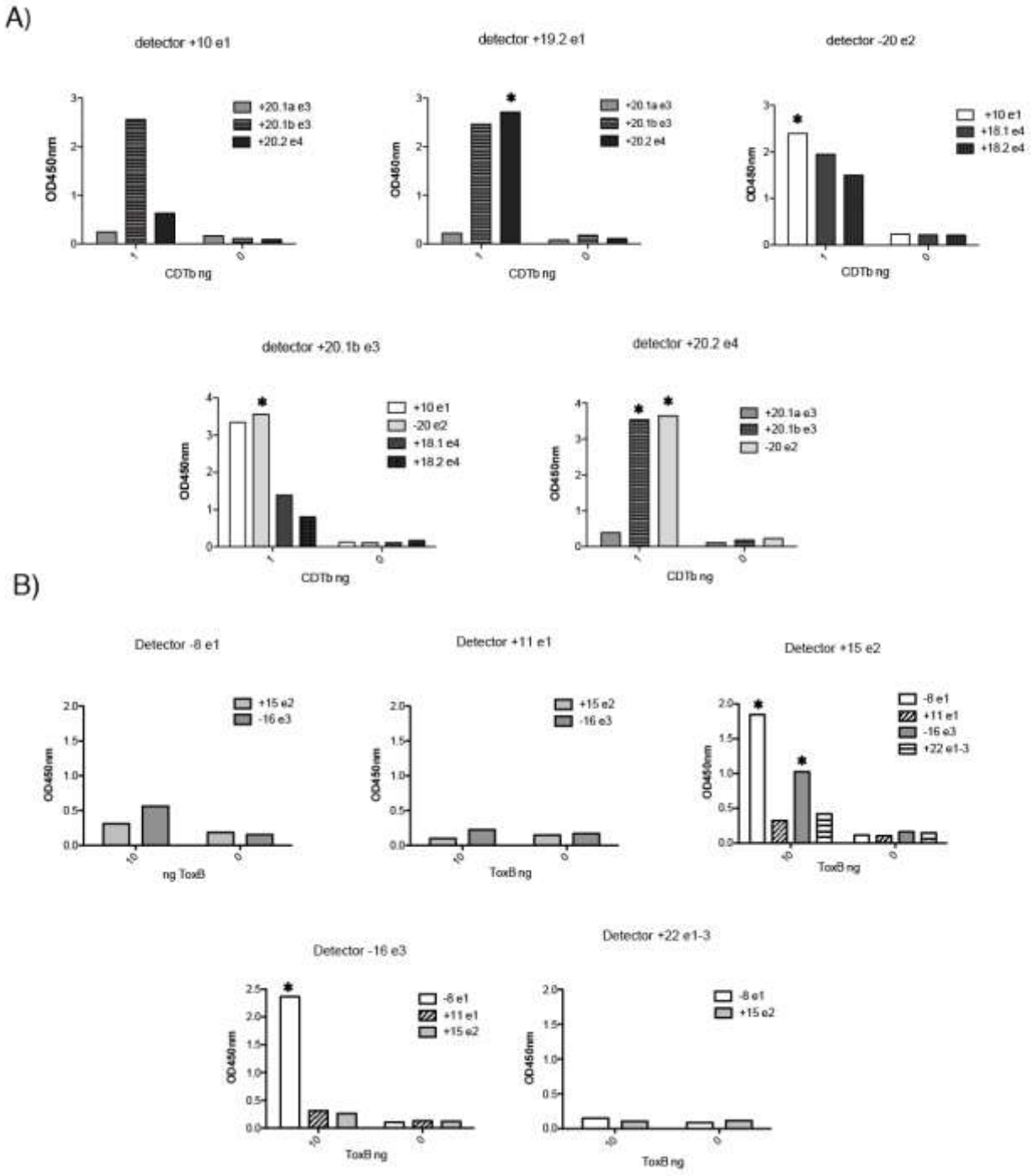

Figure 3.14. Screening pairs of hcAbs for detecting recombinant CDTb and TcdB (GTD-CPD). The screening was performed by a sandwich ELISA system as illustrated in Fig. 3.13. Unconjugated catcher hcAbs (100 ng/well) were coated overnight in a 96-well microtiter plate. The next day, free binding sites were blocked using 5% BSA-PBS for 2 h at room temperature. After washing, CDTb (1ng/well) or TcdB (10ng/well) were added to the wells for 2 h RT. After 6 cycles of washing with 0.05% Tween20-PBS, the indicated second biotinylated detector hcAbs (10ng/well) were added to the wells for 1 h at RT. After washing, bound hcAbs were detected by incubating wells with HRP-conjugated streptavidin for 1 h at RT, then washing and addition of TMB as substrate for 15 min at RT. The reaction was stopped with H_2SO_4 and measurement was performed using a plate reader at 450nM. Epitopes recognized by the hcAbs are indicated by e1 (white), e2 (light grey), e3 (dark grey) and e4 (black). Asterisk-marked columns represent the pairs of selected for the next experiments. The data points are from single measurements. The experiment in A was performed twice with similar results. The experiment in B was performed only once.

3.4.2 Evaluating the detection-sensitivity of the sandwich ELISA System

To determine the sensitivity of detection of the selected hcAb pairs, assays were set up using serially diluted recombinant CDTb and TcdB (GTD-CPD) to establish dose-response curves (**Fig. 3.15**). The results show sigmoidal curves when plotting optical density (substrate) versus log concentration of recombinant toxin components. The limit of detection (LOD) of the biotin-streptavidin capture ELISA was in the range of 50-100 pg for CDTb **(Fig. 3.15A)** and 10-30 pg for TcdB **(Fig. 3.15B)**.

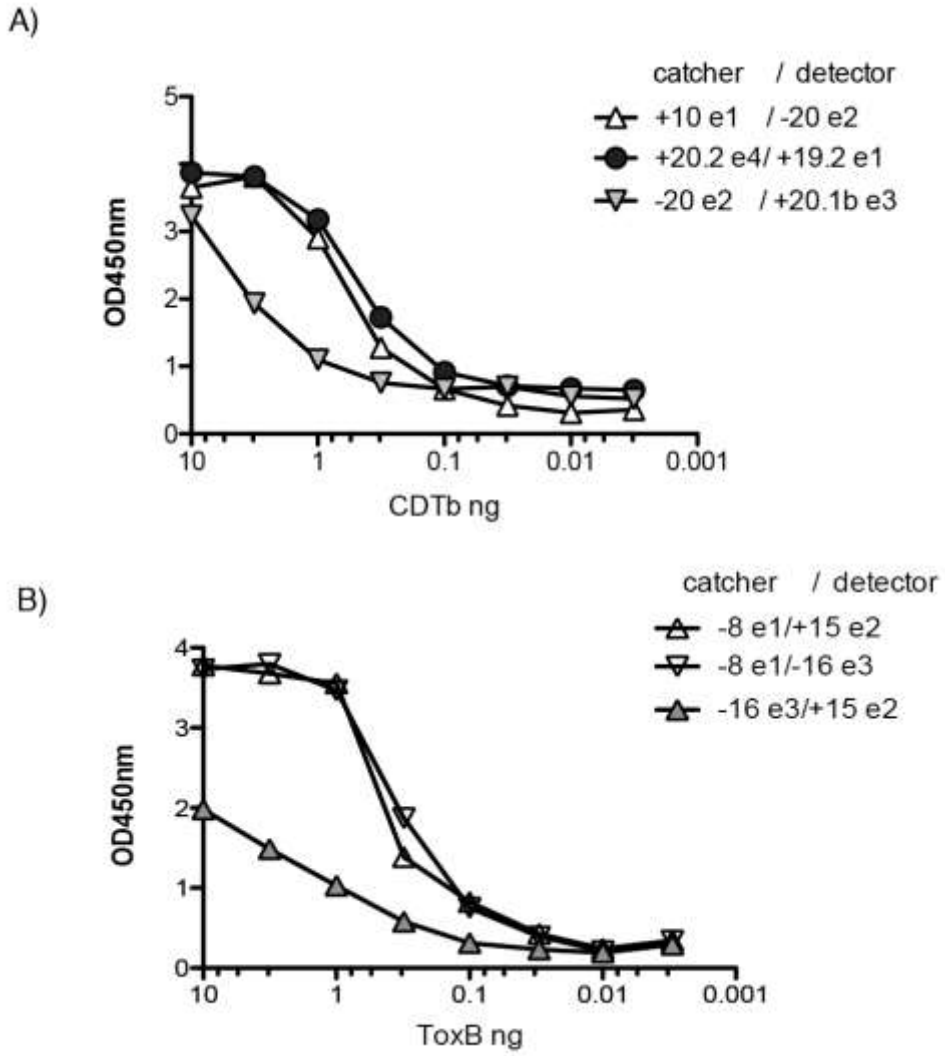

Figure 3.15. Dose-response curves for detecting recombinant CDTb (A) and TcdB (B) with selected pairs of hcAbs. The standard curves were obtained by titrating the CDTb and TcdB (GTD-CPD) using the indicated pairs of hcAbs as capture and detector. Unconjugated catcher hcAb (100ng/well) was coated overnight in a 96-well microtiter plate. Free binding sites were blocked using 5% BSA-PBS for 2 h at RT. Recombinant CDTb and TcdB were √10 serially diluted from a starting concentration of 10 ng/well, transferred to the wells for 2 h at RT. After 5 cycles of washing with 0.05% Tween20-PBS and PBS, biotinylated detector hcAb (100ng/well) was added to the wells for 1 h at RT. Bound hcAbs were detected by sequential incubation with HRP-conjugated streptavidin for 1 h at RT and TMB substrate for 15 min at RT. The reaction was stopped with H_2SO_4 and measurement was performed using a plate reader at 450nM. The data points are from single measurements. The experiment was performed only once.

3.4.3 The presence of CDTa does not interfere with the detection of CDTb

Upon proteolytic activation, the binding subunit CDTb binds to the cell surface receptor LSR as a heptamer, and to the enzymatic subunit CDTa. In order to determine whether detection of CDTb by our ELISA is affected by the presence of CDTa, I next performed the CDTb ELISA in the presence of the CDTa subunit using three pairs of catcher and detector hcAbs. Recombinant CDTb and CDTa (10ng+1ng/well) were mixed in 7:1 molar ratio and titrated in a √10 dilution series (**Fig. 3.16**). The results indicate that CDTb can be detected with high sensitivity in the presence of CDTa with all pairs of hcAbs tested.

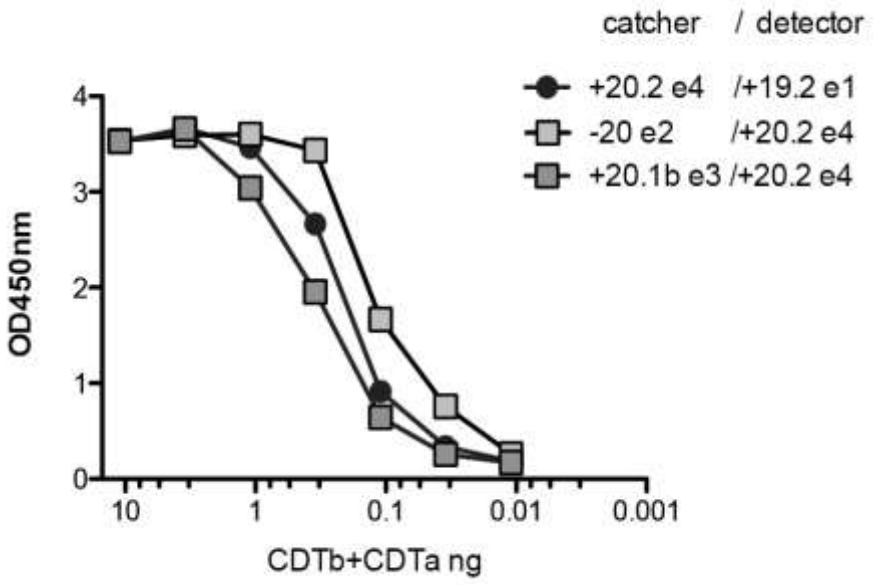

Figure 3.16. Sandwich ELISA with pairs of hcAbs can detect CDTb even in the presence of CDTa. Dose response curves were obtained using titrations of a mixture of CDTb and CDTa in a 7:1 molar ration and the indicated pairs of CDTb-specific hcAbs as detector/catcher in a sandwich ELISA. Unconjugated catcher hcAb was coated and free binding sites were blocked with BSA as in Fig 3.15. Recombinant CDTb and CDTa were mixed in a 7:1 molar ration and √10 diluted with starting concentration of 10 ng /well, and transferred to the well for 2h at RT. After 7 cycles of washing, biotinylated detector hcAb (100ng/well) was added to the wells for 1h at RT. Bound hcAbs were detected using HRP-conjugated streptavidin and TMB substrate as in Fig. 3.15. The data points are from single measurements. The experiment was performed only once.

3.4.4 Detection of CDTb and TcdB in spiked stool samples

To evaluate the capacity of the established sandwich ELISA system for detecting the recombinant toxin components in stool samples, a spiked stool assay was set up. To this end, 360 mg of healthy mouse feces was collected and homogenized with 1x protease inhibitor cocktail (cOmplete,Roche) in 7.2 ml of 5% BSA-PBS for 1 hour at room temperature (corresponding to a concentration of 50 mg feces/ml of PBS). Samples were vortexed every 15 min. Insoluble material was pelleted by centrifugation for 25 min at 4600 rpm. The supernatant was removed to new tubes and spiked with a serial dilution of recombinant CDTb and TcdB (GTD-CPD) at a starting concentration 10 ng/ml (1

ng/well) for CDTb and 100 ng/ml (10 ng/well) for TcdB (GTD-CPD). As controls, the same dilution series for both toxin components was performed in 1% BSA-PBS (see above, **Fig. 3.15**). Sandwich ELISA was performed using the previously tested pairs of hcAbs as detector/catcher (**Fig. 3.17**). The results indicate that CDTb and TcdB can be detected effectively even in the presence of mouse stool extracts. The limit of detection in the spiked stool samples was similar to the values obtained when the toxins were diluted in buffer (1%BSA-PBS); i.e. approximately 50-100 pg for CDTb **(Fig. 3.17A)** and 10-30 pg for TcdB (**Fig. 3.17B**).

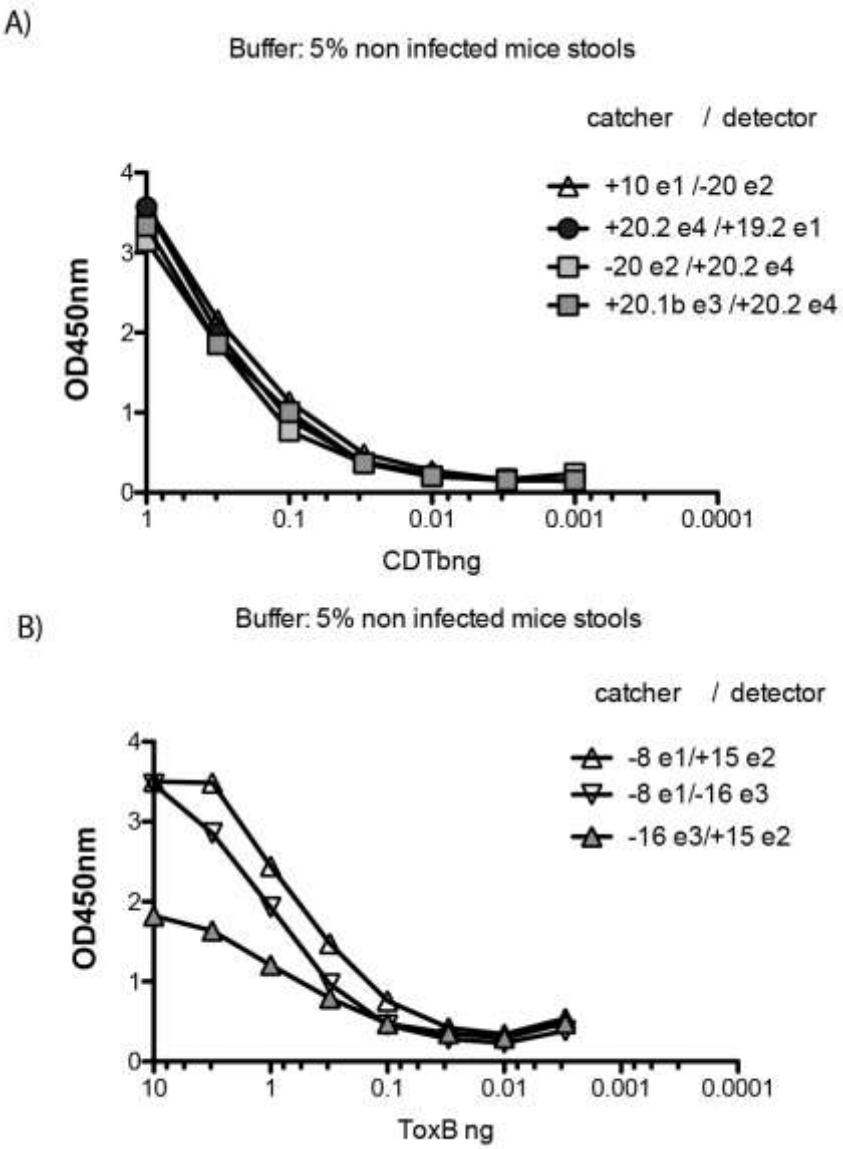

Figure 3.17. Sandwich ELISA with pairs of hcAbs can detect CDTb and TcdB in spiked stool samples. 360 mg of healthy mouse feces was collected and homogenized in 20 volumes of PBS containing 1x protease inhibitor cocktail (cOmplete,Roche) and 5%BSA for 2 h on ice. Samples were vortexed every 15 min and then centrifuged for 25 min at 4600rpm. The supernatant was spiked with a $\sqrt{10}$ serial dilution of recombinant CDTb and ToxB with a starting concentration of 1 ng/well and 10 ng/well respectively. Coating of wells with catcher hcAbs and detection of bound toxin components with biotinylated hcAbs, HRP-conjugated streptavidin and TMB substrate was performed as in Fig. 3.15. The data points are from single measurements. The experiment in A was performed twice. The experiment in B was performed only once.

3.4.5 Detection of CDTb and full length TcdB in stool samples of *C. difficile*-infected mice

To evaluate the feasibility of the developed ELISA for detecting native CDTb and ToxB in stool samples of *C. difficile* infected mice, I used two pairs of hcAbs as catcher/detector that had shown high sensitivity in the previous assays with recombinant toxin components, i.e. +20.2 e4/+19.2 e1 and +10 e1/-20 e2 for CDTb and -8 e1/+15 e2 and -8 e1/-16 e3 for ToxB (**Fig. 3.18**). The stool samples were collected from mice one day and two days after infection with 10^6 spores of *C. difficile* ribotype 027 (a strain that is known to produce ToxA, ToxB and CDT). Stools from healthy mice were used as control.

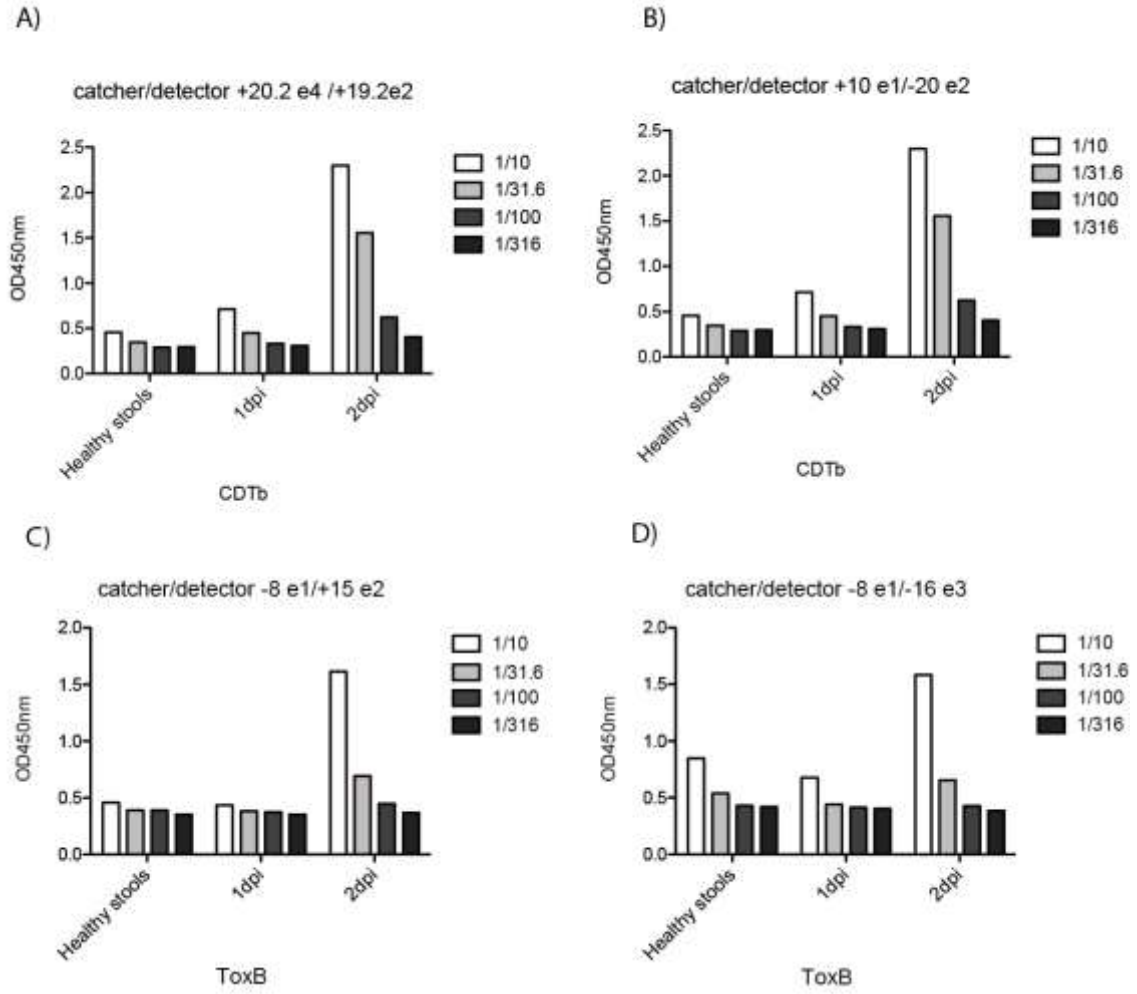

Figure 3.18. Detection of CDTb and ToxB in stool samples of *C. difficile*-infected mice. Feces of healthy mice and mice infected with 10^6 spores of *C. difficile* ribotype 027 (CDT-producing) were collected and homogenized at a weight:volume ratio of 1:4 with PBS containing 1x protease inhibitor cocktail, EDTA-free (Halt, Thermofisher) and 5% BSA for 2 h on ice. Samples were vortexed every 15 min and insoluble material was removed by centrifugation for 20 min at 8000 rpm at 4˚C. The supernatants were centrifuged again for 15 min at 8000 rpm at 4˚C and were then filtered and serially diluted with √10 dilution factor. 100 µl of diluted stool extracts were loaded per well. Coating of wells with catcher hcAbs and detection of bound toxins with biotinylated hcAbs, HRP-conjugated streptavidin and TMB substrate was performed as in Fig. 3.15. 1dpi : one day post infection, 2dpi:two days post infection. The data points are from single measurements. The experiment in B was performed twice with similar results. The experiment in A, C, D, was performed only once.

Fecal extracts were prepared by resuspending feces in 4 volumes (weight/volume) in PBS containing 5% BSA and a protease inhibitor cocktail for 2 h on ice with vortexing every 15 min (corresponding to ≈250 mg feces/ml PBS). Insoluble material was pelleted by high-speed centrifugation and filtered supernatants were diluted in PBS/BSA in a $\sqrt{10}$ dilution series. The results indicate that CDTb can be detected already one day post infection with *C.difficile* ribotype 027 (**Figs. 3.18A-B**) and that levels of CDTb rise during the second day of infection (**Figs. 3.18A-B**). In contrast, TcdB is undetectable by the established system on the first day after infection but becomes clearly detectable the day thereafter (**Figs. 3.18C-D**).

To quantify CDTb and ToxB in the stool samples, I used the standard curves obtained with stool samples spiked with recombinant CDTb and TcdB using the CDTb-specific pair of hcAbs +20.2 e4/+19.2 e1 and the TcdB-specific pair of hcAbs -8 e1/+15 e2 (**Table 3.2**). The results indicate levels of CDTb on day 1 after infection of approximately 0.8 ng per mg of feces rising to 5.7 ng/mg on the second day post infection (**Table 3.2**). TcdB is undetectable on day 1 and rises to 1.6 ng /mg feces on day 2 post infection (**Table 3.2**).

	1d post-infection (ng toxin/mg feces)	2d post-infection (ng toxin/mg feces)
TcdB	------	1.6
CDTb	0.8	5.7

Table 3.2. Quantification of toxin level in feces samples Standard curves were calculated with Excel. Standard curve for CDTb (+20.2 e4/+19.2 e1): Y=0,1009x+0,3445, R^2 = 0,96; Standard curve for TcdB (-8 e1/+15 e2): Y=0,0631x+0,3673, R^2 = 0,98.

4. Discussion

In this thesis, specific VHHs against *Clostridium difficile* toxins were selected from dromedary immune phage libraries. These VHHs were produced and reformatted into bivalent heavy chain antibodies (hcAbs). The potential use of these VHHs and hcAbs for diagnosis and neutralization of *Clostridium diffcile* toxins was investigated. Eight CDTb-specific VHHs from six distinct VHH families and five distinct TcdB-specific VHHs were isolated from immune dromedary libraries by phage display panning (**Table 3.1**). The VHHs were expressed in HB2151 *E. coli* and human HEK-6E cells (**Figs. 3.2 and 3.4**). Their specific binding to their targets was confirmed by ELISA (**Figs. 3.3 and 3.5**).

In dromedaries, approximately half of the natural serum IgG repertoire consists of heavy-chain antibodies, while llamas have a lower proportion of hcAbs of 25 to 45% (Muyldermans, 2001). Although similar in structure, VHHs from llamas and dromedaries display differences in CDR3 length and disulfide linkages within the antigen binding loops that may affect their biochemical properties and application as diagnostics and therapeutics (Muyldermans, 2001). An additional non-canonical disulfide bond is more frequent in dromedary compared to llamas. In dromedary VHHs, this additional disulfide bridge typically is located between CDR1 and CDR3, while in llama it tends to be located between CDR2 and CDR3 (Govaert et al., 2012, Mendoza et al., 2020). The small size of nanobodies (15kDa) and the convex shape of their paratope, in combination with a long complementarity determining region (CDR3), enhances their capacity to bind to cryptic epitopes, e.g. an enzyme active site or conserved epitopes of virus particles (Crasson et al., 2015, Fumey et al., 2017, Kunz et al., 2017, Li et al., 2012).

CDTb-specific nanobodies

```
Dr 1406

#IC +19.2    LSCEASGFIFEDSDMG.....WYHQAPGNECEQVAAISRDGRT.YYGASWKGRFTISRNNAENTVYLQMSSLKPEDTGMYYCAGRNPRDLQNYGGACQGPFGY.WG
#IC   -20    LSCEASGLPFSRNLMA.....WFRQGPGKEREGIAAIVAGGTSTAYARNVEGRFAISQDNAKNTVYLEMNSLKPEDSAVYYCAANSRQWVPAASRFLYETSYNNWG
#IC +20.1 a LSCVVPSSAYCMG........WFRQAPGKEREAVAATNRGSSNEYYTASAKDRFTISHDHKKNMVTLQMRSLQPEDTGTYYCAAGEYGGVCRDWMRGPPEDYTDWG
          b LSCVVPSSAYCMG........WFRQTPGKEREAVAATNRGTSNEYYSDSVKDRAIISHDYTKNMVTLRMRRLQPEDTGTYYCAAGQYGGVCRDWMRGPPECGYTDWG
#IC +18   a LSCAANDDAYSRCSVG.....WFRQAPGKERELVSTIKHDGRT.YYADSVKGRFTISQDNAKKTVYLQMNSLKAEDTAMYYCNIVPGSFASGGACYPDGHSY..WG
          b LSCTASDYVRSRCSVY.....WSRQAPGKERELVSSIRNDGSTY.YADFVKGRFTISEDKAKKTVYLQMNSLKPEDTAMYFCTIVPGDFASGGACYPTGHTY..SG
#IC +20.2    LSCAASGYIVGSYCMA.....WFRQAPGKEREGVAAINSGGGKPYYADSVKGRFSISPDNARNTVYLQMNSLKPEDTAIYYCAATLAGSGGACYSPLDQYGQSYWG

Dr 1409

#IC +10      LSCTASGIVFEASDMA.....WYHLPPGKGCELVSRISSDGRTY.YTDSVKGRFTISRDNAKNTVSLQMNSLKPEDTAMYYCAAPNWRLESPCY.............SG
#IC +19.2    LSCEASGFTFEDSDMG.....WYHQAPGNECEQVAAITRDGRTY.YGASWKGRFTISRNNAENTVYLQMSSLKPEDTGMYYCAGRNPRDLQNYGGACQGPFGY....WG
```

TcdB-specific nanobodies

```
Dr 1406

#IC -8     LSCAASGLTFSISRYVLNWVRQAPG..KGLEWVSTINPHRGGTT..YADSVKGRFTASSDDAKNTLYLRMDSLRTEDTAMYYCTLGSVWALGT.............RGQ
#IC +11    LSCAASGFTFSRNSMS..WVRQAPG..KDLEWVSIISIDGSRT..YYADSVKGRFTISRDDAENTLYLQMNSLKAEDTAMYYCLRGDGRFCRGDCY...........RGQ
#IC +15    LSCAASGDIVSRRCMG..WFRQAPG..KEREGVATIYTPLGIGTAEYGASVKGRFTISQDNAKNTLYLEMNNLEPEDSGIYYCAASEGVFCYLRTNAYNY.......WG
#IC -16    LSCAADRDTYSMYSMA..WFRQAPG..KEREGVATISSTSGRT..YYADDVKGRFTISRDNAKNTMYLQMNGLKPEDTAIYYCAARALGDIRRLQPVDWSL......WG
#IC +22    LSCAASGSMYRANCMA..WFRQAPGPGKEREGVAAINRGSGTT..YYADSVKGRFTISQDAAKNTWYLQMNSLKPEDTAIYYCAADRYDYCSDSWSDADLVEYGYNYWG
```

Figure 4.1. Sequence alignment of CDTb and TcdB specific VHHs selected from two immunized dromedaries Dr1406 and Dr1409 by phage display panning. VHHs are grouped into families according to their CDR3 (blue), CDR1 (red) and CDR2 (green). The framework regions are colored in black. Amino acid differences between two members of a family are highlighted in grey. The canonical Cys residues and additional Cys pairs likely involved in disulfide bonding are highlighted in yellow.

Inspection of the VHH amino acid sequences selected in this thesis reveals that the VHHs have CDR3 loops from 8 to 23 amino acids. Seven of eight CDTb-specific VHHs have an additional pair of cysteines, five of these for a potential disulfide bridge between CDR1 and CDR3 and three for a potential disulfide between FR2 and CDR3. Three of five TcdB-specific VHH have an additional pair of cysteines, two of these for a potential disulfide bridge between CDR1 and CDR3 and one for a potential disulfide bridge within the CDR3 (**Fig. 4.1**). Our lab had previously selected four CDTb-specific and five CDTa-specific VHHs from immunized llamas. These VHHs contained CDR3 loops of 3 to 21 amino acids and most lacked an extra-disulfide bridge (Unger et al., 2015). For comparison, the average CDR3 length in human and mouse VHs is 12 and 9 amino acids, respectively (Wu et al., 1996).

It has been proposed that the role of the additional disulfide bond in *Camleus dromedarius* is related to biophysical adaptations of the VHH domain to the absence of the light chain and/or to high body temperatures. Camels are adapted to arid, hot climates, while llamas and alpacas generally occupy more temperate zones (Govaert et al., 2012, Kunz et al., 2018, Mendoza et al., 2020). To survive the extreme desert climate, camels conserve water by increasing their internal body temperature. The temperature of healthy camels at rest may vary from 34°C at night to more than 40°C during the day. This temperature variation is a means to conserve water by storing heat during the day (Gebreyohanes and Assen, 2017). In addition to providing protection against heat-mediated degradation or aggregation, it is conceivable that the non-canonical disulfide linkage affects the affinity of the VHH for its target antigen, e.g by according greater stability to the VHH and/or reducing the entropic penalty associated with antigen binding. This hypothesis is supported by the results of mutational analysis of several VHHs (Govaert et al., 2012). However, other authors favor the notion that the non-canonical disulfide bond found in camel VHH has evolved to stabilize the biophysical properties of the domain, rather than playing a role in antigen binding (Mendoza et al., 2020). Further structural and biophysical studies are needed to determine the role of the additional disulfide bond for particular camel VHHs.

In order to assess the neutralizing potential of bivalent CDTb-specific hcAbs, I performed cytotoxicity assays using HT29 human colon carcinoma cells. The integrity of actin cytoskeleton was assessed by Phalloidin staining. The results indicate that the CDTb-specific hcAb +20.1a effectively protects HT29 cells from the cytotopathic effects of the binary CDTa/CDTb toxin (**Figs. 3.9**). CDTb engages host cells through the lipolysis-stimulated lipoprotein receptor (LSR), undergoes proteolytic cleavage and forms a heptamer that interacts with a single molecule of CDTa before internalization into the cell. The formation of the CDT complex relies on the interaction of an N-terminal adaptor and pseudoenzyme domain of CDTa with the subunits of the CDTb heptamer (**Figs. 4.2A-B)** (Anderson et al., 2019, Sheedloa et al., 2020).

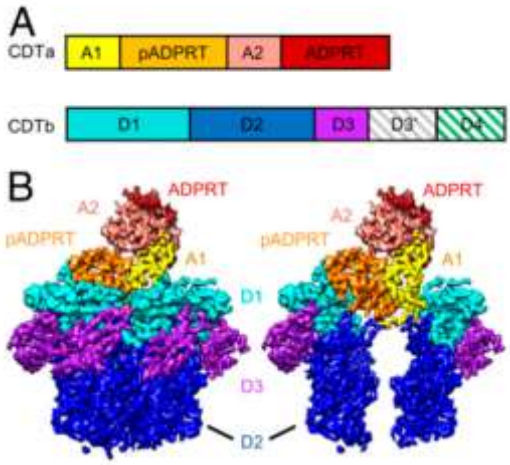

Figure 4.2. Structure of the Clostridiidium difficile transferase toxin (CDT). (A) The binary CDT toxin consists of of two polypeptide chains termed CDTa and CDTb. CDTa consists of two domains called the pseudo-ADP ribosyltransferase domain (pADPRT, orange) and the ADP ribosyltransferase domain (ADPRT, red). Encoded within the N terminus of each domain is an adaptor (termed either A1 or A2 and shown in yellow and pink, respectively). CDTb consists of four domains termed D1–D3, D3′ and D4. (B) Cryo–electron microscopy (cryo-EM) structure model of binary CDT, containing one molecule of CDTa and seven CDTb subunits, colored as in A. On the left is a model of CDTa in complex with a complete CDTb heptamer, and on the right is a split view showing the positioning of CDTa with only two CDTb subunits (Sheedloa et al., 2020).

Since the VHHs generated in this study were selected from dromedaries immunized with the recombinant CDTb subunit, the neutralization mechanism could be explained by hcAb-mediated steric hindrance of the assembly of CDTb heptamers, and/or the binding of the CDTb heptamer to CDTa or to LSR. Our group had previously selected a CDTa-specific VHH (l+8) from immunized llamas that also effectively protected HT29 cells from CDTa/CDTb-mediated disintegration of the actin cytoskeleton (**Fig. 3.9**). This nanobody also blocked the ADP ribosylation of actin by CDTa *in vitro* (Unger et al., 2015). Combining CDTb-specific nanobodies developed in the present study with llama-derived CDTa-specific VHHs may present a strategy to neutralize CDT toxin even more efficiently.

In order to assess the neutralizing potential of TcdB-specific hcAbs, all of which bound to the N-terminal glycosyltransferase domain of TcdB with low nM affinites, I treated HT29 cells with TcdB in the presence or absence of hcAbs and monitored cells for rounding and detachment by microscopy. Even at high molar excess, none of the TcdB-specific hcAbs, was able to effectively inhibit TcdB-mediated cytotoxicity (**Fig. 3.12**). The lack of effective neutralization may be related to the extremely high potency of TcdB, which can effectively kill cells at sub-picomolar concentrations (0.74 pMol in **Fig. 3.12**). Other studies have shown that TcdB is 100–10,000 times more potent than TcdA against several cell types (Di Bella et al., 2016). Recent data support the notion that toxin B alone is sufficient to cause disease and likely is much more potent than toxin A also *in vivo* (Johnson and Gerding, 2019).

Other groups have selected TcdB-specific VHHs that bind to the central delivery/translocation domain or the C-terminal combined repetitive oligopeptides (CROPs) region. Hussack et *al.* isolated 29 VHHs targeting these domains. Despite their high affinities of up to Kd=70 pM, none of the monomeric VHHs showed a neutralizing effect; however, when the VHHs were reformatted into bivalent hcAbs, inhibition of cytotoxic effect of TcdB was detected, presumably due to steric and/or avidity effects not afforded to monomeric VHHs (Hussack et al., 2018). Yang et *al.* generated a tetravalent, bispecific construct (designated "ABA") composed of two VHHs against the GTD and translocation domain (TD) of TcdA, and two VHHs recognizing the GTD of TcdB. ABA was able to bind to both toxins simultaneously and showed a significantly enhanced neutralizing activity *in vitro* and *in vivo* (Yang et al., 2014). Other VHHs with high-affinity binding to the C-terminal CROPs region of TcdB failed to inhibit TcdB cytotoxicity (Wang et al., 2012, Yang et al., 2014). ABA was subsequently reengineered into a tetraspecific construct (designated VNA2-Tcd), consisting of two different TcdB-GTD-specific VHHs linked to two different TcdA-specific VHHs. VNA2-Tcd showed toxin neutralization at subnanomolar concentrations for both toxins in cellular assays. Protection from CDI was observed in piglets treated with an adenovirus encoding VNA2-Tcd (Schmidt et al., 2016). Kandalaft et *al*. opted for another target to inhibit CDI, i.e. the SLP surface protein of *C. difficile*. This group developed VHHs that bind SLPs from various strains. A combination of three SLP-specific VHHs inhibited the motility of the bacteria *in vitro* (Kandalaft et al., 2015).

Bezlotoxumab is a fully humanized IgG1/kappa monoclonal antibody of 148 kDa approved by the US Food and Drug Administration (FDA) to reduce the recurrence of CDI (Navalkele and Chopra, 2018). This antibody targets *C. difficile* TcdB, more precisely, a peptide corresponding to the N-terminal half of the CROP domain of TcdB. Fab fragments of Bezlotoxumab bind side-by-side to two highly homologous epitopes within the CROP domain (Orth et al., 2014). Intravenous infusion of bezlotoxumab in conjunction with antibacterial treatment reduced the risk of recurrent CDI for patients with known risk factors (Johnson and Gerding, 2019, Navalkele and Chopra, 2018).

Early detection of *C. difficile* and its toxins is important, as this allows earlier treatment that can significantly reduce the morbidity, mortality, and medical cost of CDI. The current recommended diagnostic strategy is based on a multi-step algorithmic testing to maximize diagnostic accuracy (Cohen et al., 2010, Crobach et al., 2016). As none of these assays suffices as a stand-alone diagnostic test for *C. difficile*, alternative diagnostic tools are needed. Despite the rapidity and low cost of the enzyme immunoassays (EIA) for toxins A and/or B detection, their sensitivity and specificity vary widely, and sometimes their positive predictive values (PPVs) are inadequate (Burnham and Carroll, 2013).

In this study, I established a sensitive sandwich ELISA immunoassay using pairs of TcdB-specific and pairs of CDTb-specific heavy chain antibodies. In both cases, the two hcAbs recognize non-

overlapping epitopes. An unconjugated hcAb is used for capturing the toxin and the second, biotinylated hcAb in conjunction with peroxidase-conjugated streptavidin for detection. The ultrahigh affinity biotin-streptavidin bond can resist severe environments such as organic solvents, proteolytic enzymes and extremes of temperature and pH. The sandwich ELISA exhibited high specificity and sensitivity. The limit of detection was determined to be approximately 1 ng/ml and 0.1 ng/ml for CDTb and TcdB, respectively (**Fig. 3.15**), i.e. in the range of the analytical limits of detection (LODs) for enzyme immunoassays (Pollock, 2016). The established ELISA showed good performance also in mouse stool samples spiked with recombinant toxins, with little unspecific binding to other proteins or substances in the stool (**Fig. 3.17**). The ELISA assay was also able to detect endogenous toxins in stool samples collected from a *C. difficile* infected mice (Schumacher, 2020). In the CDI mouse model, Schumacher detected signs of infection through diarrhea, soiling of cages and weight loss. Two days after infection with *C. difficile* spores, the nesting paper and cages of mice showed a greater level of soiling compared to the first day post-infection, in addition to a significant weight loss (Schumacher, 2020). These clinical symptoms correspond well with the increased levels of CDTb and TcdB detected by the established ELISA, between day 1 and day 2 post infection (**Fig. 3.18**).

Studies of CDI in humans also indicate a correlation between fecal CDT levels, disease severity and mortality (Akerlund et al., 2006, Burdon et al., 1981, Cohen et al., 2018, Pollock, 2016). Cohen et *al.* found that the fecal CDT level is a good predictor for disease severity (high leukocyte count, deterioration in serum creatinine levels, and low serum albumin levels). They noticed that fecal CDT level was significantly higher in patients with severe disease compared to those with mild to moderate disease. They also found that high levels of fecal toxins might predict increased short-term mortality. The use of fecal CDT level as a risk stratification tool may help in decision making for early aggressive therapy initiation (Cohen et al., 2018). In human, toxin levels in stools could potentially be clinically valuable to predict disease and treatment outcomes and in identifying those who need aggressive therapy(Pollock, 2016).

The ELISA immunoassay established in this thesis may provide a basis for the rapid detection of CDT levels in human stool samples and thereby help to simplify and improve the efficiency of *C. difficile* laboratory diagnosis.

IgA is the most abundant antibody at the mucosal surfaces. The induction of an effective mucosal IgA antibody response may require cumbersome adjustments of the antigen, adjuvant, and delivery route. Passive immunization, i.e. delivery of preformed antibodies, presents an alternative for the protection of mucosal surfaces (de Sousa-Pereira and Woof, 2019). As a potential basis for a passive mucosal vaccine, I reformatted VHHs that bind to distinct epitopes of CDTb into chimeric VHH-mouse IgA heavy chain antibodies. Transfection into HEK-6E cells yielded monomeric IgA hcAbs, co-transfection with the mouse J-chain yielded dimeric IgA hcAbs. Both formats were produced as

secretory proteins in HEK293-6E cells and could be purified by affinity chromatography using immobilized protein A. Both, monomeric and dimeric IgA were produced at high yields (**Fig. 3.6**).

Other studies have evaluated recombinant VHH-IgA hcAbs. Virdi et *al.* generated such hcAbs (designated SIgA) against diarrhea-causing enterotoxigenic Escherichia coli (ETEC). When produced by bioencapsulated *Arabidopsis thaliana* seeds or by yeast cells *in vivo*, these hcAbs showed efficient protection in a piglet model (Virdi et al., 2013) (Virdi et al., 2019). Another group fused VHHs, directed against the Campylobacter flagella and major outer membrane proteins, to the hinge and Fc-domains of chicken IgA. Chickens are considered as the main reservoir of this zoonotic infectious disease. The selected chimeric hcAbs were produced in *N. benthamiana* leaves and *Arabidopsis thaliana* seeds and showed binding to their specific antigens and to Campylobacter cells (Vanmarsenille et al., 2018). Both groups used Arabidopsis plants as a production platform. Compared to mammalian cells, plant-based production has cost advantages and provides a safe delivery route. Furthermore, the *N*-glycosylation pathway in plants has been engineered to facilitate expression of antibodies with humanized *N*-glycans (Bosch et al., 2013, Virdi et al., 2016, Westerhof et al., 2015).

Gut microbiota act as a protective barrier against the colonization of the intestine with *C. difficile*. This barrier is disrupted when the normal gut microbiota is altered by antibiotic therapy. A new promising therapeutic approach involves the restoration of gut microbiota by fecal microbiota transplantation (FMT) (Kachrimanidou and Tsintarakis, 2020). Restoration of the gut microbial community can help to restore gut homeostasis and resistance against colonization by pathogens. This is achieved either by inhibition of pathogens via metabolites (bacteriocins, antibiotics, short-chain fatty acids (SCFA), secondary bile acids) produced by commensal microbes, by competition for available nutrients, or by stimulating immune defense mechanisms (Kachrimanidou and Tsintarakis, 2020). SCFA, including carboxylic acids from bacterial fermentation of dietary fibers, have been shown to inhibit the development of *C. difficile in vitro*, and to induce regulatory T cells and inhibit the activation of macrophages and neutrophils (Belkaid and Hand, 2014, Kachrimanidou and Tsintarakis, 2020). A decrease in bacteria that produce SCFA can alter the defense of the host against *C. difficile* and can increase the sensitivity toward the infection. Moreover, microbiota-mediated bioconversion of primary into secondary bile acids has been shown to inhibit *C. difficile* vegetative growth (Kachrimanidou and Tsintarakis, 2020, Seekatz and Young, 2014). *C. difficile* carriers were found to have fewer Proteobacteria and a larger proportion of Firmicutes and Bacteroidetes than CDI patients. The microbiome of healthy carriers resembles that of other healthy individuals, suggesting the importance of Bacteroidetes and the non-pathogenic Clostridia member (Firmicutes) in suppressing *C. difficile* outgrowth (Kho and Lal, 2018, Zhang et al., 2015). Consistently, following FMT, the composition of the gut microbiome shifts towards an increase in Bacteroidetes and

Clostridium cluster IV and XIVa (Firmicutes), and a reduction in Proteobacteria phylum (Kho and Lal, 2018). Although FMT is often effective in treating and preventing recurrent CDI, it still not approved by the FDA due to risks associated with the transfer of foreign, potentially infectious material (Dieterle et al., 2019). Ongoing research aims to develop alternatives to FMT such as standardized bacterial replacement and defined cultures of one or more microbial species. It is hoped that such bio-therapeutic tools can correct the dysbiosis that accompanies CDI, by replacing the depleted bacterial species and re-establishing gut homeostasis while circumventing the safety issues of fecal matter (Kachrimanidou and Tsintarakis, 2020, Lazar et al., 2018). The impact of these emerging therapies will likely not only affect CDI, but also other microbial illnesses that are dependent on an interaction between the host, native microbiota, and pathogen (Dieterle et al., 2019). It is conceivable that FMT or related bio-therapeutics could be combined in a synergistic fashion with the VHH-IgA hcAbs generated in this study to improve the treatment of CDI.

Commensal gut microbiota can potentially be used as vectors for the *in situ* delivery of recombinant antibodies and other therapeutic proteins. Lactic acid bacteria (LAB) are commensal gram-positive bacteria belonging to Firmicutes phylum. They are widely used in food fermentation and as probiotics. They are ideal candidates as live delivery vehicles surviving the passage through the gastrointestinal tract to release therapeutic and prophylactic molecules directly at the oral, nasal, and genital mucosae (del Rio et al., 2019, Lazar et al., 2018). Several studies have explored the use of LAB for the *in situ* production of VHHs at the gut mucosa after oral delivery (del Rio et al., 2019). In one study, recombinant *L. paracasei* strains were engineered to either secrete TcdB-specific VHHs into the extracellular medium or to produce these VHHs as proteins anchored to the cell wall. The oral administration of such engineered *L. paracasei* displaying cell wall-anchored TcdB-specific VHHs delayed the development of *C. difficile* infection and provided partial protection in a hamster model of CDI (Andersen et al., 2016). In contrast, oral administration of purified TcdB-specific VHHs did not provide protection, probably due to the acidic or proteolytic degradation of the antibodies (Vandenbroucke et al., 2010). The oral administration of engineered lactobacilli that either secrete recombinant VHH-IgA or display cell wall-anchored VHH-IgA (with single or multiple valencies and specificities) may also represent a promising approach for further development of the toxin-specific nanobodies generated in this thesis.

4.1 Perspectives

The generated nanobodies represent new diagnostic and therapeutic approaches for *Clostridium difficile* associated disease. Our aim was to develop an easy immunoassay to detect toxins in infected stool samples and establish an efficient non antibiotic alternative therapy that prevent persistence of toxin damages produced by *C. difficile* and minimally disrupt the gut microflora. In a long-term perspective, the efficacy of the obtained Nbs could be improved by using in silico site-directed mutagenesis to improve their affinity, or by reformatting them into bispecific or tetraspecific format that could target both toxins simultaneously thereby enhancing their neutralizing potential.

The generation of recombinant IgA VHHs represent a promising novel therapeutic against CDI, compared to the traditional IgG-based therapeutic, by their unique mechanisms of action in reaching the antigen in the luminal side via the polymeric immunoglobulin receptor (pIgR). IgA fusion antibodies have broad potential as a novel therapeutic platform, which could be applied against many other antigens invading the mucosal surfaces such as SARS CoV-2 virus that caused the pandemic COVID-19 (coronavirus disease 2019).

Microbiome plays also a crucial role in maintaining barrier defenses and gut homeostasis, bio-therapeutics derived from microbiota are emerging approaches to tackle infections. Combining recombinant IgA nanobodies and microbial therapy could be a promising strategy in enhancing therapeutic arsenal to fight c.*diff* infection. However, the transition of IgA into clinical development still challenging in terms of expression and production systems, more studies to improve the production platforms of IgA are needed.

5. Zusammenfassung

5.1 Abstract (Englisch)

Clostridium difficile is the major cause of antibiotic associated diarrhea and pseudomembranous colitis in Europe and North America. The increasing incidence and severity of *C. difficile* associated disease has been associated with the emergence of hyper virulent strains (BI/NAP1/027). Additionally to the large glucosylating toxins TcdA and TcdB, these strains produce a third binary toxin called CDT, an actin-specific ADP-ribosyltransferase which consists of the enzymatic component CDTa and the heptameric binding component CDTb. There remains a need for better diagnostic assays and specific therapies. Nanobodies, soluble single variable immunoglobulin domains (VHHs) derived from camelid heavy chain antibodies are promising tools for new diagnostics and therapeutics owing to their high solubility, stability, easy reformatting, and cost-effective production.

The goals of this thesis were to generate and characterize nanobodies directed against the enzymatic domains of TcdB (GTD-CPD) and the heptameric binding component of CDT (CDTb) and to develop nanobody-based heavy chain antibodies (hcAbs) as sensitive tools for detection these toxins in biological samples.

Eight CDTb-specific and five TcdB-specific nanobody families were selected from VHH phage display libraries obtained from immunized dromedaries by panning on immobilized recombinant toxin domains. These nanobodies were reformatted into rabbit-IgG (hcAbs) and produced as recombinant proteins in transiently transfected HEK cells. Rabbit hcAbs recognizing non-overlapping epitopes were further developed as capture/detector tools for sandwich ELISA. The best antibody pairs achieved detection limits of 50-100 pg for CDTb and 10-30 pg for TcdB. Both ELISAs were able to specifically detect these toxins in stool samples of mice infected with *C.difficile* spores. One of the selected CDTb-specific hcAbs effectively inhibited cytotoxicity toward human HT29 cells induced by CDT. However, even at very high concentrations, TcdB-specific hcAbs showed little if any toxin neutralization on HT29 cells. As a basis for adapting the generated nanobodies for therapeutic applications in the gastrointestinal tract, selected CDTb-specific nanobodies were reformatted into monomeric and dimeric mouse IgA hcAbs. These IgA hcAbs were produced at high yield in HEK cells and purified for future evaluation in preclinical mouse models.

The nanobody-based IgG hcAbs developed in this thesis provide a basis for rapid, sensitive and specific detection of *C.difficile* toxins in biological samples. If validated in preclinical mouse models, the nanobody-based IgA hcAbs may be applicable for the treatment of *C. difficile* associated disease.

5.2 Zusammenfassung (Deustch)

Clostridium difficile ist die Hauptursache für Antibiotika-assoziierten Durchfall und pseudomembranöse Kolitis in Europa und Nordamerika. Die zunehmende Inzidenz und Schwere der *C. difficile* assoziierte Erkrankung korreliert mit dem Auftreten hypervirulenter Stämme (BI/NAP1/027). Zusätzlich zu den großen glucosylierenden Toxinen TcdA und TcdB produzieren diese Stämme ein drittes binäres Toxin namens CDT, mit der enzymatischen Komponente CDTa - eine aktinspezifische ADP-Ribosyltransferase - und der hepatameren Bindungskomponente CDTb. Es besteht Bedarf an besseren diagnostischen Assays und spezifischen Therapien zur Behandlung der C. difficile assoziierten Erkrankung. Nanobodies, einzelne variable Immungloblulindomänen (VHHs) aus den Schwerekettenantikörpern (hcAb) der Cameliden, sind aufgrund ihrer hohen Löslichkeit, Stabilität, einfachen Neuformatierung und kostengünstigen Produktion, wertvolle Bausteine für neue Diagnostika und Therapeutika.

Ziele der vorliegenden Arbeit waren, Nanobodies zu erzeugen und zu charakterisieren, die gegen die enzymatischen Domänen von TcdB (GTD-CPD) und die heptamere Bindungskomponente von CDT (CDTb) gerichtet sind, und mit diesen Nanobodies neue sensitive Nachweismethoden für diese Toxine in biologischen Proben zu entwickeln.

Acht TcdB (CPD-GTD)-spezifische und fünf CDTb spezifische Nanobody-Familien wurden aus VHH-Phagen Display-Bibliotheken (die aus immunisierten Dromedaren hergestellt worden waren) mittels Panning an rekombinanten Toxinen gewonnen. Diese VHHs wurden in Kaninchen-IgG Schwereketten Antikörper (hcAb) umkloniert und als rekombinante Proteine in transient transfizierten HEK Zellen produziert. Kaninchen-hcAb, die nicht überlappende Epitope erkennen, wurden als Capture/Detektor Reagenzien für die Entwicklung von sensitiven Sandwich-ELISA verwendet. Die besten Antikörperpaare erreichten dabei eine Nachweisgrenze von 50-100 pg für CDTb und 10-30 pg für TcdB. Beide ELISAs konnten diese Toxine spezifisch in Stuhlproben von Mäusen nachweisen, die mit *C. difficile*-Sporen infiziert waren. Ein CDTb-spezifischer hcAb hemmte effektiv die durch CDT induzierte Zytotoxizität von humanen HT29 Zellen. Hingegen konnten, selbst in sehr hoher Konzentration, TcdB-spezifische hcAb die TcdB-vermittelte Zytotoxizität gegenüber HT29 Zellen nicht neutralisieren. Als Basis für therapeutische Anwendungen im Magen-Darm-Trakt wurden ausgesuchte CDTb-spezifische Nanobodies zudem in monomere und dimere Maus-IgA Schwereketten Antikörper formatiert, und in hoher Ausbeute in HEK Zellen hergestellt und für zukünftige Anwendungen in präklinischen Mausmodellen aufgereinigt.

Die in dieser Arbeit entwickelten Nanobody-basierten IgG hcAb bilden die Grundlage für einen schnellen, sensitiven und spezifischen Nachweis von *C. difficile* Toxinen in biologischen Proben. Nach Validierung in präklinischen Mausmodellen könnten die Nanobody-basierten IgA hcAb für die Therapie von *C. difficile* assoziierte Erkrankung verwendet werden.

6. Appendix

6.1 Plasmids maps

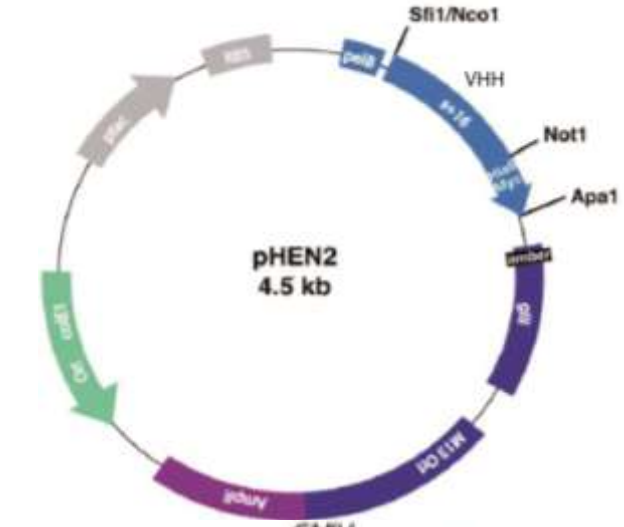

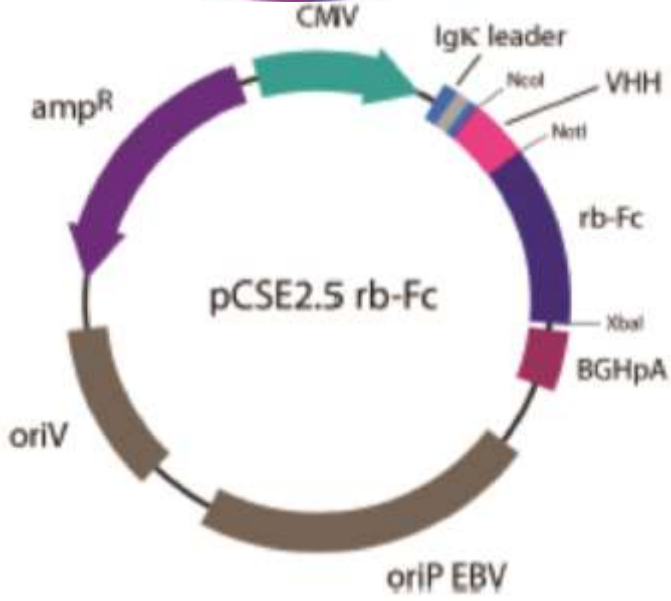

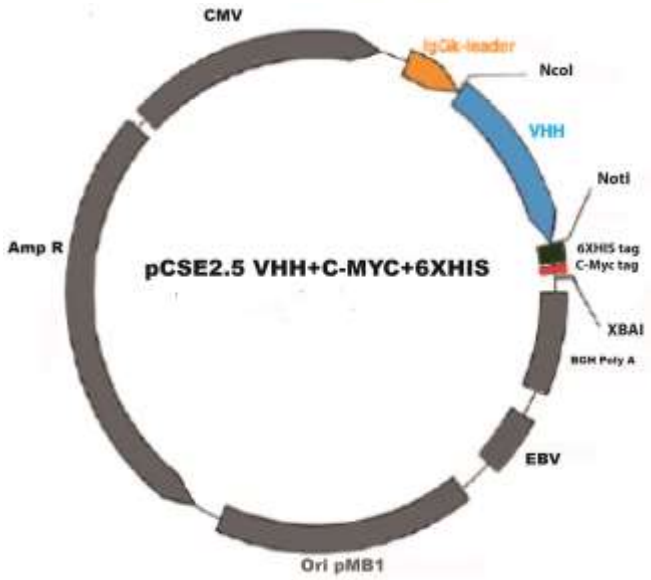

6.2 Oligonucleotides

Primer	Sequence (5‘ - 3‘)
Drom_cVHH_Lead_f	GTCCTGGCTGCTGCTCTTCTACAAGG
Drom_cVHH_CH2_reverse	GGTACGTGCTGTTGAACTGTTCC
Drom_for_cVHH_FR1_ Forward	TCGCGGCCCAGCCGGCCATGGCAGATGTGCAGCTGCAGGAGTCTGGR GGAGG
Drom_nested_cVHH_FR4 reverse	GGACTAGTGCGGCCGCTGAGGAGACGGTGACCTGGGT
CMV_F (pCSE2.5, forward)	CGCAAATGGGCGGTAGGCGTG
LMB3 (pHEN2, forward)	CAGGAAACAGCTATGAC
Fdseq1 (pHEN2, reverse)	GAATTTTCTGTATGAGG

6.3 Sequence alignment of VHHs obtained from primary TG1 Libraries

```
Dr 1406

01 LSCVGSGYVHDRHCMGWFRQAPGKEREGVAVIDSRDDSSYYGDSVKGRFTISQDKSKNTVHLLMNSLKVEDTAIYYCAAEYGMCTSGYVTILVNEFDYRGQGTQVTVSS
02 LSCTTSGSMPRTYYVGWVRQAPGKEREGVAIINNVGGNTYYADSVKGRFTISQDNAQVTVYLQMNSLKPEDTSKYVCALGPGFLADASLLGRLATD--WGQGTQVTVSS
03 LSCVVSGYTYRTNCMGWFRQAARKEREGVAAIWIGGSS-RYADSVKGRFTISLDNGNNTVYLHMNSLKPEDTALYYCAAATTCFWNRALNSARYEY--WGQGTQVTVSS
04 LSCRASDYTYRGGCMGWFRQIPGKEREGVAAVNSGAGSTYYADSVKGRFTISQDNAKRTVYLQMNRLAPEDTAIYYCAAAWWCGSDDWDSTRRINS--WGQGTQVTVSS
05 LSCQVSGDTYTGTCAGWFRQAPGKGREGVAFINRPGTFTSYTDSVKGRFIISQDNTKNTWSLQMKNLKPEDTATYYCAAEGFGCYTGGAPYGFSY---WGQGTQVTVSS
06 LSCAASGYTGSRNCMAWFRQAPGKEREALAAIYTGGGTTYYADSVKGRFTISQDAHKNTVYLQMNNLKPEDTAVYYCAGEGRYNDYEGCFGYNS----WGQGTQVTVSS
07 LSCAASGYIYSTYSMGWFRQAPGKEREVVATINTRTGSTYYADSVKGRFTISQDNAKHTVSLQMNSLKPEDTAIYYCAAGSCSRPWHVCRDSAD----WGQGTQVTVSS
08 LSCAASGDIFSSYVMGWFRKAPGKECELVATIESDGRTTY-ADSVKGRFTISRDNALSPAHLQMNNLKPEDTAVYYCAADVSRFTTRCVGSY------WGQGTQVTVSS
09 LSCAASGFTFSSYDMSWVRQAPGKGLEWVSVIGSGGGSTYYADSVKGRFTISRDNAKNTVTLQMNRLKPEDTAVYYCATEGALDRYYSLDY-------WGKGTQVTVSS
10 LSCAASGSLPSTCSLGWYRQAPGQARELVATIRTDGST-YYADSVKGRFTISQDNAKNTVYLQMNNLKPEDTALYYCNNSNARPWCGPLTA--------GQGTQVTVSS
11 LSCTVSGNPYSRCTMAWYRQAPGKQREFVSDINSESTT-YYADSVKGRFTISKDAAEKTVHLQMNNLNPEDTAMYTCNIRCLVSRMWYNY--------WGHGTQVTVSS


Dr 1409

01 LSCSASGYTFSDYGMGWFRQAPGKECELVSAIGGDGTTN--YADTVKGRFTISRDNSKNTVVLQMNSLKPEDTAVYYCVGEVFSGSMLYTSSSYRRADCATLFGYNYWGQGTQVTVSS
02 LSCAASGYTVSSICMGWFRQAPGKEREGVALISGLGGS--IYYADSVKGRFTISQDNAKNTVYLQMNSLKPEDTAIYYCAATELCGSWHLPRGAYGYNY---------WGQGTQVTVSS
03 LSCAVSGDTISRMCVSWFRQPPGREREAVARIGFGGNY--TWYTDSVRGRFTVSQDNARNLVYLQMSSLKPEDTAMYYCAAVEGSGRYCDWRVPRSYV----------WGQGTQVTVSS
04 LDCATSGESGSRWCMGWFRQAPGKEREGVAFINRSNGN--TYYTDSVKGRFTIAQDNAKNTVYLLMNNLKPEDTAAYYCAAPSRPIRCGNLVAGDFAH----------WGQGTQVTVSS
05 LSCLASGFAFGTFPMSWVRRTPGKGLEWVSGINSGGGS--TYYADSVKGRFTISRDNAKNTLYLQLNSLKTEDTAMYYCAKDDDSGTYIDLGVWYNY----------WGQGTQVTVSS
06 LSCTVSGFNFDDSDMGWYHQPPGKTCELISTITSDGLS--TWYADSVKGRFTISRNNAENTMYLQMNNLNPEDTAMYYCAAVDHGGRWYCGYT--------------GQGTQVTVSSA
07 LSCTASGFTFADTKMGWFRQAPGNECDLVSVIDKDGTE---YYITPVEGRFTISRDNAKNTIYLQMNDLKPEDTAMYYCAANPTKTRDDAVCT--------------WGLGTQVTVSS
08 LSCAYSGYAFTCPMGWYRQAPGKERELISRIMTDGDTF----YADSVKGRFTISQDNAKNMVYLQMNSLEPEDTGRYYCSTARPCPLFGY-----------------WGQGTQVTVSS
09 LSCAASRYGQTRYFMHWFRQVPGKERERVASLNPFNGI--AWYDDSVKGRFTISQGGAENTVNLKMDKLTPEDTAIYYCVAGFGSGLYTY-----------------WGQGTQVTVSS
10 LSCTVPGFSSGRCGVTWSRLAAGRSLEWVASISTGGDTASSDSRFAVSSDKAEDTVYLQLNTLRPEDTGRYSCKASGVCSGD-------------------------WGQGTQVTVSS
12 LSCTVPGFSSGRCGVTWSRLAAGRSLEWVASISTGGDTASSDSRFAVSSDKAEDTVYLQLNTLRPEDTGRYSCKASGVCSGD-------------------------WGQGTQVTVSS
```

Figure 6.3. Sequence alignment of the VHHs after TG1 transfection. The CDR1, CDR2 and CDR3 loops are coloured in red, green, and blue, respectively. The framework regions are coloured black. Cys residues likely involved in disulfide bonds are highlighted in yellow

6.4 Direct ELISA using Biotinylated nanobodies

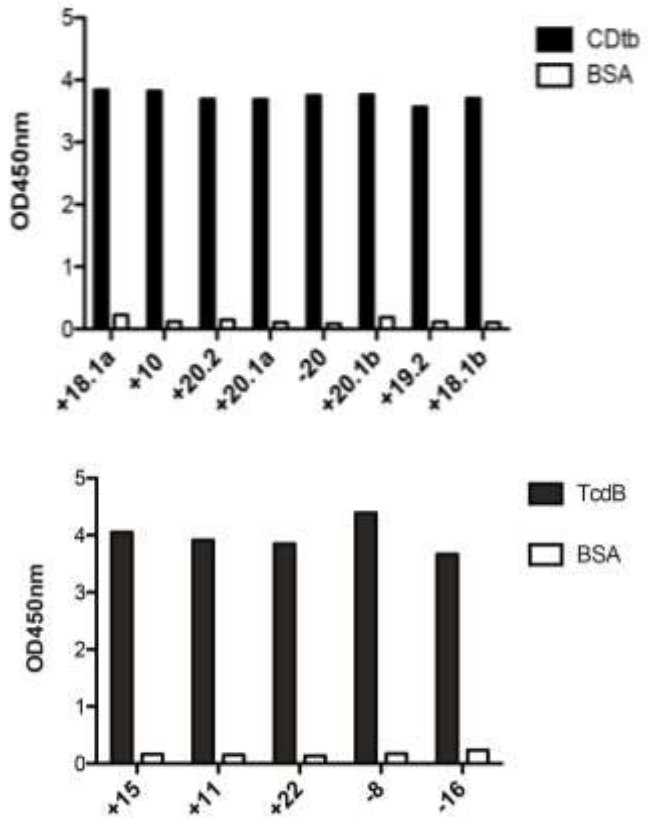

Figure 6.4. Analysis of binding specificity of nanobodies after Biotinylation by Direct ELISA

6.5 Sequence of Hinge-CH2-CH3 of mouse IgA and J chain

- Amino acids sequence of Hinge-CH2-CH3 of mouse IgA [Mus musculus domesticus] with NOTI and XBAI sites ordered as gene blocks

QPAAASGPTPPPPITIPSCQPSLSLQRPALEDLLLGSDASITCTLNGLRNPEGAAFTWEPSTGKDAVQKKAAQN
SCGCYSVSSVLPGCAERWNSGASFKCTVTHPESGTLTGTIAKVTVNTFPPQVHLLPPPSEELALNELLSLTCLV
RAFNPKEVLVRWLHGNEELSPESYLVFEPLKEPGEGATTYLVTSVLRVSAETWKQGDQYSCMVGHEALPMNFTQ
KTIDRLSGKPTNVSVSVIMSEGDGICY**SRKA

- Amino acids sequence of J-chain, [Mus musculus] with NcoI and NOTI sites ordered as gene blocks

PAMADDEATILADNKCMCTRVTSKIIPSTEDPNEDIVERNIRIVVPLNNRENISDPTSPLRRNFVYHLSDVCKK
CDPVEVELEDQVVTATQSNICNEDDGVPETCYMYDRNKCYTTMVPLRYHGETKMVQAALTPDSCYPD
VQAALTPDSCYPD--AAAHH

7. Abbreviations

AA	Amino acid
ADP	adenosine diphosphate
AEBSF	4-(2-Aminoethyl) benzenesulfonyl fluoride
AP	Alkaline Phosphatase
ATP	adenosine triphosphate
BCA	bicinchoninic acid
BSA	bovine serum albumin
CCCNA	cell culture cytotoxicity neutralization assay
CDAD	Clostridium difficile associated disease
CDI	Clostridium difficile infection
cDNA	complementary DNA
CDR	complementary determining region
CDT	Clostridium difficile transferase
CH	constant domain of the antibody heavy chain
CL	constant domain of the light chain
CPD	cysteine protease domain
CROPs	c-terminally-located combined repetitive oligopeptides
DMEM	Dulbecco's modified Eagle medium
DNA	deoxyribonucleic acid
dNTP	deoxyribonucleotide triphosphate
DTT	dithiothreitol
EDTA	ethylendiamintetraacetate
ELISA	enzyme-linked immunosorbent assay
Fab	fragment antigen binding
Fc	fragment of crystalization
FCS	foetal calf serum
Fig.	figure
FR	framework regions
GDH	glutamate dehydrogenase
GTD	glucosyl transferase domain
HCl	hydrochloric acid
HCAbs	heavy chain only antibodies
HEK	human embryonal kidney cells
HEPES	4-(2-hydroxyethyl)-1-piperazineethanesulfonic acid
HRP	horseradish peroxidase
HSP90	heat shock protein 90
IDSA	Infectious Diseases Society of America
Ig	immunglobulin
$InsP_6$	inositol hexakisphosphate
IPTG	isopropylthio-β-galactoside
kDa	kilodalton
LCT	large clostridial toxin
LSR	lipolysis-stimulated lipoprotein receptor
mAb	monoclonal antibody
MW	molecular weight
NAATs	nucleic acid amplification tests
NaCl	sodium chloride
NAD^+	nicotinamide adeninine dinucleotide
Nb	nanobody
OD	optical density
PBS	phosphate buffer saline
Pfu	Plaque-Forming Unit
PCR	polymerase chain reaction
PelB	pectate lyase B
PMC	pseudomembranous colitis

RNA	ribonucleic acid
Rpm	revolutions per minute
sdAb	single domain antibody
SDS-PAGE	sodium dodecyl sulfate polyacrylamide
SHEA	The Society for Healthcare Epidemiology of America
SOC	super optimal broth with catabolite repression
TAE	tris-acetate-EDTA
TcdA	toxin A (of Clostridium difficile)
TcdB	toxin B (of Clostridium difficile)
TMB	3,3′,5,5′-tetramethylbenzidine
U	unit
UV	ultraviolet
V	volt
VH	variable domain of the heavy chain
VHH	variable domain of the heavy chain only antibody
VL	variable domain of the light chain

8. References

AGHEBATI-MALEKI, L., BAKHSHINEJAD, B., BARADARAN, B., MOTALLEBNEZHAD, M., AGHEBATI-MALEKI, A., NICKHO, H., YOUSEFI, M. & MAJIDI, J. 2016. Phage display as a promising approach for vaccine development. *J Biomed Sci,* 23**,** 66.

AKERLUND, T., SVENUNGSSON, B., LAGERGREN, A. & BURMAN, L. G. 2006. Correlation of disease severity with fecal toxin levels in patients with Clostridium difficile-associated diarrhea and distribution of PCR ribotypes and toxin yields in vitro of corresponding isolates. *J Clin Microbiol,* 44**,** 353-8.

AKTORIES, K., SCHWAN, C. & JANK, T. 2017. Clostridium difficile Toxin Biology. *Annu Rev Microbiol,* 71**,** 281-307.

ANDERSEN, K. K., STROKAPPE, N. M., HULTBERG, A., TRUUSALU, K., SMIDT, I., MIKELSAAR, R. H., MIKELSAAR, M., VERRIPS, T., HAMMARSTROM, L. & MARCOTTE, H. 2016. Neutralization of Clostridium difficile Toxin B Mediated by Engineered Lactobacilli That Produce Single-Domain Antibodies. *Infect Immun,* 84**,** 395-406.

ANDERSON, D. M., SHEEDLO, M. J., JENSEN, J. L. & LACY, D. B. 2019. Structural insights into the transition of Clostridioides difficile binary toxin from prepore to pore. *Nature Microbiology,* 5**,** 102-107.

BANAWAS, S. S. 2018. Clostridium difficile Infections: A Global Overview of Drug Sensitivity and Resistance Mechanisms. *Biomed Res Int,* 2018**,** 8414257.

BARTLETT, J. G. 2002. Antibiotic-associated diarrhea. *New England Journal of Medicine,* 346**,** 334–349.

BARTLETT, J. G. 2017. Bezlotoxumab — A New Agent for Clostridium difficile Infection. *New England Journal of Medicine,* 376**,** 381-382.

BARTLETT, J. G. & GERDING, D. N. 2008. Clinical recognition and diagnosis of Clostridium difficile infection. *Clin Infect Dis,* 46 Suppl 1**,** S12-8.

BELKAID, Y. & HAND, T. W. 2014. Role of the microbiota in immunity and inflammation. *Cell,* 157**,** 121-41.

BLANKE, S. R., SCHWAN, C., STECHER, B., TZIVELEKIDIS, T., VAN HAM, M., ROHDE, M., HARDT, W.-D., WEHLAND, J. & AKTORIES, K. 2009. Clostridium difficile Toxin CDT Induces Formation of Microtubule-Based Protrusions and Increases Adherence of Bacteria. *PLoS Pathogens,* 5**,** e1000626.

BOSCH, D., CASTILHO, A., LOOS, A., SCHOTS, A. & STEINKELLNER, H. 2013. N-glycosylation of plant-produced recombinant proteins. *Curr Pharm Des,* 19**,** 5503-12.

BREEDVELD, A. & VAN EGMOND, M. 2019. IgA and FcalphaRI: Pathological Roles and Therapeutic Opportunities. *Front Immunol,* 10**,** 553.

BURDON, D. W., GEORGE, R. H., MOGG, G. A., ARABI, Y., THOMPSON, H., JOHNSON, M., ALEXANDER-WILLIAMS, J. & KEIGHLEY, M. R. 1981. Faecal toxin and severity of antibiotic-associated pseudomembranous colitis. *J Clin Pathol,* 34**,** 548-51.

BURNHAM, C. A. & CARROLL, K. C. 2013. Diagnosis of Clostridium difficile infection: an ongoing conundrum for clinicians and for clinical laboratories. *Clin Microbiol Rev,* 26**,** 604-30.

CHANDRASEKARAN, R. & LACY, D. B. 2017. The role of toxins in Clostridium difficile infection. *FEMS Microbiol Rev,* 41**,** 723-750.

COHEN, N. A., MILLER, T., NA'AMINH, W., HOD, K., ADLER, A., COHEN, D., GUZNER-GUR, H., SANTO, E., HALPERN, Z., CARMELI, Y. & MAHARSHAK, N. 2018. Clostridium

difficile fecal toxin level is associated with disease severity and prognosis. *United European Gastroenterol J,* 6**,** 773-780.
COHEN, S. H., GERDING, D. N., JOHNSON, S., KELLY, C. P., LOO, V. G., MCDONALD, L. C., PEPIN, J., WILCOX, M. H., SOCIETY FOR HEALTHCARE EPIDEMIOLOGY OF, A. & INFECTIOUS DISEASES SOCIETY OF, A. 2010. Clinical practice guidelines for Clostridium difficile infection in adults: 2010 update by the society for healthcare epidemiology of America (SHEA) and the infectious diseases society of America (IDSA). *Infect Control Hosp Epidemiol,* 31**,** 431-55.
CRASSON, O., RHAZI, N., JACQUIN, O., FREICHELS, A., JEROME, C., RUTH, N., GALLENI, M., FILEE, P. & VANDEVENNE, M. 2015. Enzymatic functionalization of a nanobody using protein insertion technology. *Protein Eng Des Sel,* 28**,** 451-60.
CROBACH, M. J., PLANCHE, T., ECKERT, C., BARBUT, F., TERVEER, E. M., DEKKERS, O. M., WILCOX, M. H. & KUIJPER, E. J. 2016. European Society of Clinical Microbiology and Infectious Diseases: update of the diagnostic guidance document for Clostridium difficile infection. *Clin Microbiol Infect,* 22 Suppl 4**,** S63-81.
CZEPIEL, J., DROZDZ, M., PITUCH, H., KUIJPER, E. J., PERUCKI, W., MIELIMONKA, A., GOLDMAN, S., WULTANSKA, D., GARLICKI, A. & BIESIADA, G. 2019. Clostridium difficile infection: review. *Eur J Clin Microbiol Infect Dis,* 38**,** 1211-1221.
DALEY, L. P., GAGLIARDO, L. F., DUFFY, M. S., SMITH, M. C. & APPLETON, J. A. 2005. Application of monoclonal antibodies in functional and comparative investigations of heavy-chain immunoglobulins in new world camelids. *Clin Diagn Lab Immunol,* 12**,** 380-6.
DE MARCO, A. 2020. Recombinant expression of nanobodies and nanobody-derived immunoreagents. *Protein Expr Purif,* 172**,** 105645.
DE SOUSA-PEREIRA, P. & WOOF, J. M. 2019. IgA: Structure, Function, and Developability. *Antibodies (Basel),* 8.
DEL RIO, B., REDRUELLO, B., FERNANDEZ, M., MARTIN, M. C., LADERO, V. & ALVAREZ, M. A. 2019. Lactic Acid Bacteria as a Live Delivery System for the in situ Production of Nanobodies in the Human Gastrointestinal Tract. *Frontiers in Microbiology,* 9.
DI BELLA, S., ASCENZI, P., SIARAKAS, S., PETROSILLO, N. & DI MASI, A. 2016. Clostridium difficile Toxins A and B: Insights into Pathogenic Properties and Extraintestinal Effects. *Toxins (Basel),* 8.
DIETERLE, M. G., RAO, K. & YOUNG, V. B. 2019. Novel therapies and preventative strategies for primary and recurrent Clostridium difficile infections. *Ann N Y Acad Sci,* 1435**,** 110-138.
FUMEY, W., KOENIGSDORF, J., KUNICK, V., MENZEL, S., SCHUTZE, K., UNGER, M., SCHRIEWER, L., HAAG, F., ADAM, G., OBERLE, A., BINDER, M., FLIEGERT, R., GUSE, A., ZHAO, Y. J., CHEUNG LEE, H., MALAVASI, F., GOLDBAUM, F., VAN HEGELSOM, R., STORTELERS, C., BANNAS, P. & KOCH-NOLTE, F. 2017. Nanobodies effectively modulate the enzymatic activity of CD38 and allow specific imaging of CD38(+) tumors in mouse models in vivo. *Sci Rep,* 7**,** 14289.
GEBREYOHANES, M. G. & ASSEN, A. M. 2017. Adaptation Mechanisms of Camels (Camelus dromedarius) for Desert Environment: A Review. *Journal of Veterinary Science & Technology,* 08.
GERDING, D. N., JOHNSON, S., RUPNIK, M. & AKTORIES, K. 2014. Clostridium difficile binary toxin CDT: mechanism, epidemiology, and potential clinical importance. *Gut Microbes,* 5**,** 15-27.
GERHARD, R. 2017. Receptors and Binding Structures for Clostridium difficile Toxins A and B. *Curr Top Microbiol Immunol,* 406**,** 79-96.

GHIZZONE, M. V. 2019. *Clostridioides difficile : What's in a name?* [Online]. springer. Available: https://http://www.healio.com/news/infectious-disease/20190301/clostridioides-difficile-whats-in-a-name.
GOVAERT, J., PELLIS, M., DESCHACHT, N., VINCKE, C., CONRATH, K., MUYLDERMANS, S. & SAERENS, D. 2012. Dual beneficial effect of interloop disulfide bond for single domain antibody fragments. *J Biol Chem,* 287**,** 1970-9.
GUPTA, P., ZHANG, Z., SUGIMAN-MARANGOS, S. N., TAM, J., RAMAN, S., JULIEN, J.-P., KROH, H. K., LACY, D. B., MURGOLO, N., BEKKARI, K., THERIEN, A. G., HERNANDEZ, L. D. & MELNYK, R. A. 2017. Functional defects inClostridium difficileTcdB toxin uptake identify CSPG4 receptor-binding determinants. *Journal of Biological Chemistry,* 292**,** 17290-17301.
HANSEN, I. S., BAETEN, D. L. P. & DEN DUNNEN, J. 2019. The inflammatory function of human IgA. *Cell Mol Life Sci,* 76**,** 1041-1055.
HUSSACK, G., RYAN, S., VAN FAASSEN, H., ROSSOTTI, M., MACKENZIE, C. R. & TANHA, J. 2018. Neutralization of Clostridium difficile toxin B with VHH-Fc fusions targeting the delivery and CROPs domains. *PLoS One,* 13**,** e0208978.
JOHNSON, S. & GERDING, D. N. 2019. Bezlotoxumab. *Clin Infect Dis,* 68**,** 699-704.
JOVCEVSKA, I. & MUYLDERMANS, S. 2020. The Therapeutic Potential of Nanobodies. *BioDrugs,* 34**,** 11-26.
KACHRIMANIDOU, M. & TSINTARAKIS, E. 2020. Insights into the Role of Human Gut Microbiota in Clostridioides difficile Infection. *Microorganisms,* 8.
KALAKUNTLA, A. S., NALAKONDA, G., NALAKONDA, K., PIDIKITI, C. V. & AASIM, S. A. 2019. Probiotics and Clostridium Difficile: A Review of Dysbiosis and the Rehabilitation of Gut Microbiota. *Cureus,* 11**,** e5063.
KANDALAFT, H., HUSSACK, G., AUBRY, A., VAN FAASSEN, H., GUAN, Y., ARBABI-GHAHROUDI, M., MACKENZIE, R., LOGAN, S. M. & TANHA, J. 2015. Targeting surface-layer proteins with single-domain antibodies: a potential therapeutic approach against Clostridium difficile-associated disease. *Appl Microbiol Biotechnol,* 99**,** 8549-62.
KHO, Z. Y. & LAL, S. K. 2018. The Human Gut Microbiome - A Potential Controller of Wellness and Disease. *Front Microbiol,* 9**,** 1835.
KUNZ, P., FLOCK, T., SOLER, N., ZAISS, M., VINCKE, C., STERCKX, Y., KASTELIC, D., MUYLDERMANS, S. & HOHEISEL, J. D. 2017. Exploiting sequence and stability information for directing nanobody stability engineering. *Biochim Biophys Acta Gen Subj,* 1861**,** 2196-2205.
KUNZ, P., ZINNER, K., MUCKE, N., BARTOSCHIK, T., MUYLDERMANS, S. & HOHEISEL, J. D. 2018. The structural basis of nanobody unfolding reversibility and thermoresistance. *Sci Rep,* 8**,** 7934.
LAZAR, V., DITU, L. M., PIRCALABIORU, G. G., GHEORGHE, I., CURUTIU, C., HOLBAN, A. M., PICU, A., PETCU, L. & CHIFIRIUC, M. C. 2018. Aspects of Gut Microbiota and Immune System Interactions in Infectious Diseases, Immunopathology, and Cancer. *Front Immunol,* 9**,** 1830.
LI, J. W., XIA, L., SU, Y., LIU, H., XIA, X., LU, Q., YANG, C. & REHEMAN, K. 2012. Molecular imprint of enzyme active site by camel nanobodies: rapid and efficient approach to produce abzymes with alliinase activity. *J Biol Chem,* 287**,** 13713-21.
LUBBERT, C., ZIMMERMANN, L., BORCHERT, J., HORNER, B., MUTTERS, R. & RODLOFF, A. C. 2016. Epidemiology and Recurrence Rates of Clostridium difficile Infections in Germany: A Secondary Data Analysis. *Infect Dis Ther,* 5**,** 545-554.
MANTIS, N. J., ROL, N. & CORTHESY, B. 2011. Secretory IgA's complex roles in immunity and mucosal homeostasis in the gut. *Mucosal Immunol,* 4**,** 603-11.

MASTRANTONIO, P., AND RUPNIK, M 2018. updates on Clostridium difficile in Europe.
MENDOZA, M. N., JIAN, M., KING, M. T. & BROOKS, C. L. 2020. Role of a noncanonical disulfide bond in the stability, affinity, and flexibility of a VHH specific for the Listeria virulence factor InlB. *Protein Sci,* 29**,** 1004-1017.
MUYLDERMANS, S. 2001. Single domain camel antibodies: current status. *J Biotechnol,* 74**,** 277-302.
MUYLDERMANS, S. & SMIDER, V. V. 2016. Distinct antibody species: structural differences creating therapeutic opportunities. *Curr Opin Immunol,* 40**,** 7-13.
NAVALKELE, B. D. & CHOPRA, T. 2018. Bezlotoxumab: an emerging monoclonal antibody therapy for prevention of recurrent Clostridium difficile infection. *Biologics,* 12**,** 11-21.
OOIJEVAAR, R. E., VAN BEURDEN, Y. H., TERVEER, E. M., GOORHUIS, A., BAUER, M. P., KELLER, J. J., MULDER, C. J. J. & KUIJPER, E. J. 2018. Update of treatment algorithms for Clostridium difficile infection. *Clin Microbiol Infect,* 24**,** 452-462.
ORRELL, K. E., ZHANG, Z., SUGIMAN-MARANGOS, S. N. & MELNYK, R. A. 2017. Clostridium difficile toxins A and B: Receptors, pores, and translocation into cells. *Crit Rev Biochem Mol Biol,* 52**,** 461-473.
ORTH, P., XIAO, L., HERNANDEZ, L. D., REICHERT, P., SHETH, P. R., BEAUMONT, M., YANG, X., MURGOLO, N., ERMAKOV, G., DINUNZIO, E., RACINE, F., KARCZEWSKI, J., SECORE, S., INGRAM, R. N., MAYHOOD, T., STRICKLAND, C. & THERIEN, A. G. 2014. Mechanism of action and epitopes of Clostridium difficile toxin B-neutralizing antibody bezlotoxumab revealed by X-ray crystallography. *J Biol Chem,* 289**,** 18008-21.
PENG, Z., LING, L., STRATTON, C. W., LI, C., POLAGE, C. R., WU, B. & TANG, Y. W. 2018. Advances in the diagnosis and treatment of Clostridium difficile infections. *Emerg Microbes Infect,* 7**,** 15.
POLLOCK, N. R. 2016. Ultrasensitive Detection and Quantification of Toxins for Optimized Diagnosis of Clostridium difficile Infection. *J Clin Microbiol,* 54**,** 259-64.
RAO, K. & MALANI, P. N. 2020. Diagnosis and Treatment of Clostridioides (Clostridium) difficile Infection in Adults in 2020. *JAMA*.
SCHMIDT, D. J., BEAMER, G., TREMBLAY, J. M., STEELE, J. A., KIM, H. B., WANG, Y., DEBATIS, M., SUN, X., KASHENTSEVA, E. A., DMITRIEV, I. P., CURIEL, D. T., SHOEMAKER, C. B. & TZIPORI, S. 2016. A Tetraspecific VHH-Based Neutralizing Antibody Modifies Disease Outcome in Three Animal Models of Clostridium difficile Infection. *Clin Vaccine Immunol,* 23**,** 774-84.
SCHUMACHER, L. 2020. *Characterisation of llama-derived single domain antibodies for the Clostridium difficile toxin CDTb and the establishment*
of a murine infection model of the pathogen. Universität Hamburg.
SEEKATZ, A. M. & YOUNG, V. B. 2014. Clostridium difficile and the microbiota. *J Clin Invest,* 124**,** 4182-9.
SHEEDLOA, M. J., ANDERSON, D. M., THOMAS, A. K. & LACYA, D. B. 2020. Structural elucidation of the Clostridioides difficile
transferase toxin reveals a single-site binding
mode for the enzyme. *PNAS,* 117**,** 6139-6144.
SONG, J. H. & KIM, Y. S. 2019. Recurrent Clostridium difficile Infection: Risk Factors, Treatment, and Prevention. *Gut Liver,* 13**,** 16-24.
STRUGNELL, R. A. & WIJBURG, O. L. 2010. The role of secretory antibodies in infection immunity. *Nat Rev Microbiol,* 8**,** 656-67.
UNGER, M., EICHHOFF, A. M., SCHUMACHER, L., STRYSIO, M., MENZEL, S., SCHWAN, C., ALZOGARAY, V., ZYLBERMAN, V., SEMAN, M., BRANDNER, J., ROHDE, H., ZHU, K.,

HAAG, F., MITTRUCKER, H. W., GOLDBAUM, F., AKTORIES, K. & KOCH-NOLTE, F. 2015. Selection of nanobodies that block the enzymatic and cytotoxic activities of the binary Clostridium difficile toxin CDT. *Sci Rep,* 5**,** 7850.

VANDENBROUCKE, K., DE HAARD, H., BEIRNAERT, E., DREIER, T., LAUWEREYS, M., HUYCK, L., VAN HUYSSE, J., DEMETTER, P., STEIDLER, L., REMAUT, E., CUVELIER, C. & ROTTIERS, P. 2010. Orally administered L. lactis secreting an anti-TNF Nanobody demonstrate efficacy in chronic colitis. *Mucosal Immunol,* 3**,** 49-56.

VANMARSENILLE, C., ELSEVIERS, J., YVANOFF, C., HASSANZADEH-GHASSABEH, G., GARCIA RODRIGUEZ, G., MARTENS, E., DEPICKER, A., MARTEL, A., HAESEBROUCK, F., PASMANS, F., HERNALSTEENS, J. P. & DE GREVE, H. 2018. In planta expression of nanobody-based designer chicken antibodies targeting Campylobacter. *PLoS One,* 13**,** e0204222.

VIRDI, V., CODDENS, A., DE BUCK, S., MILLET, S., GODDEERIS, B. M., COX, E., DE GREVE, H. & DEPICKER, A. 2013. Orally fed seeds producing designer IgAs protect weaned piglets against enterotoxigenic Escherichia coli infection. *Proc Natl Acad Sci U S A,* 110**,** 11809-14.

VIRDI, V., JUAREZ, P., BOUDOLF, V. & DEPICKER, A. 2016. Recombinant IgA production for mucosal passive immunization, advancing beyond the hurdles. *Cell Mol Life Sci,* 73**,** 535-45.

VIRDI, V., PALACI, J., LAUKENS, B., RYCKAERT, S., COX, E., VANDERBEKE, E., DEPICKER, A. & CALLEWAERT, N. 2019. Yeast-secreted, dried and food-admixed monomeric IgA prevents gastrointestinal infection in a piglet model. *Nat Biotechnol,* 37**,** 527-530.

WANG, H., SUN, X., ZHANG, Y., LI, S., CHEN, K., SHI, L., NIE, W., KUMAR, R., TZIPORI, S., WANG, J., SAVIDGE, T., FENG, H. & BLANKE, S. R. 2012. A Chimeric Toxin Vaccine Protects against Primary and Recurrent Clostridium difficile Infection. *Infection and Immunity,* 80**,** 2678-2688.

WESTERHOF, L. B., WILBERS, R. H., VAN RAAIJ, D. R., VAN WIJK, C. Z., GOVERSE, A., BAKKER, J. & SCHOTS, A. 2015. Transient Expression of Secretory IgA In Planta is Optimal Using a Multi-Gene Vector and may be Further Enhanced by Improving Joining Chain Incorporation. *Front Plant Sci,* 6**,** 1200.

WOOF, J. M. & RUSSELL, M. W. 2011. Structure and function relationships in IgA. *Mucosal Immunol,* 4**,** 590-7.

WU, A. M., CHEN, W., RAUBITSCHEK, A., WILLIAMS, L. E., NEUMAIER, M., FISCHER, R., HU, S. Z., ODOM-MARYON, T., WONG, J. Y. & SHIVELY, J. E. 1996. Tumor localization of anti-CEA single-chain Fvs: improved targeting by non-covalent dimers. *Immunotechnology,* 2**,** 21-36.

WU, C. H., LIU, I. J., LU, R. M. & WU, H. C. 2016. Advancement and applications of peptide phage display technology in biomedical science. *J Biomed Sci,* 23**,** 8.

YANG, Z., SCHMIDT, D., LIU, W., LI, S., SHI, L., SHENG, J., CHEN, K., YU, H., TREMBLAY, J. M., CHEN, X., PIEPENBRINK, K. H., SUNDBERG, E. J., KELLY, C. P., BAI, G., SHOEMAKER, C. B. & FENG, H. 2014. A novel multivalent, single-domain antibody targeting TcdA and TcdB prevents fulminant Clostridium difficile infection in mice. *J Infect Dis,* 210**,** 964-72.

ZHANG, L., DONG, D., JIANG, C., LI, Z., WANG, X. & PENG, Y. 2015. Insight into alteration of gut microbiota in Clostridium difficile infection and asymptomatic C. difficile colonization. *Anaerobe,* 34**,** 1-7.

9. Acknowledgements

I would like to thank my supervisor, Prof. Dr. Friedrich Koch-Nolte, for providing me the opportunity to carry out my PhD on nanobodies in his Lab. I am thankful for his guidance, support, encouragement, advice, space and freedom he has provided throughout the last four years.

I would also like to thank Prof. Touhami Khorchani, Prof. Hammadi Hammadi and Prof. Imed Salhi at the Arid Regions Institute (Medenine, Tunisia) for being part of this project and take care of dromedary immunization in Tunisia.

I am thankful to Prof. Dr. Friedrich Haag, Prof. Dr. Hans-Willi Mittrücker and Prof. Dr. Eva Tolosa for their kind help and support whenever needed.

I would also like to thank lab technicians; Marion Nissen, Fabienne Seyfried, Gudrun Dubberke, Birte Albrecht and Joanna Schmidt for their excellent technical assistance.
My gratitude goes specifically to Fabienne Seyfried for her technical support in the lab and also her advices and kind help in many daily life issues related to German language, which have made my life in Germany much easier.

I must express my gratitude to all my lab mates, colleagues and research team; Dr. Mirijam Loew, Dr. Stephan Menzel, Dr. Thomas Eden, Dr. Sana Javed, Dr. Carolina Pinto Espinoza, Dr. Anna-Marei Eichhoff, Tobias Schäfer, for their help, support and guidance during the last years and for a cherished time spent together in the lab,

I also owe much gratitude to my parents for their continuous and tremendous encouragement, to my husband who has supported me throughout this process and has constantly encouraged me to move forward, to my little daughter Yesmin.

I would like to thank my grandparents, my sister and brother, my extended family and my relatives for their unwavering support and prayers.

10.Curriculum Vitae

„Lebenslauf wurde aus daten schutzrechtlichen Gründen entfernt‘‘

Eidesstattliche Erklärung

Ich versichere ausdrücklich, dass ich die Arbeit selbständig und ohne fremde Hilfe verfasst, andere als die von mir angegebenen Quellen und Hilfsmittel nicht benutzt und die aus den benutzten Werken wörtlich oder inhaltlich entnommenen Stellen einzeln nach Ausgabe (Auflage und Jahr des Erscheinens), Band und Seite des benutzten Werkes kenntlich gemacht habe. Ferner versichere ich, dass ich die Dissertation bisher nicht einem Fachvertreter an einer anderen Hochschule zur .berprüfung vorgelegt oder mich anderweitig um Zulassung zur Promotion beworben habe. Ich erkläre mich einverstanden, dass meine Dissertation vom Dekanat der Medizinischen Fakultät mit einer gängigen Software zur Erkennung von Plagiaten überprüft werden kann.

Unterschrift: .....